NATIONAL AERONAUTICS AND SPACE ADMINISTRATION

TECHNICAL REPORT

VOLUME I

COMPUTATIONS OF NON-REACTING AND REACTING VISCOUS BLUNT BODY FLOWS

By

C. P. Li

Applied Mechanics Department
Lockheed Electronics Company, Inc.

Prepared Under Contract NAS9-12200 By
Lockheed Electronics Company, Inc.
Houston Aerospace Systems Division

for

Computation and Analysis Division
National Aeronautics and Space Administration
Manned Spacecraft Center
Houston, Texas

February 1973

MANNED SPACECRAFT CENTER
HOUSTON, TEXAS

Applied Mechanics
Department 628-20
TR2007

TECHNICAL REPORT

Computations of Non-Reacting and Reacting Viscous Blunt Body Flows

By

C. P. LI

Applied Mechanics Department
Lockheed Electronics Company, Inc.

Prepared Under Contract NAS9-12200 By
Lockheed Electronics Company, Inc.
Houston Aerospace Systems Division

for

Computation and Analysis Division
National Aeronautics and Space Administration
Manned Spacecraft Center
Houston, Texas

February 1973

PRECEDING PAGE BLANK NOT FILMED

TECHNICAL REPORT

Computations of Non-Reacting and Reacting Viscous Blunt Body Flows

Prepared by C. P. Li
C. P. Li
Physical Science Section

Approved by W. J. Reicks
W. J. Reicks, Supervisor
Physical Science Section

Approved by R. T. Theobald
R. T. Theobald, Manager
Applied Mechanics Department

TABLE OF CONTENTS

FOREWORD

This report presents the analysis and the computer programs developed for computation of viscous shock layer flowfield surrounding the nose of a shuttle orbiter during its reentry. Part I describes the problem formulation and the numerical procedures used to solve the basic set of equations, and the results of flowfield properties at several trajectory points, ranging from the high altitude rarefied region to the low altitude boundary-layer region. Part II of this report describes the structure of the computer programs and the experiences gained in utilizing these programs. A user's input guide is also included along with a complete listing of programs.

ACKNOWLEDGEMENT

The author wishes to acknowledge many helpful comments and constructive criticisms offered by the members of the aerothermodynamics section of the Structures and Mechanics Division. Drs. W. Goodrich, C. Scott and R. C. Ried have provided many opportunities to discuss the results obtained. He also would like to thank Mr. W. J. Reicks for his advice in the presentation of this report.

PART I
ANALYSIS AND RESULTS FOR A SHUTTLE ORBITER

SUMMARY

This part of the report presents a numerical analysis of the viscous flow field, with and without finite-rate chemical reactions, in the nose region of a shuttle orbiter under a wide range of free stream conditions. One purpose of this study was to develop a unified calculation procedure that will provide a starting solution having detailed profiles of flow properties for subsequent flow field computations beyond the nose. Therefore, the generalized curvilinear coordinate system was used and the fluid-dynamic equations were cast in conservative form. Thus, several special coordinate systems can be chosen in the computation and the shock can be treated as either a sharp discontinuity or a thick layer. The second objective of this study was to investigate the flow field characteristics that are encountered during the orbiter descent. The effect of transport properties of the air mixture, the surface catalyticity, and the wall temperature on the flow field was studied extensively at several trajectory points for which the chemical nonequilibrium phenomena are predominant. The last objective was to analyze the flowfield in terms of the heat transfer and friction coefficients and to compare the results with available solutions. Representive trajectory points were selected for calculations using the frozen, finite-rate, and equilibrium gas models. The numerical solutions obtained are considered to be sufficiently accurate for the aforementioned objectives due to the use of exact equations, and the coordinate transformation which provides a better resolution of flow properties in the vicinity of a wall. Attempts were also made to improve the efficiency of the time-marching finite-difference technique which was used to solve the flow equation in the present analysis.

NOMENCLATURE

a	frozen speed of sound
A_i	temperature coefficients for polynomial equations of thermodynamic functions, Eq (16)
B	body configuration
c	mass fraction
c_f	friction coefficient, Eq (24)
c_H	heat transfer coefficient (Stanton number), Eq (25)
c_p	heat capacity at constant pressure
$D_{\ell m}$	binary diffusion coefficient
$D_{\ell m}$	multicomponent diffusion coefficient
e	specific internal energy, Eq (6)
F	Gibbs free energy Eq (16)
h	specific enthalpy
h_1, h_2, h_3	metric coefficients for the orthogonal coordinate system
H	molar enthalpy, Eq (16)
I_i	mass diffusion flux, Eq (9)
k	thermal conductivity, Eq (18) and (19)
k_f, k_b	rate constants of forward reaction, backward reaction
K	Boltzmann constant
K_c	equilibrium constant for mass concentrations
L	total number of species
$Le_{\ell m}$	Lewis number for a multicomponent mixture
M	molecular weight or Mach number
M_w	molecular weight of the mixture

NOMENCLATURE

n	normal to wall or shock
p	pressure, Eq (5)
Pr	Prandtl number
q_i	heat flux, Eq (8)
Q	internal partition function
R	universal gas constant
Re	Reynolds number
R_N	nose radius
p	tangent to wall or shock
S	specific entropy or shock configuration
t	time coordinate
T	temperature
u,v	velocity components
V_∞	free stream speed
x	mole fraction
x,y	space coordinates
X	flow quantity vector
β	parameter in stretching coordinate
ε	$e + \frac{1}{2}(u^2+v^2)$
δ	distance between shock and body along ξ-axis
γ	ratio of specific heats
ω	chemical rate of production
Π_{ij}	stress tensor, Eq (7)
ρ	density
τ_{ij}	defined in Eq (7)
μ	viscosity, Eq (17)
$\bar{\Omega}^{(\ell,m)}_{ik}$	collision cross section

NOMENCLATURE

ξ, η	space coordinates in orthogonal coordinate system

Subscripts

i, j	space dimensions
ℓ, m	ℓ-th, m-th species
∞	free stream
T	total condition
w	wall

Superscripts

$'$	quantities normalized by free stream conditions
—	flow variables in the transformed computational plane

1.0 INTRODUCTION

This document is the final report summarizing the work accomplished for Tasks G and K of project 3782. The primary purpose of these tasks was to study and to develop a program for analyzing the chemical nonequilibrium, viscous flowfield in the nose region of a shuttle orbiter. As discussed in Ref. 1 the full set of Navier-Stokes (N-S) equations is used and the chemical kinetic equations are coupled to the N-S equations to achieve a higher accuracy in the flowfield analysis.

1.1 Objectives of the Study

There are three particular areas which were pursued in the course of this study in order to establish an efficient and accurate calculation scheme. The first area of interest was to formulate the governing equations in an unsteady conservative form using generalized curvilinear coordinates. The conservative form of equations possesses not only mathematical simplicity, but the capability to determine the imbedded shocks in the flow. This feature is needed to compute the flowfield at high altitudes where the shock is no longer a thin layer. The equations being written in curvilinear coordinates also faciliates the flowfield computation for several particular coordinate systems that can be chosen to define a starting line for subsequent supersonic flow calculation downstream of the nose.

The second area of concern was to develop a self-contained procedure for the calculations of thermodynamic and transport properties of the air mixture. Existing procedures are either limited to a certain range of temperatures and/or

involve approximations which have not been justified in the calculation of transport properties. This study therefore uses a more satisfactory procedure that is at least as accurate as the flow model itself.

The last area of interest was to calculate the blunt body flow at several representative flight conditions to cover the entire flight trajectory. A wide spectrum of flow characteristics exist in the descent trajectory; namely, the classical boundary layer regime at low altitude, the nonequilibrium shock and boundary layer interactive region in the middle portion of the trajectory, and the rarefied flow environment at high altitude. Since the present analysis is intended to provide the complete flow solution around the orbiter nose, therefore, the flow field solutions are obtained within the scope of a continuum flow model.

1.2 Numerical Analyses for Viscous Reacting Flowfields

Because of past interest in the reentry technology and the associated experimental study of reacting gas flows, numerous analyses are available for analyzing the reacting viscous flow around a blunt body. Solutions have been obtained for both high and low Reynolds number limits because the departure from chemical equilibrium can significantly effect the flow observables and the skin heat transfer coefficient over a broad range of altitudes and speeds. The three most popular numerical methods developed in the last decade are the finite-difference method,[2-9] difference-differential method,[10], and the method of integral relations [11-13]. These methods have been used quite extensively in the investigation of non-reacting viscous problem including the boundary-layer and the thin shock layer, and considerable successes have been obtained. However, in dealing with the reacting flow problem where the chemical nonequilibrium processes couple directly with the fluid-dynamic equations these methods are not as successful. The basic difficulty lies in the fact that certain assumptions of the flow must be met, or some input data must be given in order to carry out the flowfield analysis. For boundary-layer analyses the edge condtions for all dependent variables should be specified before one can use any of the three methods. The boundary layer edge location can not be simply defined by the inviscid nonequilibrium calculation as it can for the non-reacting case, since the swallowing of inviscid flow has to be considered [2,3]. To obtain an accurate result from the nonequilibrium boundary layer analysis, several iterations are required between the outer inviscid flow calculation and the boundary layer calculation. Thus, the

modeling of flow field by an outer inviscid layer and an inner boundary layer, using the three highly developed numerical methods becomes less attractive.

The current analyses of the thin viscous shock layers are not as sophisticated as that of the boundary layer. Many analyses only provide solutions along the stagnation stream line, [4,7,9], and some analyses which yield solutions for the shock layer were developed using many simplifying assumptions for defining the transport properties, and gas models [6-9,12,13]. In addition to the basic assumption that the thickness of the shock layer is very thin compared to the nose radius, the shock wave itself has to be treated as a mathematical discontinuity. At high altitude this assumption gradually becomes less justified. Velocity slip is then introduced to the usual Rankine-Hugoniot relations with the hope that the downstream flow properties can be determined with acceptable accuracy. This scheme, known as the "two-layer" model in the literature [6], has provided valuable results up to the point where the shock wave and the boundary layer merges with each other and as long as there is no departure of chemical equilibrium in the flow. However, it appears that the chemical nonequilibrium processes would incur a certain amount of ambiguity in the shock wave calculations, as has been demonstrated in the various nonequilibrium shock layer analysis published.

On the basis of this proceeding discussion, we have come to the understanding that the finite-difference method and the method of integral relations have been developed mainly for the boundary-layer type equations. The necessary conditions for such analyses to be valid are that the thick-

ness of the boundary layer or shock layer must be thin compared to the nose radius and that boundary conditions be specified on the edge of the layer. These requirements reduce the applications of these methods to a rather small portion on the entire orbiter trajectory. Therefore, a satisfactory theory that can analyze the flow field for the flight altitudes between 200 and 300K FT, where the orbiter will experience significant aerodynamic heating, is still in demand.

The time-marching finite-difference method used in the present study has received considerable attention in recent years. It appeals to the flow field analyst mainly because the exact governing equations can be used, and the accuracy of the solution is dependent on the mesh size only. The essential concept of this method is to simulate the flow field development from a given set of initial conditions until the flow settles down to its steady state. Although the steady solution is what one seeks, the introduction of the unsteady term in the equations is necessary from the mathematical point of view, because it changes the parabolic or the elliptical type of equation into a hyperbolic type for which a powerful numerical method is available. This method has been used by many investigators to solve inviscid flow problem of practical interest, including cases of high angle of attack, finite-rate chemical reaction and radiative heat transfer. But there exist few practical applications for the viscous flow problem. Most of the applications have been two-dimensional problems with a simple gas model,[14] presumably due to the requirement of long computer time and the fact that the previous viscous, nonequilibrium flow analyses are quite adequate for designing many re-entry vehicles.

The presently, more strigent, design of a reusable orbiter requires more exact flow field analyses, that can only be achieved by means of the time-marching finite-difference method.

A partial list of recent publications on the subject of viscous flow problems and their approximate range of validity is given in Table 1. It is not intended to comprise a complete bibliography of significant research in this area, but to indicate the state-of-art of the viscous flow analyses under these groups; namely, the reacting multicomponent and binary mixtures, and the non-reacting gas. It is seen that although the previous analyses can be used to cover a wide range of flight conditions, such a complete solution can only be obtained for the stagnation region.

A comparison of the afore-discussed numerical methods can be made on the basis of their applications to the multicomponent nonequilibrium blunt body flow problem. The flow characteristics of interest are the shock location, and the properties inside the shock layer and along the body downstream of the stagnation point. The calculation of the stagnation flow is not included in this comparison. It is seen in Table 2 that the analysis based on the time-marching method may represent a unified numerical approach and provide more satisfactory results because of the coupling of chemical kinetic equations and the Navier-Stokes equations, and the use of the rigorous theory on the transport properties. The ease of application and the cost of computer time are also listed in approximate terms, to aid one in making an evaluation of the three methods.

2.0 GOVERNING EQUATIONS AND BOUNDARY CONDITIONS

2.1 Assumptions and Governing Equations

The present flow field analysis is based on the following major assumptions:

1) Navier-Stokes model and non-slip velocity and no-jump temperature on the wall;
2) negligible radiation transfer;
3) flow in both vibrational and rotational equilibria;
4) gas consists of a mixture of perfect gases;
5) heat flux and mass diffusion flux are approximated by the Fourier and Fick laws, respectively;
6) transport coefficients are derived for a multi-component mixture;
7) negligible bulk viscosity.

The preceeding assumptions except the first were used in part or wholly by previous analyses dealing with a thin viscous shock layer or a boundary layer. They define a reasonably realistic model for the flow of interest, and allow the solution of the model to be manageable.

$$\frac{\partial \rho}{\partial t} + \frac{\partial}{\partial x_j} \rho u_j = 0 \tag{1}$$

$$\frac{\partial}{\partial t} \rho u_i + \frac{\partial}{\partial x_j} (\rho u_j u_i + \Pi_{ji}) = 0 \tag{2}$$

$$\frac{\partial}{\partial t} \rho(e+\frac{1}{2} u_j u_j) + \frac{\partial}{\partial x_j} \left[\rho u_j (e+\frac{1}{2} u_j u_j) + \Pi_{ji} u_i + q_j\right] = 0 \tag{3}$$

$$\frac{\partial}{\partial t} \rho c_l + \frac{\partial}{\partial x_j} (\rho u_j c_l + I_{l_j}) = \rho \omega_l \tag{4}$$

$$p = R\rho T \sum_l \frac{c_l}{M_l} \tag{5}$$

$$e = \sum_l c_l e_l \tag{6}$$

where ω_l is the net rate of production of species l as a result of chemical reaction, e_l is the specific internal energy and is defined as $e_l = \int c_{v_l} dT$. The stress tensor is defined as

$$\Pi_{ij} = p\delta_{ij} - \tau_{ij} \tag{7}$$

$$= p\delta_{ij} - \mu e_{ij} + \frac{1}{3} \mu e_{jj} \delta_{ij}, \quad \delta_{ij} = 1, \ i=j \quad = 0, \ i \neq j$$

where

$$e_{ij} = \frac{\partial u_i}{\partial x_j} + \frac{\partial u_j}{\partial x_i}$$

The heat flux vector is defined as

$$q_i = -k \frac{\partial T}{\partial x_i} + \sum_l h_l I_{l_i} \tag{8}$$

where

$$h_l = e_l + \frac{p}{c_l \rho}$$

The mass diffusion vector for species 1 is defined as

$$I_{l_i} = \rho c_l \bar{V}_{l_i} = -\frac{M_l}{M_w}\sum_m \rho D_{lm} \frac{\partial c_m}{\partial x_i} \tag{9}$$

Seven unknown scalers and vectors appear in Eqn (1-6), i.e., ρ, u_i, ρ, e, c_l, p and T. All unknowns except T can be determined explicitly from the set of equations. T must be calculated iteratively using Eq (6). Since a mixture of reacting pure gases is considered here, e_l is treated as a function of temperature. A polynominal function of T is given for e_l in Section 3.1.

In Eqn (7-9), transport coefficients μ,k and D_{lm} are determined from T, p, M_l, C_l, and $\bar{\Omega}_{(l,m)}$. The method of calculation of transport coefficients is discussed in section 3.2.

2.2 Orthogonal Coordinate System

Governing equations of Eqn (1-4) can be recast in the generalized orthogonal coordinates. Making use of the relations shown in Ref. 15 for a set of non-conservative form of equation, Eqn (1-4) become

$$\frac{\partial U}{\partial t} + \frac{\partial F}{\partial \xi} + \frac{\partial G}{\partial \eta} + H = 0 \tag{10}$$

where U, F, G and H are the column vectors that have the following expressions:

$$U = h_1 h_2 h_3 (\rho, \rho u, \rho v, \rho \varepsilon, \rho c_l).$$

$$F = h_2h_3(\rho u, \rho u^2+\Pi_{\xi\xi}, \rho uv+\Pi_{\xi\eta}, (\rho\varepsilon+\Pi_{\xi\xi})u+\Pi_{\xi\eta}v+q_\xi, \rho uc_1+I_{1_\xi})$$

$$G = h_3h_1(\rho v, \rho vu+\Pi_{\eta\xi}, \rho v^2+\Pi_{\eta\eta}, (\rho\varepsilon+\Pi_{\eta\eta})v+\Pi_{\eta\xi}u+q_\eta, \rho vc_1+I_{1_\eta})$$

$$H = (0, h_3\frac{\partial h_1}{\partial\eta}(\rho uv+\Pi_{\xi\eta})-h_3\frac{\partial h_2}{\partial\xi}(\rho v^2+\Pi_{\eta\eta})-h_2\frac{\partial h_3}{\partial\xi}\Pi_{\zeta\zeta},$$
$$-h_3\frac{\partial h_2}{\partial\xi}(\rho vu+\Pi_{\eta\xi})-h_3\frac{\partial h_1}{\partial\eta}(\rho u^2+\Pi_{\xi\xi})-h_1\frac{\partial h_3}{\partial\eta}\Pi_{\zeta\zeta}, 0, h_1h_2h_3\rho\omega_1)$$

where $\varepsilon = e+\frac{1}{2}(u^2+v^2)$ is the specific total energy, ξ,η are the space coordinates. The stress and heat flux are defined by

$$\Pi_{\xi\xi} = p-\mu e_{\xi\xi}+\frac{1}{3}\mu(e_{\xi\xi}+e_{\eta\eta}+e_{\zeta\zeta})$$

$$\Pi_{\eta\eta} = p-\mu e_{\eta\eta}+\frac{1}{3}\mu(e_{\xi\xi}+e_{\eta\eta}+e_{\zeta\zeta})$$

$$\Pi_{\zeta\zeta} = p-\mu e_{\zeta\zeta}+\frac{1}{3}\mu(e_{\xi\xi}+e_{\eta\eta}+e_{\zeta\zeta})$$

$$\Pi_{\xi\eta} = -\mu e_{\xi\eta} = \Pi_{\eta\xi}\ ,\ e_{\xi\xi} = 2(\frac{1}{h_1}\frac{\partial u}{\partial\xi}+\frac{v}{h_1h_2}\frac{\partial h_1}{\partial\eta})\ ,$$

$$e_{\eta\eta} = 2(\frac{1}{h_2}\frac{\partial v}{\partial\eta}+\frac{u}{h_1h_2}\frac{\partial h_2}{\partial\xi})\ ,\ e_{\zeta\zeta} = 2(\frac{u}{h_1h_2}\frac{\partial h_3}{\partial\xi}+\frac{v}{h_2h_3}\frac{\partial h_3}{\partial\eta})$$

$$e_{\xi\eta} = \frac{h_2}{h_1}\frac{\partial}{\partial\xi}(\frac{u}{h_2})+\frac{h_1}{h_2}\frac{\partial}{\partial\eta}(\frac{v}{h_1}) = e_{\eta\xi}$$

$$q_\xi = -\frac{k}{h_1}\frac{\partial T}{\partial\xi}+\sum_1 h_1I_{1_\xi}$$

$$q_\eta = -\frac{k}{h_2}\frac{\partial T}{\partial\eta}+\sum_1 h_1I_{1_\eta}$$

$$I_{1_\xi} = \frac{-M_1}{M_w}\rho \sum_m D_{1m} \frac{\partial c_m}{h_1 \partial \xi} \quad , \quad I_{1_\eta} = -\frac{M_1}{M_w}\rho \sum_m D_{1m} \frac{\partial c_m}{h_2 \partial \eta}$$

Equation (10) reduces to a simpler form along the axis of symmetry for an axisymmetric flow.

$$\frac{\partial \bar{U}}{\partial t} + 2\frac{\partial \bar{F}}{\partial \xi} + \frac{\partial \bar{G}}{\partial \eta} + \bar{H} = 0 \tag{11}$$

where $\bar{U} = \frac{U}{h_3}$, $F = \frac{F}{h_3}$, $\bar{G} = \frac{G}{h_3}$ and

$$\bar{H} = \left(0, \frac{\partial h_1}{\partial \eta}(\rho uv + \Pi_{\xi\eta}) - \frac{\partial h_2}{\partial \xi}(\rho v^2 + \Pi_{\eta\eta}) \right.,$$
$$-\frac{\partial h_2}{\partial \xi}(\rho uv + \Pi_{\eta\xi}) - \frac{\partial h_1}{\partial \eta}(\rho u^2 + \Pi_{\xi\xi}),$$
$$\left. -\frac{1}{\frac{\partial h_3}{\partial \xi}} \frac{\partial^2 h_3}{\partial \xi \partial \zeta} \Pi_{\zeta\zeta} \quad , \quad 0 \quad , -h_1 h_2 \rho \omega_1 \right)$$

The singularity has been elminated from Eqn (11) since h_3 no longer appears in the column vectors.

The space coordinates and the metric coefficients for three different versions of coordinate systems in the generalized orthogonal coordinate system are given in Table 3 and illustrated in Figure 1.

2.3 Transformation to Computational Planes

Conventional parameters such as the Reynolds number, the Prandtl number, and the Lewis number can be introduced in Eqn (10) by the following normalization procedure. Let

$$p' = \frac{p}{p^\infty} \ , \ \rho' = \frac{\rho}{\rho^\infty} \ , \ T = \frac{T'}{T^\infty} \ , \ e' = \frac{e}{(p^\infty/\rho^\infty)}, \ u' = u/(p_\infty/\rho_\infty)$$

be the nondimensional dependent variables, and $\xi' = \xi/R_N$,

$t' = t/(\sqrt{p_\infty/\rho_\infty}/R_N)$ be the nondimensional independent variables. Substituting these quantities into Eqn (10), one obtains the dimensionless governing equations which have the same form as Eqn (10) except for the parameters appearing with the stress tensor, heat flux and mass diffusion vectors.

$$\tau'_{\xi\xi} = \frac{\sqrt{\gamma_\infty} M_\infty}{Re} \tau_{\xi\xi} \text{ , etc.}$$

$$q'_{\xi'} = -\frac{\sqrt{\gamma_\infty} M_\infty \gamma}{(\gamma-1) PrRe} \frac{\partial T'}{\partial \xi'} + \frac{\sqrt{\gamma_\infty} M_\infty}{PrRe} \sum_1 I'_{1\eta} \; h'_1 \text{ , etc.}$$

$$I'_{1\xi'} = -\frac{\sqrt{\gamma_\infty} M_\infty}{PrRe} \sum_m Le_{1m} \frac{\partial c_m}{\partial \xi'} \text{ , etc.}$$

where $Re = \frac{\rho_\infty V_\infty R_N}{\mu}$, $Pr = \frac{c_p \mu}{k}$, and $Le_{1m} = \frac{\rho D_{1m} C_p}{k}$

The governing equations are then transformed to a computational coordinate system, on which both the shock (or the outer surface) and the body are made boundary mesh lines of the computational region. Let $y = \xi$, $z = 1-\frac{\eta-B}{\delta}$, where $\delta=S-B$; the distance between the shock and body, or between the outer surface and the body (see figure 1). The transformed equation becomes

$$\frac{\partial \delta U}{\partial t} + \frac{\partial \delta F}{\partial y} + \frac{\partial}{\partial z} ((1-z)(\delta_t U + \delta_y F) - G) + \delta H = 0 \qquad (12)$$

at every point except the axis of symmetry, on which the following form is used:

$$\frac{\partial \delta \bar{U}}{\partial t} + 2\frac{\partial \delta \bar{F}}{\partial y} + \frac{\partial}{\partial z} ((1-z)(\delta_t U + \delta_y \bar{F}) - \bar{G}) + \delta \bar{H} = 0 \qquad (13)$$

The stress tensor, heat flux and mass diffusion vectors in the computational coordinates are:

$$\frac{1}{2} e_{yy} = \frac{1}{h_1} \left(\frac{\partial u}{\partial y} + (1-z) \frac{\delta_y}{\delta} \frac{\partial u}{\partial z} \right) + \frac{v}{h_1 h_2} \left(-\frac{1}{\delta} \frac{\partial h_1}{\partial z} \right)$$

$$\frac{1}{2} e_{yz} = \frac{h_2}{h_1} \left(\frac{\partial}{\partial y} \left(\frac{v}{h_2} \right) + (1-z) \frac{\partial_y}{\delta} \frac{\partial}{\partial z} \left(\frac{v}{h_2} \right) \right)$$

$$+ \frac{h_1}{h_2} \left(-\frac{1}{\delta} \frac{\partial}{\partial z} \left(\frac{u}{h_1} \right) \right) = \frac{1}{2} e_{zy}$$

$$\frac{1}{2} e_{\zeta\zeta} = \frac{1}{h_2} \left(-\frac{1}{\delta} \frac{\partial v}{\partial z} \right) + \frac{u}{h_1 h_2} \left(\frac{\partial h_2}{\partial y} + (1-z) \frac{\delta_y}{\delta} \frac{\partial h_2}{\partial z} \right)$$

$$q_y = -\frac{1}{h_1} \left(\frac{\partial T}{\partial y} + (1-z) \frac{\delta_y}{\delta} \frac{\partial T}{\partial z} \right) + \sum_1 h_1 I_{1_y}$$

$$q_z = -\frac{1}{h_2} \left(-\frac{1}{\delta} \frac{\partial T}{\partial z} \right) + \sum_1 h_1 I_{1_z}$$

$$I_{1_y} = -\rho \frac{M_1}{M_W} \sum_m D_{1m} \left(-\frac{1}{\delta} \frac{\partial c_m}{\partial z} \right) ,$$

$$I_{1_z} = -\rho \frac{M_1}{M_W} \sum_m D_{1m} \left(\frac{\partial c_m}{\partial y} + (1-z) \frac{\delta_y}{\delta} \frac{\partial c_m}{\partial z} \right)$$

The conversion from the generalized orthogonal coordinate system to its special versions; namely, the body intrinsic, polar and cylindrical coordinate systems can be easily made with the use of Table 4.

The computational region is further mapped to another plane to allow higher space resolution near the body. This transformation of coordinates is desirable for an accurate calculation of momentum and energy transfer from the flow to the body. Let $\bar{y}$ and $\bar{z}$ be the coordinates of the second computational plane, and $\bar{z} = (1-\exp(\beta z))/(1-\exp(\beta))$ $\bar{y} = y$. The relations have been shown to be valuable in Ref. 14. Making use of $\frac{\partial}{\partial z} = \frac{-\beta\exp(\beta z)}{1-\exp(\beta)} \frac{\partial}{\partial \bar{z}}$ and $\frac{\partial}{\partial y} = \frac{\partial}{\partial \bar{y}}$, one can obtain the governing equations cast in the new computational plane as follows:

$$\frac{\partial U}{\partial t} + \frac{\partial F}{\partial \bar{y}} + \frac{\partial G}{\partial \bar{z}} + H = 0 \qquad (14)$$

for every where in the computational region except on the axis of symmetry; and

$$\frac{\partial \bar{U}}{\partial t} + 2\frac{\partial \bar{F}}{\partial \bar{y}} + \frac{\partial \bar{G}}{\partial \bar{z}} + \bar{H} = 0 \qquad (15)$$

for the axis of symmetry.

The variables U, F, G, *and* H and variables with overline are defined by:

$$U = \delta U,\ F = \delta F,\ G = \frac{-\beta\exp(\beta z)}{1-\exp(\beta)}((1-z)(\delta_t+\delta_y F)-G),$$

$$H = \delta H - \beta((1-z)(\delta_t+\delta_y F)-G)$$

$$\bar{U} = U/h_3,\ \bar{F} = F/h_3,\ \bar{G} = G/h_3,\ \bar{H} = \delta\bar{H} - \beta((1-z)(\delta_t+\delta_y \bar{F})-\bar{G})$$

A detailed expression of Eqns (14) and (15) can be worked out by substituting U, F, G, H, $\bar{U}$, $\bar{F}$, $\bar{G}$, $\bar{H}$ into Eqns (12) and (13).

2.4 Boundary Conditions

The velocity non-slip and temperature no-jump conditions are used in this analysis as the wall conditions.

$$u = 0 = v$$

$$T = T_w \qquad \text{for an isothermal wall}$$

$$\frac{\partial T}{\partial n} = 0 \qquad \text{for an adiabatic wall}$$

Where e_w and T_w are related by $e_w = c_v T_w$ for a highly cooled wall.

The wall catalycity is only considered in two limiting forms, i.e.;

$$c_1 = c_1(T_w) \qquad \text{for a fully catalytic wall}$$

$$\frac{\partial c_1}{\partial n} = 0 \qquad \text{for a non-catalytic wall}$$

The boundary conditions on the outer surface of the computational region are the free stream conditions when the shock is to be computed inside the region. If the shock is used as the outer surface then the Rankine-Hugoniot relations are employed to determine the flow variables immediately behind the shock. The assumption of frozen composition of species across the shock is also utilized.

3.0 THERMODYNAMIC AND TRANSPORT PROPERTIES AND CHEMICAL KINETICS

3.1 Method of Calculation of Thermodynamic Properties of Perfect Gases

Numerous methods are presently available for the calculation of the thermodynamic properties of species of perfect gases. The program of Reference 16, which was written at the NASA Lewis Research Center, was used as a matter of convenience. The difference between the method used in Ref. 16 and others include one or more of the following: different forms for the partition function, different spectroscopic data, inclusion of excited-state data, and different heats of formation. The major aspects involved in the calculation of thermodynamic properties of the air species will be briefly included here, in order to present the analysis in a self-contained manner. More complete details can be found in Ref. 16.

Equations for evaluating thermodynamic functions from the partition function and its first and second derivatives are

$$\frac{c_p}{R} = \frac{T^2}{Q}\frac{d^2Q}{dT^2} - \left(\frac{T}{Q}\frac{dQ}{dT}\right)^2 + \frac{2T}{Q}\frac{dQ}{dT} + \frac{5}{2}$$

$$\frac{H_T - H_0}{RT} = \frac{T}{Q}\frac{dQ}{dT} + \frac{5}{2}$$

$$-\frac{F_T - H_0}{RT} = \ln Q + \frac{3}{2}\ln M + \frac{5}{2}\ln T - 3.66511$$

The internal partition function Q contains vibrational, rotational, and electronic contributions. The last term

in each of the equations is the translational contribution.

The partition function for monatomic gases is given by

$$Q = \sum_{m=1}^{L} g_m \exp\ (-E_m/KT)$$

where g_m and E_m are the statistical weight and electronic energy of the m^{th} state, respectively. The way to terminate the number of energy levels L is to include all energy levels that are less than or equal to the ionization potential lowered by an amount KT. This cutoff method is temperature dependent and is used in this study.

For diatomic gases, Q involves vibrational and rotational as well as electronic energy.

$$Q = Q_e^m\ Q_v^m\ Q_R^m\ Q_{corr}$$

The quantities Q_e^m, Q_v^m, Q_R^m are the electronic, harmonic oscillator, and classical rotation contributions to the partition function, respectively. The remaining term is the correction term given by the modified Pennington and Kobe method (Ref. 29 in Ref. 16).

After calculating the thermodynamic data for the species, a least-square technique is used to fit these data into polynomials. The input spectroscopic data and the resultant coefficients of the empirical equations for thermodynamics functions are given in Appendix I. The following shows the thermodynamic functions in terms of the coefficients:

$$C_p/R = A_1 + A_2T + A_3T^2 + A_4T^3 + A_5T^4$$

$$H/RT = A_1 + \frac{A_2}{2}T + \frac{A_3}{3}T^2 + \frac{A_4}{4}T^3 + \frac{A_5}{5}T^4 + \frac{A_6}{T} \qquad (16)$$

$$F/RT = A_1(1-\ln T) - \frac{A_2}{2}T - \frac{A_3}{6}T^2 - \frac{A_4}{12}T^3 - \frac{A_5}{20}T^4 + \frac{A_6}{T} - A_7$$

3.2 Method of Calculations of Transport Property of a Mixture

The Chapman-Enskog theory, as extended to a multi-component mixture by Herschfelder, etc.,[17], is used to calculate the transport coefficients.

The first approximation to the coefficient of viscosity, for a mixture of gases, is given as

$$\mu = -\frac{\begin{vmatrix} F_{11} & F_{12} & F_{13} & \cdots & F_{1n} & x_1 \\ F_{12} & F_{22} & F_{23} & \cdots & F_{2n} & x_2 \\ F_{13} & F_{23} & F_{33} & \cdots & F_{3n} & x_3 \\ \vdots & \vdots & \vdots & & & \vdots \\ F_{1n} & F_{2n} & F_{3n} & \cdots & F_{nn} & x_n \\ x_1 & x_2 & x_3 & \cdots & x_n & 0 \end{vmatrix}}{\begin{vmatrix} F_{11} & F_{12} & F_{13} & \cdots & F_{1n} \\ F_{12} & F_{22} & F_{23} & \cdots & F_{2n} \\ F_{13} & F_{23} & F_{33} & \cdots & F_{3n} \\ \vdots & \vdots & \vdots & & \vdots \\ F_{1n} & F_{2n} & F_{3n} & \cdots & F_{nn} \end{vmatrix}} \qquad (17)$$

where the principal diagonal elements are given by

$$F_{ii} = \frac{x_i^2}{\eta_{ii}} + \sum_{\substack{k=1 \\ k\neq i}}^{n} \left(\frac{2x_i x_k}{\eta_{ik}}\right) \frac{M_i M_k}{(M_i + M_k)^2} \left(\frac{5}{3A^*_{ik}} + \frac{M_k}{M_i}\right)$$

and the off-diagonal elements by

$$F_{ij} = F_{ji} = -\left(\frac{2x_i x_j}{\eta_{ij}}\right) \frac{M_i M_j}{(M_i + M_j)^2} \left(\frac{5}{3A^*_{ij}} - 1\right), i \neq j$$

The quantity η_{ik} in above equations is given by

$$\eta_{ik} \times 10^6 = \frac{26.693 \sqrt{\frac{2M_i M_k T}{(M_i + M_k)}}}{\bar{\Omega}_{ik}(2,2)}$$

The quantity η_{ii} represents the viscosity coefficient for molecule i and may be obtained by letting k=i in the same equation.

The first approximation to the coefficient of thermal conductivity of a mixture of reacting gases contains two terms

$$k = k_{monatomic} + k_{internal}$$

An expression for $k_{monatomic}$ is given as

$$k_{monatomic} = 4 \frac{\begin{vmatrix} L_{11} & L_{12} & L_{13} & \cdots & L_{1n} & x_1 \\ L_{21} & L_{22} & L_{23} & \cdots & L_{2n} & x_2 \\ L_{31} & L_{32} & L_{33} & \cdots & L_{3n} & x_3 \\ \vdots & \vdots & \vdots & & \vdots & \vdots \\ L_{n1} & L_{n2} & L_{n3} & \cdots & L_{nn} & x_n \\ x_1 & x_2 & x_3 & \cdots & x_n & 0 \end{vmatrix}}{\begin{vmatrix} L_{11} & L_{12} & L_{13} & \cdots & L_{1n} \\ L_{21} & L_{22} & L_{23} & \cdots & L_{2n} \\ L_{31} & L_{32} & L_{33} & \cdots & L_{3n} \\ \vdots & \vdots & \vdots & & \vdots \\ L_{n1} & L_{n2} & L_{n3} & & L_{nn} \end{vmatrix}} \qquad (18)$$

where the principal diagonal elements are given by

$$L_{ii} = \frac{-16x_i^2 M_i}{15R\eta_{ii}} - \sum_{\substack{k=1 \\ k\neq i}}^{n} \frac{16x_i x_k \left(\frac{15}{2}M_i^2 + \frac{25}{4}M_k^2 - 3M_k^2 B_{ik}^* + 4M_i M_k A_{ik}^*\right) M_i M_k}{15R(M_i + M_k)^3 A_{ik}^* \eta_{ik}}$$

and the off-diagonal elements by

$$L_{ij} = L_{ji} = \frac{16x_i x_j M_i^2 M_j^2}{15R(M_i + M_j)^3 A_{ij}^* \eta_{ij}} \left(\frac{55}{4} - 3B_{ij}^* - 4A_{ij}^*\right) \quad i \neq j$$

An expression for $k_{internal}$ is given as

$$k_{mixture\ internal} = \sum_{i=1}^{n} \frac{\frac{6}{5} A^*_{ii} \left(c_{p_i} - \frac{5}{2} \frac{R}{M_i} \eta_{ii} \right)}{1 + \left[\frac{A^*_{ii}}{A^*_{ij}} \left(\frac{2M_j}{M_i + M_j} \right) \frac{\eta_{ii}}{\eta_{ij}} \frac{x_j}{x_i} \right]} \quad (19)$$

Finally, the first approximation to the coefficient of binary diffusion is given as

$$D_{ij} = \frac{3}{5} \frac{(M_i + M_j)}{M_i M_j} \frac{RT}{P} A^*_{ij} \eta_{ij} \quad (20)$$

The multicomponent diffusion coefficients are calculated by the following formula

$$D_{ij} = \frac{1}{M_j} M_w \frac{K^{ji} - K^{ii}}{|K|} \quad (21)$$

where $K_{ii} = 0$

$$K_{ij} = \frac{x_i}{D_{ij}} + \frac{M_j}{M_i} \sum_{k \neq i} \frac{x_k}{D_{ik}} \ ;$$

$|K|$ is the determinant of the K_{ij} and K^{ij} are the minors:

$$K^{ji} = (-1)^{i+j} \begin{vmatrix} 0 & \cdots & K_{1,i-1} & K_{1,i+1} & \cdots & K_{1,n} \\ \vdots & & \vdots & \vdots & & \vdots \\ K_{j-1,1} & \cdots & K_{j-1,i-1} & K_{j-1,i+1} & \cdots & K_{j-1,n} \\ K_{j+1,1} & \cdots & K_{j+1,i-1,} & K_{j+1,i+1} & \cdots & K_{j+1,n} \\ \vdots & & \vdots & \vdots & & \vdots \\ K_{n,1} & \cdots & K_{n,i-1} & K_{n,i+1} & \cdots & K_{n,n} \end{vmatrix}$$

Note that all the transport coefficients are expressed in terms of the quantity η_{ij} to facilitate computer calculations. Simple derivations and references based on which these formulae are obtained are shown in Reference (17).

The calculation procedure for solving μ and k monatomic is essentially the same one used in Reference 18 in which the equations (17) and (18) are written as a set of simultaneous linear algebraic equations and the Gauss-Jordan reduction scheme is used. In situations where the mole fraction of some species is zero, such as in the frozen flow, problems occur in solving the algebraic equations. In this case, the mole fraction is set to 10^{-8} in order to avoid the round-off errors in the calculation and to prevent more than negligible contributions to the results.

The binary collision cross sections and their ratios are needed in the calculation of transport properties,

$$A^*_{ik} = \bar{\Omega}^{(2,2)}_{ik} / \bar{\Omega}^{(1,1)}_{ik}$$

$$B^*_{ik} = (5\bar{\Omega}^{(1,2)}_{ik} - 4\bar{\Omega}^{(1,3)}_{ik}) / \bar{\Omega}^{(1,1)}_{ik}$$

There are 25 possible binary interactions for dissociating air having five species for which the data of cross section $\bar{\Omega}^{(\ell,m)}_{ik}$ are generally available up to 10000°K. Extrapolation is used whenever the temperature is outside of the given range. In case the binary cross section is not available, a simple combination rule is used; i.e.

$$A_{ik} = (A_{ii} + A_{kk})/2$$

$$B_{ik} = (B_{ii} + B_{kk})/2$$

When the cross section is unknown for two like neutral species, the rigid sphere cross section is used. Since the data are scarce for changed species, their contribution to the transport properties are not accounted for, consequently the calculation of transport properties as described in this section is only satisfactory when the ionization is not significant. The data of cross sections used in this study are summarized in Appendix II.

3.3 Chemical Reactions

The calculation of the net rate of production ω_1 for species 1 can be carried out in a number of ways because of the number of the relations governing the chemical

reaction rate is more than the number of species. The redundancy of the chemical system is caused by two extra relations for the conservation of atoms or nuclei of the molecular species and the conservation of charge for ionized species in addition to the chemical reactions. The usual approach is to obtain the ω_1 of the molecular and the ionized species from the chemical reactions, and the ω_1 of the atomic species and electrons from the conservation relations. In dealing with a complicated chemical system involving a large number of species, however, it is found in Ref. 19 that the calculation of ω_1 simply from the chemical reactions alone is more expedient. Since the conservation of atoms and charge is satisfied with a chosen set of chemical reactions, the unique solutions of ω_1 is obtained.

In the present analysis six different types of reactions can be considered. They are listed as follows:

I	$A+B \rightleftharpoons C+D$
II	$A+B+(M) \rightleftharpoons C+(M)$
III	$A+B \rightleftharpoons C+D+E$
IV	$A+B \rightleftharpoons C$
V	$A+(M) \rightleftharpoons B+C+(M)$
VI	$A+B+C \rightleftharpoons D+E$

A,B,C,D and E refer to the reacting species and M denotes the third body. The production and dimunition rate of species involved in the reactions are respectively $(\omega_1)_f$ and $(\omega_1)_b$.

	$(\omega_1)_f$	$(\omega_1)_b$
I.	$k_f\rho^2[A][B]$	$k_b\rho^2[C][D]$
II.	$k_f\rho^3[A][B]/M_w$	$k_b\rho^2[C]/M_w/RT$
III.	$k_f\rho^2[A][B]$	$k_b\rho^3[C][D][E]RT$
IV.	$k_f\rho^2[A][B]$	$k_b\rho[C]/RT$
V.	$k_f\rho^2[A]/M_w$	$k_b\rho^3[B][C]RT/M_w$
VI.	$k_b\rho^3[A][B][C]RT$	$k_f\rho^2[D][E]$

where $k_b = k_f/K_c$, K_c is the equilibrium constant.

$$k_f = A\, T^{\eta}\exp(-\varepsilon/T) \quad , \quad \left[\frac{cm^3}{mole\ sec}\right]$$

the coefficients A, η, and ε are given Appendix III, where k_f is usually given in literature in the cgs-Kelvin unit. In the formulas for calculations of $(\omega_1)_f$ and $(\omega_1)_b$ [ ] indicates the mass concentration per mole of the species and R = 82.07835 atm-cm^3/°K/mole. The net rate of production is obtained by the following relation to reduce the round-off error

$$\omega_1 = \left(\sum_{r=1}^{N} (\omega_1)_{f,r} - \sum_{r=1}^{N} (\omega_1)_{b,r}\right) \frac{M_1}{\rho} \qquad (22)$$

where r refers to the number of chemical reactions.

4.0 TIME-MARCHING FINITE-DIFFERENCE METHOD

4.1 Predictor-Corrector Technique

Among several versions of the Lax-Wendroff second-order difference scheme for solving an initial-value problem, the predictor-corrector technique proposed by MacCormack[20] is probably the most widely used. This technique not only yields better accuracy, but is easier to use than other versions, especially for mesh points located on the computational boundaries. The essence of this technique can be described as follows:

$$x_{n,m}^{k+1} = x_{n,m}^{k} + \left(\frac{\partial x}{\partial t}\right)_{n,m}^{k} \Delta t \tag{23a}$$

$$x_{n,m}^{k+1} = \frac{1}{2}\left(x_{n,m}^{k} + x_{n,m}^{k+1} + \left(\frac{\partial x}{\partial t}\right)_{n,m}^{k+1} \Delta t\right) \tag{23b}$$

where x is the unknown vector to be solved, and $\left(\frac{\partial x}{\partial t}\right)$ is given by Eqn (14) and (15). To achieve the formal second-order accuracy in both space and time, $\left(\frac{\partial x}{\partial t}\right)^{k}$ and $\left(\frac{\partial x}{\partial t}\right)^{k+1}$ are computed using one-side difference quotients to replace the space derivatives, and alternations between the backward and the forward formulas are to be made in Eqn (23a) and (23b) for spatial derivatives. On the boundaries of the computational region, i.e., body and shock or outer surface due to the lack of mesh points outside of the region, alternations of the difference quotient can not be applied. However, physical boundary conditions are available for these boundaries and are taken into account in a two-step fashion consistent to the calculations inside the region. Note, the one-side difference formulas are only applied to the space derivatives

of convection terms with respect to x. However, for the stress tensor and the heat flux and mass diffusion vectors, centered-difference formulas are used.

It has been recognized that all numerical schemes introduce a certain amount of numerical dissipation and dispersion to the equations being solved and care must be taken to distinguish between the numerical and physical dampings[21]. For example, a first-order scheme could be used for wake flow studies if the flow Reynolds number is so low as to dominate the flow characteristics. On the other hand, for a high Reynolds number blunt body flow, a second-order scheme may not be sufficient to suppress the contribution from the numerical dissipation. Theoretically, one can always apply a fourth or higher-order scheme to the blunt body flow problem but the higher-order scheme involves tedious arithmetic computations and has not been developed to a stage for practical use. Therefore, the only immediate remedy for the user is to use very small mesh spacing.

4.2 Numerical Relaxations

Because of the complexities of the governing equations (14) and (15), it is advantageous to view the time-marching method not as a means to solve the mathematical initial-value problem, but rather as a relaxation method similar to the one which solves the elliptic equations of a boundary-value problem. The time-marching method yields the unique steady solution no matter what the initial conditions are as long as these conditions are compatible and reasonable to the physical problem. This point of view was first suggested by Crocco[22] and substantiated by later work on both inviscid and viscous problems. Interpretation of the time-marching method in this way is most suitable to the problem considered in this

study, since the transient solution of the problem is of no concern. Therefore, the Courant-Friedrich-Lewy (CFL) stability condition for a hyperbolic system of equations, which provides the largest possible time step size for all meshpoints in the computational region for the transient problems, will not be followed strictly. Rather it is proposed to march the solution in time on each mesh point according to its largest possible CFL step size, or to enforce the CFL condition by a local value and not by the global value.[23] This procedure is similar to the variable-time method of characteristics whereas the conventional procedure corresponds to the fixed-time method of characteristics.[24] If only the time-asymptotic solution is of interest, then the new procedure would reach its limit by a smaller number of time steps and the cost of computer time would be less than that of the conventional procedure.

There are additional freedoms available to the users in the consideration of time step sizes. If the CFL condition gives the relaxation time increment on the basis of the physical argument that the propagation of numerical signals should be larger than the flow velocity and the speed of sound across a mesh spacing, then there exists another relaxation time which is valid for chemically reacting flows. The reasoning is this: the time step size can not be larger than the chemical relaxation time across a mesh spacing in order to maintain the stability in the integration of the chemical kinetic equations. In the conventional procedure the smaller of the two time step sizes is to be used for the whole region. But in the new variable-time procedure both the CFL condition and chemical relaxation condition are applied locally to each mesh point and to different equations. Numerical

experiments using this relaxation procedure have been carried out for selective cases to be discussed in Section 4.5.

4.3 Sharp-Shock Formulation

The blunt-body flow field is characterized by the presence of gradients of flow properties upstream of the body. At high speed and low altitude the gradients are confined in a very thin-layer, and can treated mathematically as a discontinuity across which the Rankine-Hugoniot relations can be applied. Since there is no need to know the structure of the shock wave in the computation of the flow field downstream of the shock, the shock itself is treated as a boundary of the region of interest. The other boundaries consist of the axis of symmetry, the body, and a line located in the supersonic region connecting the shock and the body. The shock wave has been observed experimentally as a thin surface so it is assumed that the flow remains chemically frozen as it traverses the shock and the diffusion in the shock is negligible. In general, a correlation can be made between the flow Reynolds number and the existence of a sharp shock; namely for $Re/Rn \geq 10^5 - 10^4$ the assumption of a sharp shock is very good. Because of the high Reynolds number, the flow downstream of the shock is largely inviscid with the viscous effects located in a thin boundary layer adjacent to the body surface. The numerical procedure which relates the shock boundary conditions to the finite-difference solution are identical to the one developed for inviscid flow computations.[19]

The initial flow field conditions are based on stationary-shock results at one side of the computational region and

the assumed surface properties on the other. Flow properties between these two boundaries are obtained from a linear interpolation procedure. The shock location as well as the shock speed changes in the subsequent time steps. The shock speed, after the first one hundred steps computation, can be used to indicate the steadiness of the solution. When the ratio of the shock and the free stream speeds becomes less than one per cent, the solution can be regarded as the steady results.

To determine the shock speed on various points of the shock boundary, a locally intrinsic coordinate system is used, while the normal component of the shock speed is used in the Rankine-Hugoniot relations. Figure 3 gives the relations between the shock intrinsic coordinates and the three possible orthogonal coordinates. Details of the matching procedure are not different from the discussion in the aforementioned references.

4.4 Thick-Shock Formulation

It has been observed experimentally that the width of the gradients of flow properties upstream of a blunt body increases as the free stream Reynolds number decreases.[25] The mechanisms that cause the broadening of a shock wave are primarily due to the fact that the ambient air density is low and the physical dissipation effects become dominant in the flow field. The characteristics of the blunt body flow changes drastically as the altitude increases. The boundary layer begins to thicken while the shock may still be thin, then at higher altitudes the shock width increases and merges with the boundary layer. As the altitude further

increases there is no distinction between the shock and the boundary layer. Thus, the sharp-shock formulation fails to provide adequate analysis for flow field predictions.

The low-Reynolds number blunt body flow problem has been studied by many investigators. The continuum approach describing the flow field on the basis of the Navier-Stokes equations has provided surprisingly accurate results for Reynolds numbers as low as $Re_\infty/Rn = 1$.[26] For slightly higher Reynolds numbers, say $Re_\infty/Rn = 10^2$-10^3, the shock and boundary layer are not completely merged and the integration of equations through the shock as used in Ref. 26 and 27 can be replaced by the so-called "two-layer" model.[6] The computation of the flow field is made downstream from the inner-edge of the shock, and the dissipative Rankine-Hugoniot relations are used on that edge. Solution can be thus obtained in a manner similar to the sharp-shock formulation.[14] The drawbacks of this method of solution are: 1) it gives accurate information upstream of the body only for certain conditions and the inner-edge of the shock wave is not physically locatable;[27] 2) it does not clearly define the species concentrations on the inner-edge of the shock. Ambiguities are introduced to the calculation of species on the shock boundary as demonstrated by various investigators.[6-9]

The thick-shock formulation adopted in the present study is similar to the one for ideal or equilibrium-air-flow calculations shown in Ref. 26. The initial conditions are given within the computational region which has an outer-boundary located far upstream of the body where it is free of any disturbance from the body. The free stream properties are maintained on this outer-boundary independently of the time

steps. The flow properties inside the region are also free stream quantities initially and the body is instantaneously inserted into the free stream. Note, the use of the outer-boundary serves the same purpose as the shock boundary in the sharp-shock formulation. The finite-difference method is then used to advance the solution in time for mesh points inside the computational region, except for the outer-surface. The steadiness of the solution is indicated by the negligible changes of flow properties between two time steps.

4.5 Verification of the Calculation Procedure

The basic formulations and the method of solution discussed in previous sections have been coded in Fortran V for the UNIVAC 1108 system at NASA-MSC. Four versions of the program were developed in this study. They are the non-reacting viscous thin and thick shock codes, and the reacting viscous thin and thick shock codes. These versions can be made as options from a general viscous reacting blunt body program with some additional programming effort. Verification of the basic formulation has been concentrated on the non-reacting flows, because more reliable results are available for comparison purposes.

The concept of time-marching according to the local CFL step size was first demonstrated in a high Reynolds number flow calculation. The sharp-shock formulation was used because the steadiness of the solution can be easily judged from the magnitude of the shock speed. The free stream conditions for this case are shown in Figure 4. A spherical-cone is chosen as the body and the downstream outflow boundary of the computational region is defined by $\theta = 80°$. Flow

speeds across the outflow line are mostly supersonic. A large angle is used here to emphasize the difference between solutions which use different procedures of selecting time increment. Figure 4 shows the rate of convergence for two solutions; one proceeds according to the global CFL time increment, whereas the other proceeds according to the local CFL time increment. The range of shock speed is given by the difference between two curves. It is zero initially and should go to zero after many computational steps. With the local CFL increment the solution is very close to the steady solution after 250 steps. But the other solution indicates that more steps are needed before the steady solution is reached. Since the global CFL increment is determined most likely from the mesh points on the axis of symmetry, these time increments are several factors smaller than the CFL increment determined from mesh points on the downstream outflow boundary. The large difference in the magnitude of the CFL increments affects the numerical relaxation to the same degree. Another calculation not shown in this report indicates that with a smaller computational region, $\theta = 60°$, the improvement using the local CFL increment over the global CFL increment is not as great as shown in Figure 3. It is also found that the resulting steady solutions are in very close agreement. More investigations on the relaxation time increment will be published in a later report.

The second test case demonstrates the necessity of performing flow field computations on the second transformed computational plane for a high Reynolds number flow. The body is a hyperboloid of 10° asymptotic angle in the free stream conditions shown in Figure 5(a) and (b). Both skin friction and heat transfer coefficients were calculated by means of

the numerical techniques discussed in Section 2.2 and were summarized in Ref. 28. Figure 5 indicates that more than 100 mesh points in the first computational plane are needed across the shock layer, i.e., N=100, in order to predict the boundary layer accurately. If the second computational plane is used, and with the use of β=3 and N=45, better results can be obtained. The saving of computer cost is more than a factor of two because the difference in N used. However, it should be pointed out that in the second plane the mesh spacing between the shock boundary and the nearest mesh line is stretched to a higher degree than the squeezing of mesh spacing between the body and its nearest mesh line. The stretching of mesh spacing at the shock gives rise to difficulties in the marching procedure, and convergence of the solution may not be achieved if β is too large and N is too small.

It is also of interest to compare other flow properties obtained from the non-conservative and convervative-form of governing equations. The governing equations used in this work and in Ref. 14 represent the two forms of these equations. Figure 6 gives the density and temperature profiles on the axis of symmetry for the same free stream conditions. The temperatures are quite close, but the densities are very different. The density profile obtained from the non-conservative form of the equation is unreasonable, especially at the body. The fundamental difficulty can be traced back to the dependent variables used. Since p, u, v and s, where s is the specific entrophy were used in Ref. 14, the boundary condition of temperature could not be imposed directly upon the solution. Except for this discrepancy, other flow quantities are about the same.

The last verification case was made by solving the flow field structure around a sphere in a low Reynolds number flow. The free stream conditions are given in Figure 7 and the computational region is given in Figure 1. All the computations are carried out in the first computational plane, since sharp gradients of flow properties disappeared in this rarefied gas regime. The transient solution is given in Figure 7a. It is observed that at least 1000 time steps are required to reach the asymptotic steady solution. The overshoot shown in temperature profiles close to the body decreases with the increase in time steps. The cause of the overshoots is not clear although it is most probably from a numerical rather than a physical source. The density profile on the axis of symmetry agrees very well with experimental results [25]. Also shown in Figure 7b are the results of a Monte Carlo simulation technique [29]. They are not as good as the present results. More results for a cylinder flow can be found in Ref. 26,

5.0 NUMERICAL SOLUTIONS OF THE SHUTTLE CONDITIONS

A trajectory that corresponds to the long-range orbiter and the maximum heating load was used for the flow field computation discussed herein. Six representative points in the trajectory were selected for the purpose of investigating the characteristics of the flow field. The locations of the six points are given in the velocity-altitude diagram shown in Figure 8. Additional free stream conditions are listed in Table 5 for reference. The orbiter trajectory covers a wide range of flow regimes that can be categorized according to the free stream Reynolds number based on the nose radious of 2 ft. Points 0 and 1 are the two highest Reynolds numbers flow and are in what is usually called the boundary-layer regime. The shock can be treated as a thin discontinuity and be treated inviscidly. The viscous dissipation is confined in the boundary layer close to the nose surface. Points 4 and 5 have the smallest Reynolds' numbers and are in the rarefied gas regime. A thick shock structure appears upstream of the nose and the viscous flow extends from the nose to the free stream adjacent to the shock. The middle portion of the trajectory is represented by points 2 and 3. The shock may be treated as a discontinuity, however, the boundary-layer is sufficiently thick so that interactions between the shock and the boundary layer exist. In addition, because of the speed, significant departure of chemical equilibrium occurs in the shock layer. For the other four points either an equilibrium air or an ideal gas model would be the appropriate flow chemistry model for both low and high altitude flight, because the speed is rather low at the low altitude trajectory while the density is low at the high speed and high altitude trajectory.

5.1 Ideal and Equilibrium Flow Field Solutions

All the trajectory points except for point 5 were considered in the flow field computations using both ideal gas and equilibrium air models. A modified set of boundary conditions including velocity slip will be used in a future analysis to deal with the flow field solution of point 5 exclusively. The present analysis is unable to predict physically correct results; viz. the skin heat transfer coefficients is larger than one, etc. Furthermore, due to the difference in shock structure, the sharp shock formulation was used for the first four points. Whereas the thick-shock formulation was used for point 4. An attempt was made to calculate the flow field for point 4 using the sharp-shock formulation but the solution could not converge to the steady solution due to the small value of the Reynolds number.

Figure 9a and 9b show the temperature profiles on the axis of symmetry obtained for the ideal gas model and the equilibrium air model, respectively. Note that the wall temperatures are different among the four points in order for the highly-cooled wall assumption to be valid. The shock stand-off distances are also given in Figure 9a and 9b. The equilibrium temperature profile for point 4 is not given because of the limitation in the real gas subroutine.

Figure 10 gives the skin friction coefficients obtained from the ideal gas and the equilibrium air analyses. The air chemistry only affects the value of C_F at high altitude. It is also found in Figure 11, which presents the skin heat transfer coefficients for several points, that the departure of chemical equilibrium affects solutions of points

2 and 3. It should be pointed out that the highest heat flux to the wall is at point 3 computed on the basis of the ideal gas and equilibrium air gas models. The nondimensional formulas used are

$$c_F = \frac{e_{ns}}{1/2\ \gamma_\infty M_\infty^2} \tag{24}$$

$$c_H = \frac{q_n}{[(H)_T-(H_W)_T]\ \gamma_\infty M_\infty} \tag{25}$$

where $H = \varepsilon+p/\rho$, and e_{ns}, q_n are in body intrinsic coordinates.

The results presented in Figure 9, 10, and 11 were obtained using the local time increment to advance the solution until it has reached its asympotic state, and using the second computational plane with coordinate squeezing toward the body. The mesh was constructed by N=45, M=10, and β=3. The number of time steps needed were K=500-800. The execution time of the programs on the UNIVAC 1108 system was 45 to 75 minutes for each case. A large number of time steps was found to be necessary to bring a steady solution to the thick-shock flow field analysis.

The thermodynamic properties of the ideal gas and the equilibrium air are obtained from the following relations. $p = (\gamma-1)\rho e$, $T = (\gamma-1)e/R$ where γ and R are the ratio of specific heat and the gas constant, respectively. γ=1.4 is used in the ideal gas flow field calculations and $\gamma=\gamma_{eff}$ is used in the equilibrium air calculation. γ_{eff} is determined as a function of internal energy and density by the following equation [30]:

$$\gamma_{eff} = R_0^{\alpha} \left[0.161 + 0.255\ F_1 G_1 + 0.280\ (1-F_1)\ G_2 + 0.137\ F_2 G_3 \right] + 1$$

where

$$\alpha = 0.048\ F_1\ \log_{10} E + 0.032\ (1-F_1)\ (1-F_2)\ \log_{10} E + 0.045\ F_2$$

and

E = local internal energy (ergs/gm) X 10^{10}

$R_o = \rho/\rho_o$ where ρ = local density, ρ_o = sea level density

Also

$$E_1 = 8.50 + 0.357\ \log_{10} R_o,\ E_2 = 45.0\ R_o\ 0.0157$$

and

$$\Delta E_1 = 0.975\ R_o^{0.05},\ \Delta E_2 = 4.0\ R_o^{0.085}$$

Also

$$F_1 = \left[\exp\ (E-E_1)/\Delta E_1 + 1 \right]^{-1},\ F_2 = \left[\exp\ (-E + E_2)/\Delta E_2 + 1 \right]^{-1}$$

$G_1 = \exp\ (-E/4.46)$, $G_2 = \exp\ (-E/6.63)$, and $G_3 = \exp\ (-E/25.5)$

5.2 Finite-rate Reacting Flow Field Solutions

Flow field solutions of trajectory points 2 and 3 are discussed in more detail in this section. The effect of the body temperature conditions, the surface catalycity, and the transport coefficients of the mixture on the flow field solution were examined. Comparisons of flow properties were also made between the viscous and the inviscid analyses and between the different gas models. To simplify the investigation, limiting cases of wall conditions are used such as an isothermal or adiabatic wall, a fully-catalytic or non-catalytic wall. In addition, transport coefficients

such as those calculated by the procedure described in Section 2.2 or those simply taken from the Sutherland formula for viscosity coefficients and constant Prandtl and Lewis numbers (Pr=0.71 and Le_{lm}=1.5) were used,

$$\mu/\mu_\infty = 1.5(T/T_\infty)^{1.5}/(T/T_\infty+0.5) \quad ,$$

$$k = c_p\mu/Pr \quad , \quad D_{lm} = k\ Le_{lm}/\rho c_p$$

The thermodynamic properties of nonreacting gas models are obtained from $p = (\gamma-1)\rho e$ and $T = (\gamma-1)e/R/M_W$ where $\gamma = 1.4$ for an ideal gas and $\gamma = \gamma_{eff}$ for an equilibrium air, γ_{eff} is calculated by a procedure described in reference 25. The chemical rate constants used in the reacting gas model are given in reference 19. The influence of rate constants on the flow properties is not studied in this work, since extensive investigations are available in the inviscid flow calculations.

The temperature profiles along the stagnation line and a line normal to the wall at $S/R_N = 0.7$ are shown in figure 12 for the trajectory point 2 . The temperature profile obtained for an ideal gas model exhibits large oscillations, especially along the stagnation line where the temperature drops quickly to the specified wall temperature. In the case of an equilibrium air model, the temperature behind the shock is nearly half of that for an ideal gas, and the oscillations are relatively small. The finite-rate chemistry considered in the shock layer results in a rapidly decreasing, but smooth profile toward the wall. This curve resembles the result in a fully-viscous shock layer, except for the

sharp gradient near the wall. The dash line is the inviscid temperature profile obtained from an improved version of program reported in reference 19. The inviscid and viscous reacting temperatures are very close to each other along the stagnation line, but not so close downstream. The difference immediately behind the shock is a result of the different shock fitting procedures used, however, the present one is more accurate. From the shock locations one can obtain the velocity displacement thickness or the velocity boundary layer thickness. The boundary layer thickens as the flow moves downstream and occupies about 10 percent of the shock layer. The viscous shock location is affected qualitatively by the finite-rate chemistry as the shock in inviscid flows. The temperature boundary layer is about twice as thick as the velocity boundary layer, and much thicker than that obtained from non-reacting calculations. Nevertheless, the temperature gradient near the wall is still quite high because of the cooled wall.

The boundary-layer features are also noted in species concentration shown in figure 13. The effect of wall catalycity is examined for both adiabatic and isothermal walls. It is seen that the influence of wall catalycity is restricted to about one quarter of the stagnation line. For an adiabatic and non-catalytic wall, the species profiles of C_{O2} and C_{NO} exhibit very close resemblance to the inviscid species profiles, which are also shown in figure 13a. If the wall condition is changed to catalytic, the influence of wall catalycity is extended to one-third of the stagnation line. Since the flow properties are affected to different degrees by the wall conditions, it is therefore difficult to obtain appropriate edge conditions for boundary-layer analyses.

Another flowfield calculation was made using multicomponent transport coefficients for a high-cooled, catalytic wall. Figures 14 and 15, respectively, present the temperature profiles across the shock layer at four points on the body and species profiles at two points on the body. The flowfield results are nearly indistinguishable from each other as comparison is made between figures 12 and 14 and between 13 and 15. In terms of computation time, however, the multicomponent results requires four times as much as that for results obtained from using simple transport coefficients. The computation time per mesh point is about one-tenth of a second for viscous calculations and about one-fifteenth of a second for inviscid calculations. It is estimated for a reacting flow calculation using seven species and 19 reactions. The total time for a converged solution is 45 minutes for a mesh of 10×15, or 10 points along the body and 15 points across the shock layer, with 250 time steps. More computation time can be saved for multicomponent solution by matching the inviscid and viscous solutions outside of the boundary layer.

Because of the cost to execute the program, most of the results are obtained from a mesh of 10×15. The resultant spacing near the wall is obvisouly too coarse to predict accurate heating rates, but is sufficiently small to resolve the fine detail of the flow property profiles. The overall accuracy on the flowfield solution is checked by comparing the total specific energy with its free stream value. The dissipations of total energy are presented in figure 16 at three body points. All three curves decrease rapidly in proportion to the distance from the wall. The level of numerical dissipation is also given for an inviscid flow

calculation of same free stream condition. The accuracy of the computed flowfield results is then checked by using a finer mesh spacing. Difference in flow properties are within 5 percent between the solutions obtained from 10×15 and 10×30. However, the mesh spacing is critical to the calculation of skin friction and heat transfer coefficient.

It is shown in figure 21 that the C_H obtained using a mesh of 10×15 is almost one order of magnitude less than the existing results.[2] Improvement can be achieved by reducing the mesh spacing near the wall. It is found that the C_H values begin to level off with a mesh of 10×30 and $\beta = 2$, where the mesh spacing next to the wall is approximately one-hundredth of the shock layer thickness. More discussion on the calculations with a stretched coordinate can be found in reference 14. It should be pointed out that the multicomponent C_H is higher than the simple C_H by a factor of 2 or more. This is caused by the higher coefficients of mass diffusion and thermal conductivity of the multicomponent theory.

The flowfield results of the trajectory point 3 are presented in figures 17 through 20. The ideal gas temperature profile has larger oscillations and the reacting temperature drops more quickly behind the shock. Also, the boundary-layers are thicker than those of the trajectory point 2. There is roughly a factor of two increase for both velocity and temperature boundary-layer thickness. Due to a much higher speed, the dissociation inside the shock layer is more complete and ionization is considered in the calculation. But the boundary-layer features are still observed in the flow property profiles. Notice that the peak of C_{O_2} in

figure 17 is located approximately in the middle of the shock layer for three combinations of wall conditions. The interaction between the boundary layer and the shock is markedly stronger than that for the trajectory point 2. Figures 19 and 20 give the temperature and species profiles across the shock layer at several points on the body. Very little difference is found between the results obtained from the simple transport theory and the multicomponent theory. Finally, the heating rates are computed and presented in figure 21. Note, the agreement with existing data is not quite good. The calculations of C_H have been made on meshes of 10×20, $\beta = 1$ and 10×35; $\beta = 2$. But the value of C_H is still lower than the boundary-layer result.

Some of the results obtained for the trajectory point 4 are shown in figures 22 and 23. The assmuption of a thin shock was used in the reacting air calculation with simple transport properties. The shock layer is fully viscous, as the wall effect extends to the shock and the temperature profile no longer exhibits markedly decreasing magnitude downstream of the shock. In contrast to the temperature profile obtained for the trajectory points 2 and 3, the temperature gradients at the wall are also smaller. Another interesting result is that the shock wave is located a little farther than that of the trajectory point 3. The free stream Mach number are, respectively 27- and 29.5 for points 3 and 4. The validity of applying the thin-shock program to the trajectory point, which has a Reynolds number of 900 based on a nose radius of 2 ft, was checked by using the thick-shock program. The dash line presented in figure 22 are the ideal gas results for the trajectory point 4. Significant

differences are observed between these two sets of calculations. In addition to the effects of different gas models used, the thick-shock calculation was made for $Re_\infty = 450$ or for the same free stream condition but one foot nose radius. The computation encountered difficulty in reaching the steady state for $Re_\infty = 900$ or higher Reynolds numbers. It seems that a certain amount of physical dissipation is needed to damp the oscillations in the flowfiled results for a chosen mesh size. The mesh used in the present calculation is N = 20 and M = 10 and the computational region is defined by $S/R_N = 0.6$ $N/R_N = 1$. The computer time is about 85 minutes on the MSC-UNIVAC 1108 for K = 1500 . Since the reacting air calculation would require several fold more computer time, such a calculation has not been attempted.

Figure 23 shows the species profiles on two stations across the shock layer obtained from the thin-shock reacting program. The level of dissociation and ionization is approximately the same as that of the trajectory point 3. However, the shape of the profiles are quite different as revealed by a comparison between Figures 23 and 20, where the wall conditions are the same for both cases.

Finally, in Figure 24 the best rates are summarized for the trajectory points considered in this study.

The results for points 0 and 5 are not presented because the speed is either too low or the altitudes too high for these conditions such that the departure of chemical equilibrium is negligible in the shock layer.

The value of C_H tends to agree with the results obtained from the boundary-layer or the thin shock layer theories, although our value is consistently lower for all the points.

6.0 CONCLUSION

A time-marching finite-difference method has been developed to solve for the flow field in the nose region of an orbiter. During high altitude flight the thick-shock formulation predicts results that match with the free-molecular limit, whereas at lower altitude the thin-shock formulation with the aid of coordinate transformations provides flow field solutions that agree quite closely with the usual boundary-layer theory. The present method is particularly useful to analyze the flow field for the medium altitude when appreciable chemical nonequilibrium exists. Since an "exact" form of the governing equations is utilized and only numerical approximations are made in the method of solution, the solutions obtained are considered to be more general and satisfactory than most results obtained from nonequilibrium thin shock-layer theory. The shortcomings of existing theories; i.e., the need of accurate edge conditions for reacting boundary-layer analysis, and the use of a "two-layers" model and of simple transport coefficients analysis are absent from the present solution. Two major assumptions are employed in the present, as well as, in the previous analysis; namely that the vibrational equilibrium is maintained and mass diffusion depends only on the density gradient. These assumptions are made in order for the computers presently available to manage the computations within a reasonable time. The cost of the flow field computation is noted to increase considerably with the use of a more elaborate theory of the chemical kinetics and transport properties. The application of the time-marching method to more practical problems rests entirely on the further improvement of its efficiency. It is felt that more studies should be directed toward the

numerical experimentation that will provide new techniques with the potential to expedite the convergence to the time-asympotic solution. Also, the accuracy of the results thus obtained should be examined against the experimental data which are not currently available.

7.0 REFERENCES

1. Li, C. P. and Goodrich, W.; "A Viscous Starter Solution for Shuttle Flow Field Computations;" in the Space Shuttle Aerothermodynamics Technology Conference, Vol. 1 - Flow Fields, TM X-2506, NASA, February 1972.

2. Blottner, F. G.; "Nonequilibrium Laminar Boundary-Layer Flow of Ionized Air," AIAA J. 2, 192-27 (1964)

3. Blottner, F. G.; "Finite-Difference Methods of Solution of the Boundary-Layer Equations," AIAA J. 8, 193-25 (1970)

4. Blottner, F. G.; "Viscous Shock Layer at the Stagnation Point with Nonequilibrium Air Chemistry," AIAA J 7, 2281-2288, (1969)

5. Dellinger, T. C.; "Nonequilibrium Air Ionization in Hypersonic Fully Viscous Shock Layers," AIAA paper No. 70-806, 3rd Fluid and Plasma Dynamics Conference, Los Angeles, California, June 1970

6. Cheng, H. K.; "The Blunt-Body Problem in Hypersonic Flow at Low Reynolds Number," Rept. AF-1285-A-10 Cornell Aeronautical Laboratory, Inc. (1963)

7. Chung, P.M.; Holt, J. F.; and Lin, S. W.; "Merged Stagnation Shock Layer of a Nonequilibrium Dissociating Gas", AIAA J 6, 372-79 (1968)

8. Davis, R. T.; "Hypersonic Flow of a Chemically Reacting Binary Mixture Past a Blunt Body," Paper No. 70-808, AIAA 3rd Fluid and Plasma Dynamics Conference, Los Angeles, 1970

9. Lee, R.H.C. and Zierten, T. A.; "Merged Layer Ionization in the Stagnation Region of the Blunt Body," Proceedings of the 1967 Heat Transfer and Fluid Mechanics Institute, Ed. Lilley and Olfe, Stanford University Press, 452-68 (1967)

10. Smith, A. M. D. and Jaffe, N. S.; "General Method for Solving the Laminar Nonequilibrium Boundary-Layer Equations of a Dissociating Gas," AIAA J 4, 611-20 (1966)

11. Pallone, A. J.; Moore, J. A.; and Erdos, J. I.; "Non-equilibrium Nonsimilar Solutions of the Laminar Boundary Layer Equations," AIAA J 2, 1706-13 (1964)

12. Kang, S. W.; "Nonequilibrium, Ionized, Hypersonic Flow Over a Blunt Body at Low Reynolds Number", AIAA J 8, 1263-70, July 1970

13. Shih, W. C. and Krupp, R. S.; "Viscous Nonequilibrium Blunt-Body Flow," AIAA J 5, 16-25 (1967)

14. Li, C. P.; "Solutions of the Navier-Stokes Equations for Blunt Body Flows", submitted for publication

15. Tsien, H. S.; "The Equations of Gas Dynamics" in the "Fundamentals of Gas Dynamics", Ed. H. W. Emmons, Vol. 3 in the "High Speed Aerodynamics and Jet Propulsion" Princeton University Press (1958)

16. McBride, B. J., and Gordon, S.; "Fortran IV Program for Calculation of Thermodynamic Data", TND-4097, NASA, August 1967

17. Hirschfelder, J. O., Curtiss, C. F. and Bird, R. B.; "Molecular Theory of Gases and Liquids", John Wiley and Sons, Inc., corrected with notes added, (1964)

18. Svehla, R. A.; "Thermodynamic and Transport Properties for the Hydrogen-Oxygen System", SP-3011, NASA, (1964)

19. Li, C. P.; "Time-Dependent Solutions of Nonequilibrium Airflow Past a Blunt Body." Paper No. 71-595 AIAA 4th Fluid and Plasma Dynamics Conference, Palo Alto, California, June 1971. Also in the J of Spacecraft and Rockets, 9, 571-572 (1972)

20. MacCormack, R. W.; "Numerical Solution of the Interaction of a Shock Wave with a Laminar Boundary-Layer", 2nd International Conference on Numerical Methods in Fluid Dynamics, University of California, Berkely, Calif., Sept. 15-19, 1970

21. Cheng, S. I.; "Numerical Integration of Navier-Stokes Equations," AIAA J 8, 2155-2122 (1970)

22. Crocco, L.; "A Suggestion for the Numerical Solution of the Steady Navier-Stokes Equations," AIAA J 3, 1824-1832 (1965)

23. Goodrich, W. D.; Personal communication, July, 1971.

24. Ralston, A., and Wolf, H. S.; ed., "Mathematical Methods for Digital Computers," Vol. 1, Chapter 15. "The Numerical Solution of Hyperbolic Partial Differential Equations by the Method of Characteristics", M. Lister, John Wiley & Sons (1960).

25. Russell, D. A.; "Density Disturbance Ahead of a Sphere in Rarefied Supersonic Flow," Physics Fluid, 11, 1679-1685 (1968)

26. Li, C. P.; "Shock Layer Structures in Rarefied Gas Flow," 8th International Symposium on Rarefied Gas Dynamics, Stanford University, July 10-14, 1972

27. Kao, H. C.; "Hypersonic Viscous Flow Near the Stagnation Streamline of a Blunt Body - II. Third-Order Boundary-Layer Theory and Comparison with other Methods." AIAA J 2, 1898-1906 (1964)

28. Lewis, C. H., ed., "Nonreacting and Chemically Reacting Viscous Flows Over a Hyperboloid at Hypersonic Condition," AGARD-AC-147-70. (1970)

29. Vogenitz, F. W., Bird, G. A., Broadwell, J. E., and Rugaldier, H.," Theoretical and Experimental Study of Rarefied Supersonic Flows about several simple Shapes" AIAA J 6, 2388-2394 (1968)

30. Doan, L. R. and Nickel, G. H.; "A Subroutine for the Equation of State of Air," AFWL TM-RTD (WLR) TM-63-2, (1963)

31. Vincenti, W. G. and Kruger, C. K.; "Introduction to Physical Gas Dynamics," John Wiley & Sons, Inc. (1965)

8.0 APPENDIX

I. Temperature Coefficients for Thermodynamic Functions

II. Cross sections for Calculation of Transport Properties

III. Chemical Reactions and Rate Constants

APPENDIX I

TEMPERATURE COEFFICIENTS FOR THERMODYNAMIC FUNCTIONS

The first line indicates the range of temperatures for which the following polynomials are fitted. The first two numbers give the first temperature interval, the last two give the second temperature interval. The second line refers to the name of species that is followed by the molecular weight of the species, M, the mass concentration in the free stream, C_{i_∞}, and the molar enthalpy of the species at temperature °K, H_∂. The third to the fifth lines are two sets of temperature coefficients for the temperature intervals stated in the first line. Each set of the temperature coefficients contains seven numbers, A_i (i=1,...7).

The input to the "Fortran IV program for calculation of thermodynamic data"[16] is also given for reference.

TEMPERATURE COEFFICIENTS FOR THERMODYNAMIC FUNCTIONS

500.000 2000.000 8000.000

N
14.008
.26008039+01 -.39987245-04 -.31575438-07 .15553786-10 -.11534531-14
.56036722+05 .32329063+01 .24996236+01 .76454307-06 .13041301-09
-.84771079-12 .35063098-15 .56129009+05 .38947739+01

NO
30.008
.38207707+01 .48808920-03 -.12913346-06 .15881346-10 -.72198815-15
.94662324+04 .16414434+01 .29577293+01 .15516343-02 -.34653198-06
-.14505691-09 .55093720-13 .99314868+04 .67149494+01

N2
28.016 0.767 -2072.3
.35509203+01 .65789729-03 -.17402027-06 .21186173-10 -.95608817-15
-.12811888+04 .22934428+01 .33433281+01 -.72401132-04 .13855097-05
-.90323654-09 .17563459-12 -.99664368+03 .39716316+01

O
16.0
.26081063+01 -.10928387-03 .33239655-07 -.22177461-11 .62252686-17
.29208397+05 .45252627+01 .26966714+01 -.45365525-03 .42258613-06
-.17922861-09 .28686146-13 .29206244+05 .41194475+01

O2
32.0 0.233 -2074.7
.39440561+01 .44078616-03 -.11905731-06 .15235232-10 -.71382373-15
-.14185511+04 .16345285+01 .26888313+01 .29669142-02 -.20736354-05
.70400291-09 -.93767604-13 -.90767590+03 .85677707+01

```
1000.      8000.      30000.
N                     14.008
    .62289649+00   .75996372-03  -.68415018-07   .26029019-11  -.34945540-16
    .58479554+05   .16852908+02   .25089713+01   .33558825-04  -.50810528-07
    .17437946-10  -.12061041-14   .56115633+05   .38176968+01
NO                    30.008
    .40400914+01   .13988441-03  -.11091974-07   .42166881-12  -.56661273-17
    .98440496+04   .12764058+01   .35525990+01   .74104713-03  -.21044177-06
    .26615640-10  -.12202011-14   .96660986+04   .40007346+01
N2                    28.016     0.767     -2072.3
    .40844968+01   .12278738-03  -.96239298-08   .36313722-12  -.48569485-17
   -.13953107+04  -.90243858+00   .32748564+01   .91440295-03  -.25532029-06
    .31771812-10  -.14403937-14  -.10722559+04   .40128936+01
O                     16.0
    .38996390+01  -.36415106-03   .39166618-07  -.16293483-11   .23590944-16
    .25282127+05  -.53511900+01   .25834420+01  -.92229575-04   .29726886-07
   -.20210324-11   .10287797-16   .29209532+05   .46849012+01
O2                    32.0       0.233     -2074.7
    .41112747+01   .13318230-03  -.94655609-08   .36033593-12  -.48453159-17
   -.10319605+04   .89757341+00   .37703377+01   .59954714-03  -.16830812-06
    .21487106-10  -.99140887-15  -.12872788+04   .27182910+01
NO+                   30.008
    .40373003+01   .13743275-03  -.10814367-07   .40878651-12  -.54738251-17
    .11781023+06   .23637557+00   .32670481+01   .91953966-03  -.25578741-06
    .31790552-10  -.14399933-14   .11801990+06   .48541930+01
E-                    .00052
    .25000000+01   .00000000      .00000000      .00000000      .00000000
   -.74537492+03  -.12427286+02   .25000000+01   .00000000      .00000000
    .00000000      .00000000     -.74537498+03  -.12427286+02
LAST
```

```
   150.000  7250.000 44000.000
N                    .1401+02  .0000      .0000
  .29580086+01   .72396636-04  -.19303650-08   .65164957-14  -.85710902-21
  .52845241+05  -.35782222+00   .24773161+01   .82201024-04  -.76068977-07
  .22462038-10  -.15404079-14   .56132605+05   .39907642+01
NO                   .3001+02  .0000      .0000
  .44678487+01   .22695846-04  -.14024959-09   .16591832-14   .63494057-22
  .86956018+04  -.19150373+01   .31967976+01   .11768965-02  -.38778399-06
  .55730992-10  -.28806146-14   .98652406+04   .61134104+01
N2                   .2802+02  .7670+00 -.2072+04
  .44517456+01   .21995996-04  -.20501717-09   .24035750-14   .82543275-22
 -.23783613+04  -.36415174+01   .32066185+01   .96095003-03  -.26764111-06
  .33487899-10  -.15439933-14  -.09993079+03   .44601651+01
O                    .1600+02  .0000      .0000
  .25750267+01   .22026986-04   .50533473-10  -.11757918-13  -.13900519-20
  .28692301+05   .44633487+01   .26847763+01  -.24357548-03   .96464480-07
 -.13270647-10   .65179101-15   .29176733+05   .41135781+01
O2                   .3200+02  .2330+00 -.2075+04
  .44763073+01   .33173559-04  -.11257496-09   .13687415-14   .68543405-22
 -.20125246+04  -.18259916+01   .32206321+01   .13129468-02  -.46651373-06
  .70960134-10  -.38179530-14  -.10142978+04   .59381147+01
NO+                  .3001+02  .0000      .0000
  .44517063+01   .23790900-04  -.20057345-09   .23327397-14   .73175507-22
  .11669996+06  -.28547776+01   .32070007+01   .95463964-03  -.26312343-06
  .32660308-10  -.14945999-14   .11808876+06   .52543095+01
E-                   .5200-03  .0000     -.1481+04
  .25000000+01   .00000000      .00000000      .00000000     .00000000
 -.74537492+03  -.12427286+02   .25000000+01   .00000000     .00000000
  .00000000      .00000000     -.74537498+03  -.12427286+02
LAST                      .0000     .0000      .0000
```

```
Z RUN L73069,FD23,H3,3782,G123,C,5,5                                    CP    LI
N MSG      FILE REQ.  TAPE  1 FH432 0   FSTRN  0
N HDG       INPUT TAPE A=A11611
 ASG A=A11611
   XQT  CUR
 TRW A
IN A
   FOR,*  MAIN13,MAIN13
   FOR,*  ATOM13,ATOM13
   FOR,*  DELH13,DELH13
   FOR,*  DERV13,DERV13
   FOR,*  EFTP13,EFTP13
  FOR,* IALS,IALS
  FOR,* IARS,IARS
  FOR,* IDEN13,IDEN13
   FOR,*  INPT13,INPT13
   FOR,*  KDELTA,KDELTA
   FOR,*  LEAS13,LEAS13
   FOR,*  LINK13,LINK13
   FOR,*  LOGK13,LOGK13
   FOR,*  PAGE13,PAGE13
   FOR,*  PNCH13,PNCH13
   FOR,*  POLY13,POLY13
   FOR,*  QSUM13,QSUM13
   FOR,*  RECO13,RECO13
   FOR,*  TABL13,TABL13
   FOR,*  TEMP13,TEMP13
   XQT MAIN13
CONSTSHCK      1.4388    R       1.98726   SCONST   -3.66511
ATOM  H      1.008       H2(G) 2.                2.
ATOM  O        15.9994   O2(G)      40.               15.
ATOM  N        14.0067   N2(G)      30.               20.
ATOM  E      .000548613  E1(G)             2                 2
N1(G)                    HF298 113024.6
LSTSQST      1000.       T      8000.      T     30000.      TCONST8000.
TEMP  T        200.      I       200.      T       30000.
METHODTEMPER             FILL
DATA   1.5       0.0      2.5     19223.     1.5     19231.                          2
DATA    .5     28840.     1.5     28840.     2.5     88109.5                         2
DATA    .5     88173.0    1.5     88153.4                                            2
DATA    .5     83285.5    1.5     83319.3    2.5     83366.0    .5     86131.4      3
DATA   1.5     86223.2     .5     93582.3     .5     94772.2   1.5     94794.8      3
DATA   2.5     94832.1    3.5     94883.1     .5     95476.5   1.5     95494.9      3
DATA   2.5     95533.2    1.5     96751.7    1.5     96788.2   2.5     96864.2      3
DATA    .5     97770.1    1.5     97805.8    2.5     99665.    1.5     99658.       3
DATA   1.5    104615.4     .5    104654.9    1.5    104665.    2.5    104684.      3
```

```
DATA   3.5   104718.     4.5   104767.     2.5   104810.9    3.5   104882.7    3
DATA    .5   104864.     1.5   104890.     2.5   104957.      .5   104987.     3
DATA   1.5   104998.     2.5   105011.     3.5   105020.     1.5   105120.8    3
DATA   1.5   110521.9    2.5   110545.8     .5   112294.8    1.5   112320.8    3
DATA   2.5   105144.3                                                          3
DATA   2.5   103736.8    1.5   103668.1     .5   103618.1     .5   104142.2    4
DATA   1.5   104227.4     .5   106478.6     .5   106760.5    1.5   106780.1    4
DATA   2.5   106816.1    3.5   106870.7     .5   106982.7    1.5   106998.3    4
DATA   2.5   107039.0    1.5   107447.2    1.5   110196.     2.5   110214.     4
DATA   3.5   110248.     4.5   110304.      .5   110221.     1.5   110275.     4
DATA   2.5   110288.     3.5   110339.     1.5   110221.7     .5   110244.6    4
DATA   2.5   110311.     3.5   110373.                                         4
DATA    .5   110325.     1.5   110351.     2.5   110403.     1.5   110448.3    4
DATA   2.5   110470.                                                          4
DATA    .5   110029.2    1.5   110108.5     .5   109813.5    1.5   109857.8    5
DATA   2.5   109927.9    1.5   112751.     2.5   112763.     3.5   112799.     5
DATA   4.5   112862.     1.5   112801.      .5   112816.     2.5   112820.     5
DATA   3.5   112890.2     .5                 1.5                              5
DATA   2.5   112825.     3.5   112892.      .5   112855.     1.5   112874.     5
DATA   2.5   112912.     1.5   112929.2    2.5   112947.5                      5
DATA    .5   112565.9    1.5   112610.6    2.5   112682.6     .5   112735.     6
DATA   1.5   112823.     1.5   114160.     2.5   114160.     3.5   114160.     6
DATA   4.5   114160.      .5                 1.5                2.5   114182.  6
DATA   3.5   114248.     1.5   114193.      .5   114209.     2.5   114196.     6
DATA   3.5   114275.     1.5   114232.2    2.5   114290.5     .5                6
DATA   1.5   114259.     2.5   114274.                                         6
DATA    .5   114130.     1.5   114183.                                         7
DATA   2.5   115004.     3.5   115004.                                         7
DATA    .5   115017.     1.5   115017.                                         7
DATA   1.5   115057.5    2.5   115100.1                                        7
DATA    .5   115103.     1.5   115103.     2.5   115103.                       7
DATA    .5   114015.     1.5   114072.     2.5   114146.                       7
DATA    .5   114988.     1.5   114988.     2.5   114988.     3.5   114988.     7
DATA                                                        IP    117345.    12
FINISH
OI(G)                          HF298  59556.3
LSTSQST      1000.             T      8000.        T      30000.    TCONST8000.
TEMP  T        200.             I       200.       T      30000.
METHODTEMPER                   FILL
DATA   2      0.0               1       158.5      0       226.5    2     15867.7   2
DATA   0    33792.4                                                             2
DATA   1    73767.81            1     76794.69     1     86625.35    2     86627.37  3
DATA   3    86631.04            2     88630.84     1     88630.30    0     88631.00  3
DATA   4    97420.24            3     97420.37     2     97420.50    3     97488.14  3
DATA   2     97420.37           1     97420.50     0     97420.5     2    97488.14   3
DATA   1     97488.14                                                            3
```

```
DATA    2    95476.43     1     96225.5     1     99092.64     2     99093.31    4
DATA    3    99094.52     2     99680.4     3    102908.14     4    102865.09    4
DATA    1      99680.4    0     99680.4                                           4
DATA    2     102908.14   1    102908.14                                          4
DATA    2    102116.21    1     102411.65   2     103869.4     3     105408.58   5
DATA    4    105385.3     3    105385.3     2     105385.3     1    105385.3     5
DATA    0     105385.3    2     105408.58   1     105408.58                      5
DATA    2    105019.0     1     105164.9    2    105911.3      4     106751.2    6
DATA    3    106765.8     1     105911.3    0     105911.3     3     106751.2    6
DATA    2    106751.2     1     106751.2    0     106751.2     2     106765.8    6
DATA    1    106765.8                                                            6
DATA    2    106545.1     1     106627.9    4     107573.1     3     107582.7    7
DATA    3    107573.1     2     107573.1    1      107573.1    0      107573.1   7
DATA    2     107582.7    1     107582.7                                          7
DATA    2    107445.4     1     107497.1    5.5   108105.7     3.5   108116.6    8
DATA    2    108021.4     1     108057.6    5.5   108470.2     3.5   108477.8    9
DATA    2    108412.0     1     108436.1    3.5   108734.4     5.5   108731.5   10
DATA    2    108688.4     1      108731.5                    IP      109836.7   11

FINISH
NIO1+(G)                  HF298 236660.
LSTSQST     1000.         T     8000.        T      30000.      TCONST8000.
TEMP  T      200.         I      200.        T      30000.
METHODRANDK
DATA  STATWT   1.         WE     2377.1      WEXE     16.35     BE      2.002
DATA  ALPHAE .0202
FINISH
E1(G)                     HF298 0.
EFTAPE
LOGK
LSTSQSEXP
TEMP  T      200.         I      200.        T      30000.
DATE  7 / 24
METHODALLN
E-GAS   .5
FINISH
```

```
  XQT MAIN13
CONSTSHCK      1.4388    R        1.98726   SCONST   -3.66511
ATOM  N       14.0067    N2(G)      30.               20.
ATOM  O       15.9994    O2(G)      40.               15.
N2(G)                    HF298  0.
LSTSQST    1000.         T      8000.       T     30000.      TCONST8000.
TEMP  T     200.         I       200.       T      30000.
METHODPANDK
DATA  STATWT1.           WE     2357.78     WEXE  14.184999   BE    1.9978
DATA  ALPHAE0.01708      SYMNO  2.
FINISH
O2(G)                    HF298  0.
LSTSQST    1000.         T      8000.       T     30000.      TCONST8000.
TEMP  T     200.         I       200.       T      30000.
METHODPANDK
DATA  STATWT3.           WE     1580.1618   WEXE  12.0700001  BE    1.445306
DATA  ALPHAE0.015785     SYMNO  2.
FINISH
N1O1(G)                  HF298  21600.0
LSTSQST    1000.         T      8000.       T     30000.      TCONST8000.
TEMP  T     200.         I       200.       T      30000.
METHODPANDK
DATA  STATWT2.           WE     1903.7899   WEXE  13.97       BE    1.7056
DATA  ALPHAE0.00611      SYMNO  1.
FINISH
```

APPENDIX II

CROSS SECTIONS FOR CALCULATION OF TRANSPORT PROPERTIES

The cross section data are obtained from Ref. 18 for the neutral species of air. Each pair of the interactions is listed in the first line, also shown is the number of temperatures followed. For each temperature, $\bar{\Omega}^{(1,1)}_{l\ m}$, A_{lm} and B_{lm} are given. The subroutines responsible for the calculation of transport properties of the air mixture are written on the basis of these developed in Ref. 18. Several important modifications and numerous changes in coding have been made to the original version in order to suit the flowfield program.

C	O2		14
1000,0000	8,7780	1,1690	1,1310
1500,0000	8,0930	1,1750	1,1370
2000,0000	7,6240	1,1790	1,1410
2500,0000	7,2690	1,1820	1,1440
3000,0000	6,9850	1,1850	1,1470
3500,0000	6,7490	1,1880	1,1490
4000,0000	6,5480	1,1900	1,1520
4500,0000	6,3740	1,1920	1,1540
5000,0000	6,2190	1,1940	1,1560
6000,0000	5,9560	1,1970	1,1590
7000,0000	5,7390	1,2000	1,1620
8000,0000	5,5530	1,2020	1,1640
9000,0000	5,3920	1,2050	1,1670
10000,0000	5,2500	1,2070	1,1690
N2	O		14
1000,0000	10,6100	1,1970	1,1590
1500,0000	9,6100	1,2050	1,1670
2000,0000	8,9260	1,2110	1,1730
2500,0000	8,4060	1,2150	1,1780
3000,0000	7,9980	1,2190	1,1820
3500,0000	7,6590	1,2230	1,1860
4000,0000	7,3740	1,2260	1,1890
4500,0000	7,1260	1,2290	1,1930
5000,0000	6,8990	1,2310	1,1950
6000,0000	6,5350	1,2360	1,2010
7000,0000	6,2260	1,2400	1,2050
8000,0000	5,9710	1,2440	1,2090
9000,0000	5,7440	1,2470	1,2130
10000,0000	5,5480	1,2500	1,2170
N2	N2		20
200,0000	15,4310	1,0680	1,1050
250,0000	14,4350	1,0870	1,0930
300,0000	13,7780	1,0870	1,0870
350,0000	13,3040	1,0890	1,0800
400,0000	12,9450	1,0910	1,0830
500,0000	12,4210	1,0950	1,0890
700,0000	11,7670	1,1010	1,0950
1000,0000	11,1700	1,1100	1,0960
1500,0000	10,5400	1,1260	1,1070
2000,0000	10,0100	1,1390	1,1150
2500,0000	9,5200	1,1470	1,1200
3000,0000	9,0710	1,1560	1,1250
3500,0000	8,6970	1,1670	1,1300
4000,0000	8,3500	1,1700	1,1330
5000,0000	7,8040	1,1830	1,1420
6000,0000	7,3940	1,1950	1,1470
7000,0000	7,0350	1,2000	1,1520
8000,0000	6,7210	1,2010	1,1550
9000,0000	6,4740	1,2050	1,1580
10000,0000	6,2790	1,2080	1,1580
N2	O2		20
200,0000	14,9790	1,0900	1,1200
250,0000	13,9180	1,0870	1,0990
300,0000	13,2130	1,0870	1,0910
350,0000	12,7160	1,0870	1,0870
400,0000	12,3370	1,0890	1,0800
500,0000	11,7980	1,0920	1,0860
600,0000	11,4210	1,0970	1,0900
800,0000	10,8500	1,1100	1,0990
1000,0000	10,4800	1,1320	1,1130
1500,0000	10,0500	1,1540	1,1280
2000,0000	9,8020	1,1710	1,1400

2500,0000	9,5980	1,1800	1,1510
3000,0000	9,4120	1,1930	1,1590
4000,0000	9,0800	1,2050	1,1690
5000,0000	8,7660	1,2120	1,1760
6000,0000	8,4840	1,2170	1,1800
7000,0000	8,2320	1,2210	1,1840
8000,0000	7,9910	1,2240	1,1880
9000,0000	7,7240	1,2270	1,1910
10000,0000	7,4880	1,2300	1,1940
O2	O2		20
200,0000	14,6460	1,0920	1,1420
250,0000	13,5130	1,0890	1,1090
300,0000	12,7630	1,0870	1,0960
350,0000	12,2310	1,0870	1,0900
400,0000	11,8340	1,0870	1,0870
500,0000	11,2710	1,0900	1,0820
600,0000	10,8840	1,0930	1,0870
800,0000	10,2900	1,1020	1,0930
1000,0000	9,8960	1,1150	1,0990
1500,0000	9,4700	1,1300	1,1090
2000,0000	9,2260	1,1470	1,1170
2500,0000	9,0200	1,1550	1,1240
3000,0000	8,8400	1,1620	1,1280
4000,0000	8,5160	1,1700	1,1340
5000,0000	8,2460	1,1760	1,1390
6000,0000	7,9630	1,1800	1,1430
7000,0000	7,7020	1,1840	1,1450
8000,0000	7,4790	1,1860	1,1470
9000,0000	7,2850	1,1880	1,1490
10000,0000	7,1140	1,1900	1,1510
N	N		14
1000,0000	7,0390	1,1290	1,1440
1500,0000	6,2920	1,1340	1,1440
2000,0000	5,8120	1,1380	1,1440
2500,0000	5,4640	1,1420	1,1430
3000,0000	5,1930	1,1440	1,1430
3500,0000	4,9720	1,1470	1,1420
4000,0000	4,7860	1,1490	1,1410
4500,0000	4,6280	1,1510	1,1410
5000,0000	4,4880	1,1520	1,1410
6000,0000	4,2540	1,1550	1,1420
7000,0000	4,0620	1,1580	1,1410
8000,0000	3,9020	1,1600	1,1410
9000,0000	3,7640	1,1620	1,1410
10000,0000	3,6430	1,1630	1,1410
N	NO		10
1000,0000	9,4370	1,2040	1,1660
1500,0000	8,5030	1,2120	1,1740
2000,0000	7,8690	1,2180	1,1810
2500,0000	7,3930	1,2230	1,1860
3000,0000	7,0150	1,2270	1,1910
4000,0000	6,4390	1,2340	1,1990
5000,0000	6,0080	1,2400	1,2050
6000,0000	5,6670	1,2450	1,2110
7000,0000	5,3860	1,2490	1,2160
8000,0000	5,1480	1,2530	1,2210
N	N2		14
1000,0000	9,8240	1,1960	1,1570

1500,0000	8,8970	1,2030	1.1650
2000,0000	8,2720	1,2090	1.1710
2500,0000	7,8020	1,2140	1.1760
3000,0000	7,4270	1,2180	1.1800
3500,0000	7,1150	1,2210	1.1840
4000,0000	6,8500	1,2240	1.1870
4500,0000	6,6220	1,2270	1.1900
5000,0000	6,4190	1,2290	1.1930
6000,0000	6,0800	1,2340	1.1980
7000,0000	5,7990	1,2380	1.2030
8000,0000	5,5580	1,2410	1.2070
9000,0000	5,3550	1,2450	1.2100
10000,0000	5,1700	1,2470	1.2140
N	0		14
1000,0000	8,4180	1,1760	1.1920
1500,0000	7,2270	1,1770	1.1840
2000,0000	6,4940	1,1770	1.1760
2500,0000	5,9840	1,1760	1.1680
3000,0000	5,6060	1,1760	1.1580
3500,0000	5,3100	1,1720	1.1270
4000,0000	5,0750	1,1680	1.1260
4500,0000	4,8990	1,1690	1.1280
5000,0000	4,7450	1,1700	1.1290
6000,0000	4,4900	1,1730	1.1290
7000,0000	4,2820	1,1750	1.1330
8000,0000	4,1080	1,1770	1.1340
9000,0000	3,9590	1,1760	1.1350
10000,0000	3,8290	1,1800	1.1370
NO	NO		17
200,0000	15,1540	1,0950	1.1320
250,0000	13,9740	1,0940	1.1150
300,0000	13,1920	1,0940	1.1050
350,0000	12,6300	1,0950	1.1010
400,0000	12,2030	1,0960	1.0960
500,0000	11,5930	1,0990	1.0940
600,0000	11,1770	1,1010	1.0930
700,0000	10,8620	1,1030	1.0900
800,0000	10,6060	1,1050	1.0920
1000,0000	10,2210	1,1080	1.0900
1200,0000	9,9410	1,1100	1.0950
1500,0000	9,6130	1,1130	1.0970
2000,0000	9,2060	1,1170	1.0960
2500,0000	8,9070	1,1200	1.0950
3000,0000	8,6700	1,1220	1.0950
4000,0000	8,3110	1,1250	1.0950
5000,0000	8,0460	1,1280	1.0950
NO	0		13
500,0000	6,5510	1,2130	1.1750
1000,0000	5,3960	1,2290	1.1920
1500,0000	4,7710	1,2390	1.2040
2000,0000	4,3500	1,2470	1.2130
2500,0000	4,0370	1,2530	1.2210
3000,0000	3,7890	1,2580	1.2270
4000,0000	3,4130	1,2670	1.2360
5000,0000	3,1350	1,2750	1.2470
6000,0000	2,9160	1,2810	1.2560
7000,0000	2,7370	1,2860	1.2630
8000,0000	2,5860	1,2910	1.2690
9000,0000	2,4570	1,2950	1.2760
10000,0000	2,3440	1,3000	1.2810

0	0		14
1000,0000	7,1820	1,1600	1,1410
1500,0000	6,5640	1,1630	1,1560
2000,0000	6,1390	1,1650	1,1600
2500,0000	5,8210	1,1690	1,1630
3000,0000	5,5670	1,1730	1,1680
3500,0000	5,3550	1,1770	1,1720
4000,0000	5,1740	1,1800	1,1760
4500,0000	5,0160	1,1820	1,1840
5000,0000	4,8760	1,1840	1,1850
6000,0000	4,6400	1,1880	1,1820
7000,0000	4,4380	1,1910	1,1820
8000,0000	4,2710	1,1950	1,1820
9000,0000	4,1190	1,1980	1,1810
10000,0000	3,9960	1,1990	1,1810

APPENDIX III
CHEMICAL REACTIONS AND RATE CONSTANT

The calculation of the net rate of chemical production, ω_1, for 1-species is made in one subroutine which was written previously for the inviscid flowfield calculations.[19] The rate constants given are taken from Ref. 31.

$K = A * EXP(-B/T) * T^N$,
(UNITS - CC/MOLE/SEC)

	REACTIONS CONSDERED							A	B	N	REACTION TYPE
1	N2	+N	+	= N	+N	+N		,41000+23	,11300+06	-,15000+01	3
2	N2	+N2	+	= N	+N	+N2		,48000+18	,11300+06	-,50000+00	3
3	N2	+NO	+	= N	+N	+NO		,19000+18	,11300+06	-,50000+00	3
4	N2	+O	+	= N	+N	+O		,19000+18	,11300+06	-,50000+00	3
5	N2	+O2	+	= N	+N	+O2		,19000+18	,11300+06	-,50000+00	3
6	NO	+N	+	= N	+O	+N		,79000+22	,75500+05	-,15000+01	3
7	NO	+N2	+	= N	+O	+N2		,39000+21	,75000+05	-,15000+01	3
8	NO	+NO	+	= N	+O	+NO		,79000+22	,75500+05	-,15000+01	3
9	NO	+O	+	= N	+O	+O		,79000+22	,75500+05	-,15000+01	3
10	NO	+O2	+	= N	+O	+O2		,39000+21	,75500+05	-,15000+01	3
11	N2	+O	+	= NO	+N	+		,70000+14	,36000+05	,00000	1
12	N2	+O2	+	= NO	+NO	+		,46000+25	,64000+05	-,25000+01	1
13	NO	+O	+	= O2	+N	+		,32000+10	,19700+05	,10000+01	1
14	O2	+N	+	= O	+O	+N		,36000+20	,59500+05	-,10000+01	3
15	O2	+N2	+	= O	+O	+N2		,48000+21	,59500+05	-,15000+01	3
16	O2	+NO	+	= O	+O	+NO		,36000+20	,59500+05	-,10000+01	3
17	O2	+O	+	= O	+O	+O		,64000+24	,59500+05	-,20000+01	3
18	O2	+O2	+	= O	+O	+O2		,19000+22	,59500+05	-,15000+01	3
19	N	+O	+	= NO+	+E-	+		,85000+12	,31900+05	,00000	1

9.0 LIST OF TABLES

TABLE 1. A SUMMARY OF RECENT PUBLICATIONS ON THE VISCOUS FLOW PROBLEMS

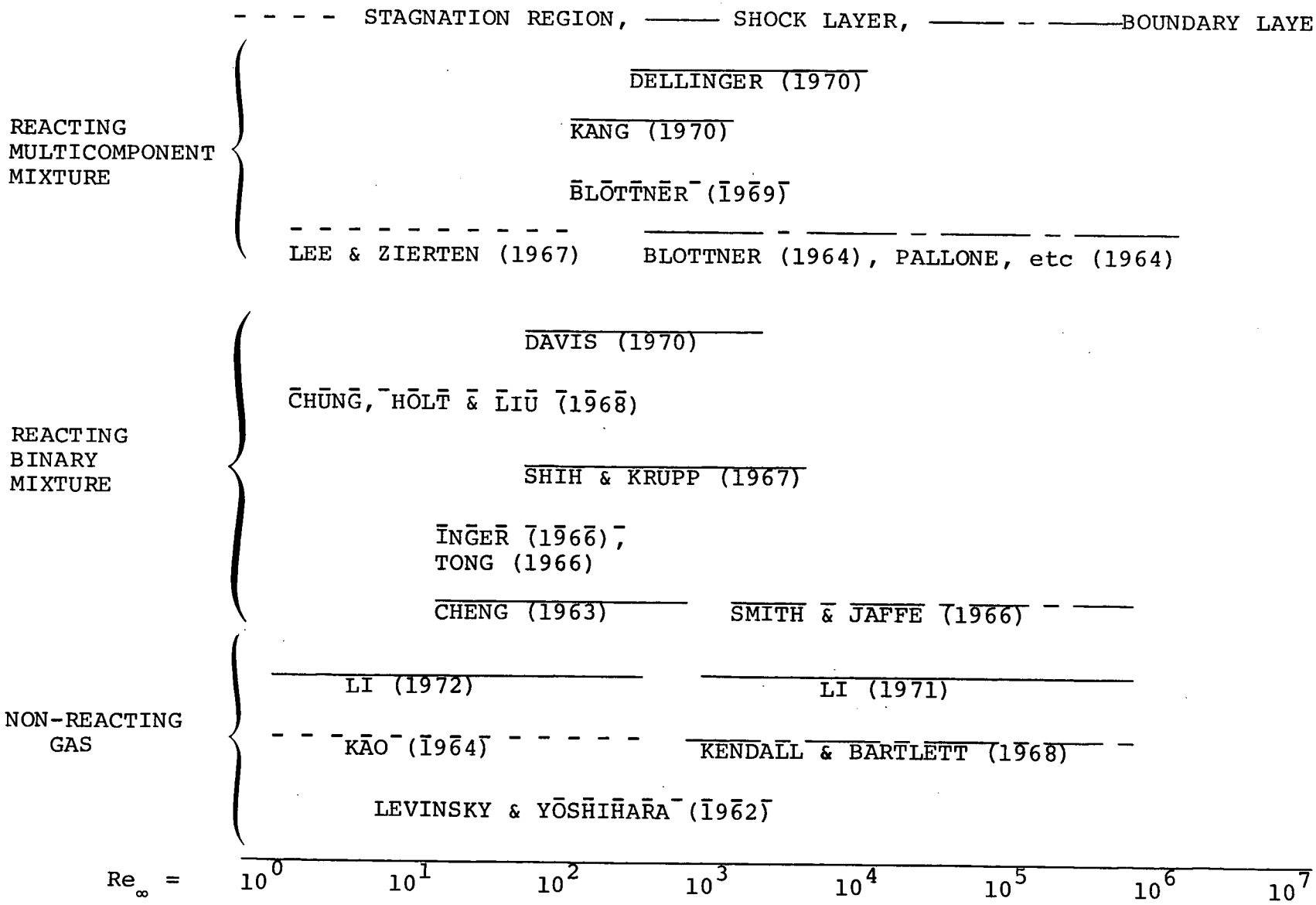

TABLE 2. NUMERICAL METHODS FOR ANALYZING VISCOUS REACTING FLOW FIELD

METHOD	EQUATION	ORBITER TRAJ. ALT.	ORBITER TRAJ. SPEED	TRANSPORT COEFFICIENT	METHOD OF SOLUTION	OUTER EDGE CONDITIONS REQUIRED	WALL CONDITION	EASE OF APPL.	COMPUTATIONS EFFICIENCY
STEADY FINITE DIFFERENCE (BLOTTNER)	BOUNDARY LAYER	LOW	NO RESTRICTION	APPROXIMATION TO CHAPMAN ENSKOG	COUPLED FLUID & KINETIC EQUATIONS	BOUNDARY-LAYER EDGE CONDITION	MASS TRANSFER	NO	MEDIUM
STEADY INTEGRAL RELATION (KANG DELLINGER)	THIN VISCOUS SHOCK LAYER	HIGH	HIGH	CONSTANT PRANDTL AND LEWIS NUMBERS	DECOUPLED FLUID & KINETIC EQUATIONS	VISCOUS SHOCK CONDITION	NONE	YES	HIGH
UNSTEADY FINITE DIFFERENCE	NAVIER STOKES	NO RESTRICTIONS	NO RESTRICTIONS	CHAPMAN ENSKOG	COUPLED FLUID & KINETIC EQUATIONS	NONE	NONE	YES	LOW

TABLE 3. ORTHOGONAL COORDINATE SYSTEM AND ITS SPECIAL FORMS

Space Coordinate / Coordinate System	ξ	η	ζ	h_1	h_2	h_3
Body Intrinsic	s	n	ϕ^j	1+kn	1	y^j
Polar	θ	r	ϕ^j	γ	1	$(r\sin\theta)^j$
Cylindrical or Cartesian	y	x	ϕ^j	1	1	y^j

j = 0 planar flow j = 1 axisymmetrical flow

k curvature

TABLE 4. METRIC COEFFICIENTS AND THEIR DERIVATIVES IN THE COMPUTATIONAL PLANE

COORDINATE SYSTEM \ METRIC COEFFICIENTS	h_1	h_2	h_3	$\frac{\partial h_1}{\partial z_1}$	$\frac{\partial h_1}{\partial z_2}$	$\frac{\partial h_3}{\partial z_1}$	$\frac{\partial h_3}{\partial z_2}$
Body Intrinsic	$1+k(1-z_2)\delta$	1	$y_b+(1-z_2)\delta\cos\phi$	$k(1-z_2)\delta_{z_1}$	$-k\delta$	$(y_{z_1}+(1-z_2))$ $(\delta_{z_1}\cos\phi-\delta\phi_{z_1}\sin\phi)^j$	$(-\delta\cos\phi)^j$
Polar	$h+(1-z_2)\delta$	1	$h_1\sin Z_1$	$(1-z_2)s_{z_1}$ $+ b_{z_1}$	$-\delta$	$\left(\frac{\partial h_1}{\partial z_2}\sin Z_2+h_1\cos Z_1\right)^j$	$\left(\frac{\partial h_1}{\partial z_2}\sin Z_1\right)^j$
Cylindrical or Cartesian	1	1	z_2	0	0	j	0

$$\frac{\partial h_2}{\partial z_1} = \frac{\partial h_2}{\partial z_2} = 0 \quad , \quad j = 0 \quad \text{planar flow,} \quad j = 1 \quad \text{axisymmetric flow}$$

TABLE 5. FREE STREAM CONDITIONS FOR THE ORBITER TRAJECTORY POINTS INVESTIGATED IN THIS STUDY

Point	Altitude	Speed	Temp °R	Pressure lb/ft^2	Density $slug/ft^3$	Enthalpy $(ft/sec)^2$	Mach Number	Reynolds Number Re/RN
0	100,000	2,500	420	23.08	3.21×10^{-5}	2.52×10^{6}	2.5	257,000
1	150,000	8,000	503	3.06	3.56×10^{-6}	3.02×10^{6}	7.3	80,000
2	200,000	14,000	447	.4715	6.12×10^{-7}	2.69×10^{6}	13.1	39,000
3	250,000	24,000	328	4.364×10^{-2}	7.78×10^{-8}	1.98×10^{6}	27.0	7,200
4	300,000	26,000	300	2.118×10^{-3}	4.12×10^{-9}	1.79×10^{6}	30.7	450
5	350,000	25,000	426	2.38×10^{-4}	3.54×10^{-10}	2.56×10^{6}	19.3	30

TABLE 6. DESCRIPTIONS OF CASES CALCULATED FOR AN ORBITER

RUN NUMBER		1	2	3	4	5	6	7	8	9	10	11	12	13	14	15	16	17	18	19	20
TRAJECTORY POINT		0	1			2							3							4	
IDEAL GAS		X	X			X							X							X	
EQUILIBRIUM AIR				X			X							X							
NONEQUILIBRIUM AIR					X			X	X	X	X	X			X	X	X	X	X		X
WALL TEMPERATURE	ISOTHERMAL	X	X	X	X	X	X	X	X			X	X	X	X	X			X	X	X
	ADIABATIC									X	X						X	X			
WALL CATALYTITY	CATALYTIC				X			X		X		X			X		X				X
	NON-CATALYTIC								X		X					X		X	X		
TRANSPORT PROPERTY	SIMPLE	X	X	X	X	X	X	X	X	X	X		X	X	X	X	X	X		X	
	MULTI-COMPONENT											X							X		X

NOTE: 1) Trajectory point 0, 1, 2 and 3 are calculated using the sharp-shock formulation, point 4 using thick-shock formulation. 2) Isothermal wall temperature is $T_w=T\infty$ for points 0 and 1, $T_w=8T\infty$ for points 2, 3, and 4. 3) Simple transport properties are given by the Sutherland formula and constant Prandtl and Lewis numbers.

10.0 LIST OF FIGURES

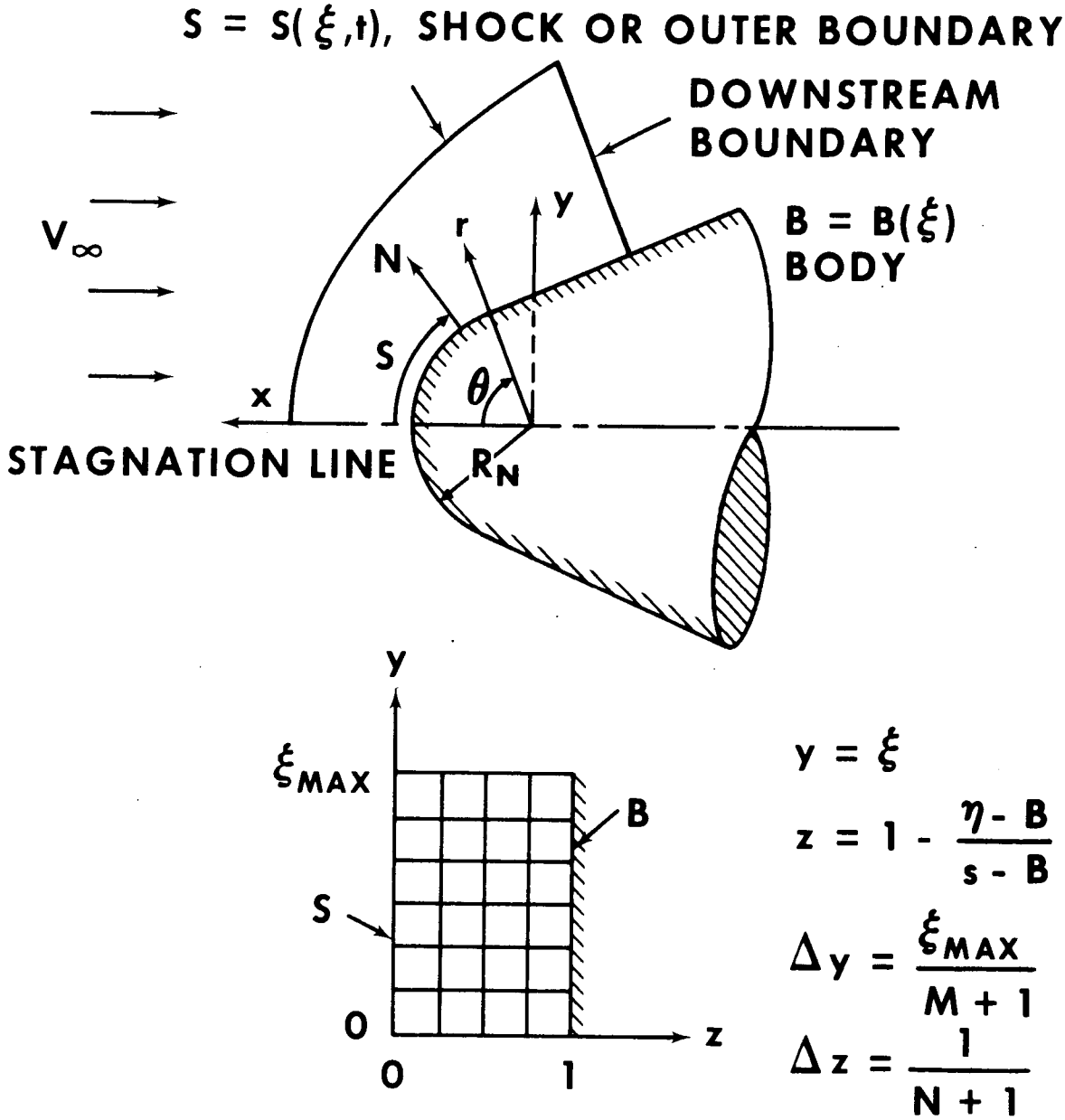
S = S(ξ,t), SHOCK OR OUTER BOUNDARY
DOWNSTREAM BOUNDARY
B = B(ξ) BODY
V∞
N
r
y
S
θ
x
STAGNATION LINE
R_N
y
ξ_MAX
B
S
0
z
0
1
y = ξ
z = 1 - (η - B)/(s - B)
Δy = ξ_MAX/(M + 1)
Δz = 1/(N + 1)

FIGURE 1

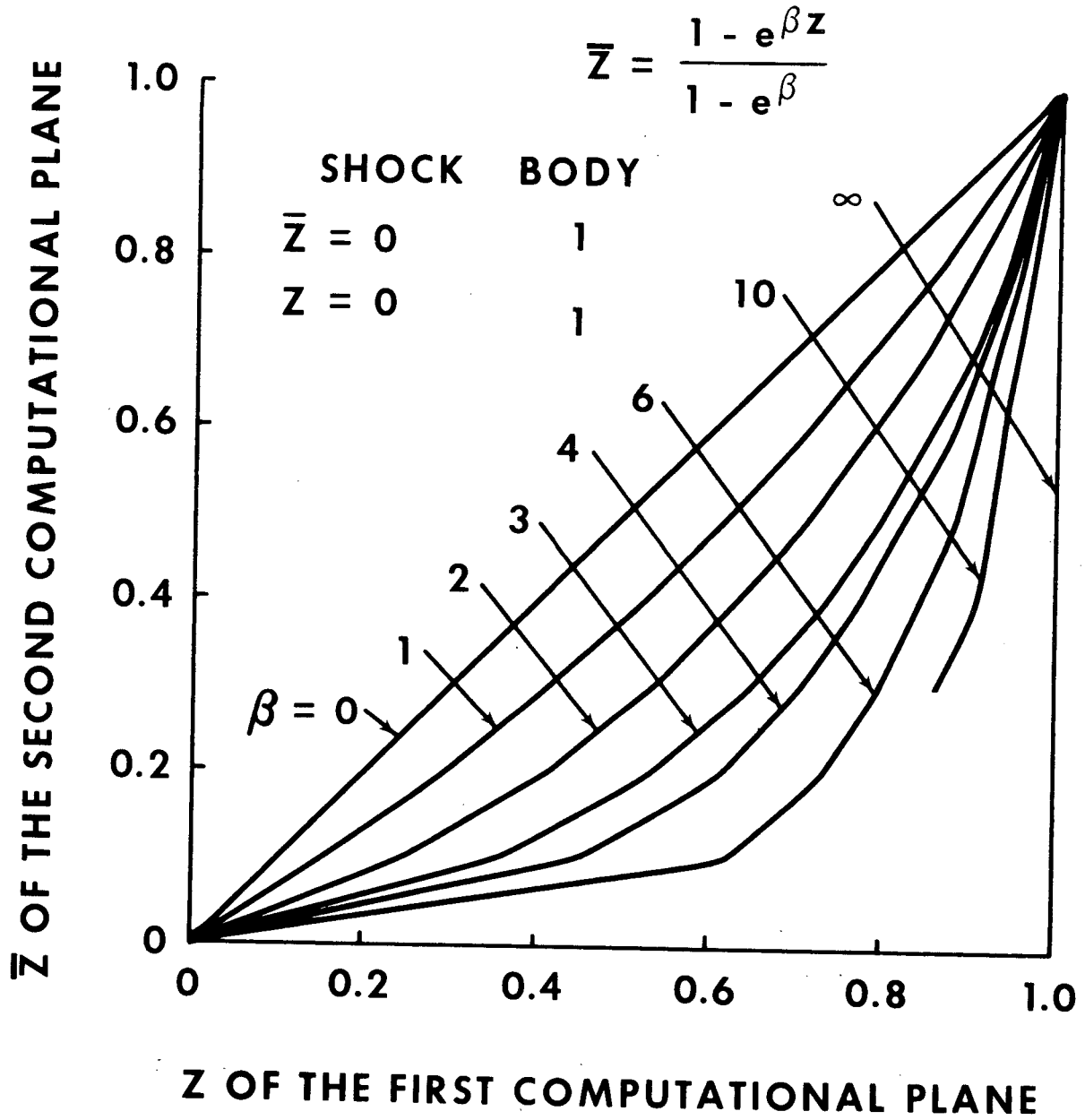
$\bar{Z} = \frac{1 - e^{\beta z}}{1 - e^{\beta}}$
SHOCK BODY
$\bar{Z} = 0$ 1
$Z = 0$ 1
$\beta = 0$
1
2
3
4
6
10
∞
1.0
0.8
0.6
0.4
0.2
0
0
0.2
0.4
0.6
0.8
1.0
$\bar{Z}$ OF THE SECOND COMPUTATIONAL PLANE
Z OF THE FIRST COMPUTATIONAL PLANE

FIGURE 2

$$\begin{pmatrix} r \\ \theta \end{pmatrix} = \begin{pmatrix} \cos\psi & -\sin\psi \\ \sin\psi & \cos\psi \end{pmatrix} = \begin{pmatrix} n \\ s \end{pmatrix}$$

$$\begin{pmatrix} V \\ U \end{pmatrix} = \begin{pmatrix} \cos\psi & -\sin\psi \\ +\sin\psi & \cos\psi \end{pmatrix} = \begin{pmatrix} -V_S \\ U_S \end{pmatrix}$$

$$\begin{pmatrix} -V_S \\ U_S \end{pmatrix} = \begin{pmatrix} \cos\psi & \sin\psi \\ -\sin\psi & \cos\psi \end{pmatrix} = \begin{pmatrix} V \\ U \end{pmatrix}$$

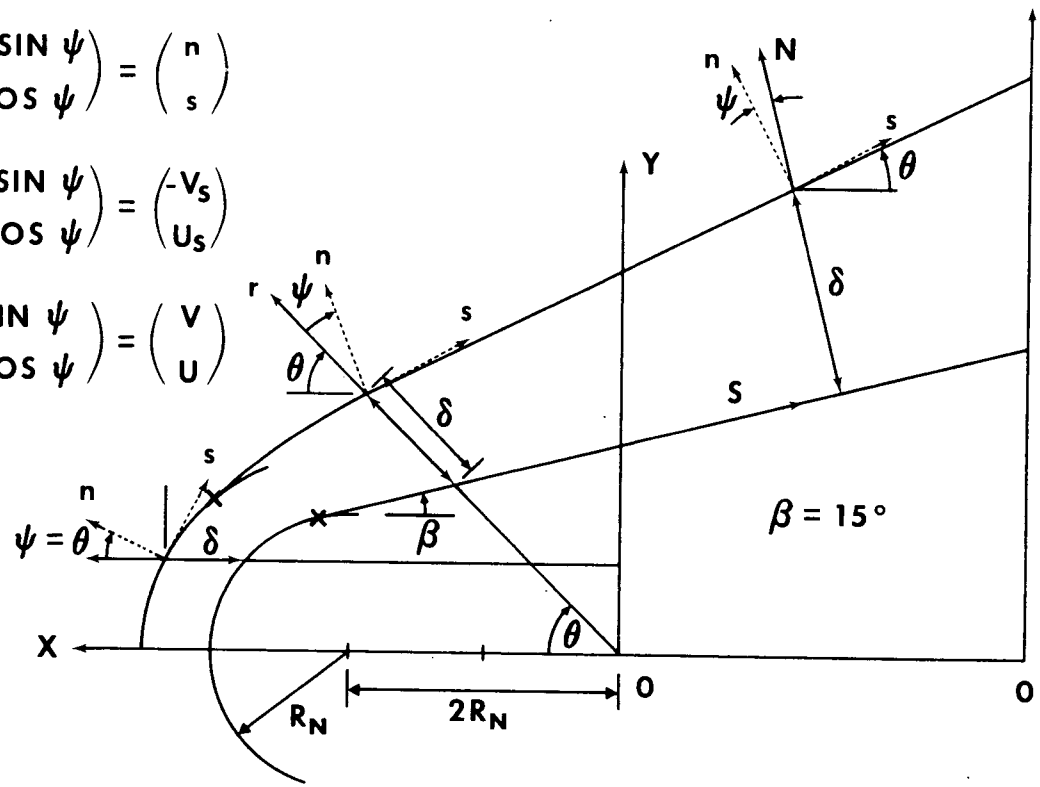

$$\begin{pmatrix} S \\ N \end{pmatrix} = \begin{pmatrix} -\sin\psi & \cos\psi \\ \cos\psi & \sin\psi \end{pmatrix} = \begin{pmatrix} n \\ s \end{pmatrix}$$

$$\begin{pmatrix} U \\ V \end{pmatrix} = \begin{pmatrix} -\sin\psi & \cos\psi \\ \cos\psi & \sin\psi \end{pmatrix} = \begin{pmatrix} -V_S \\ U_S \end{pmatrix}$$

$$\begin{pmatrix} -V_S \\ U_S \end{pmatrix} = \begin{pmatrix} -\sin\psi & \cos\psi \\ \cos\psi & \sin\psi \end{pmatrix} = \begin{pmatrix} U \\ V \end{pmatrix}$$

FIGURE 3

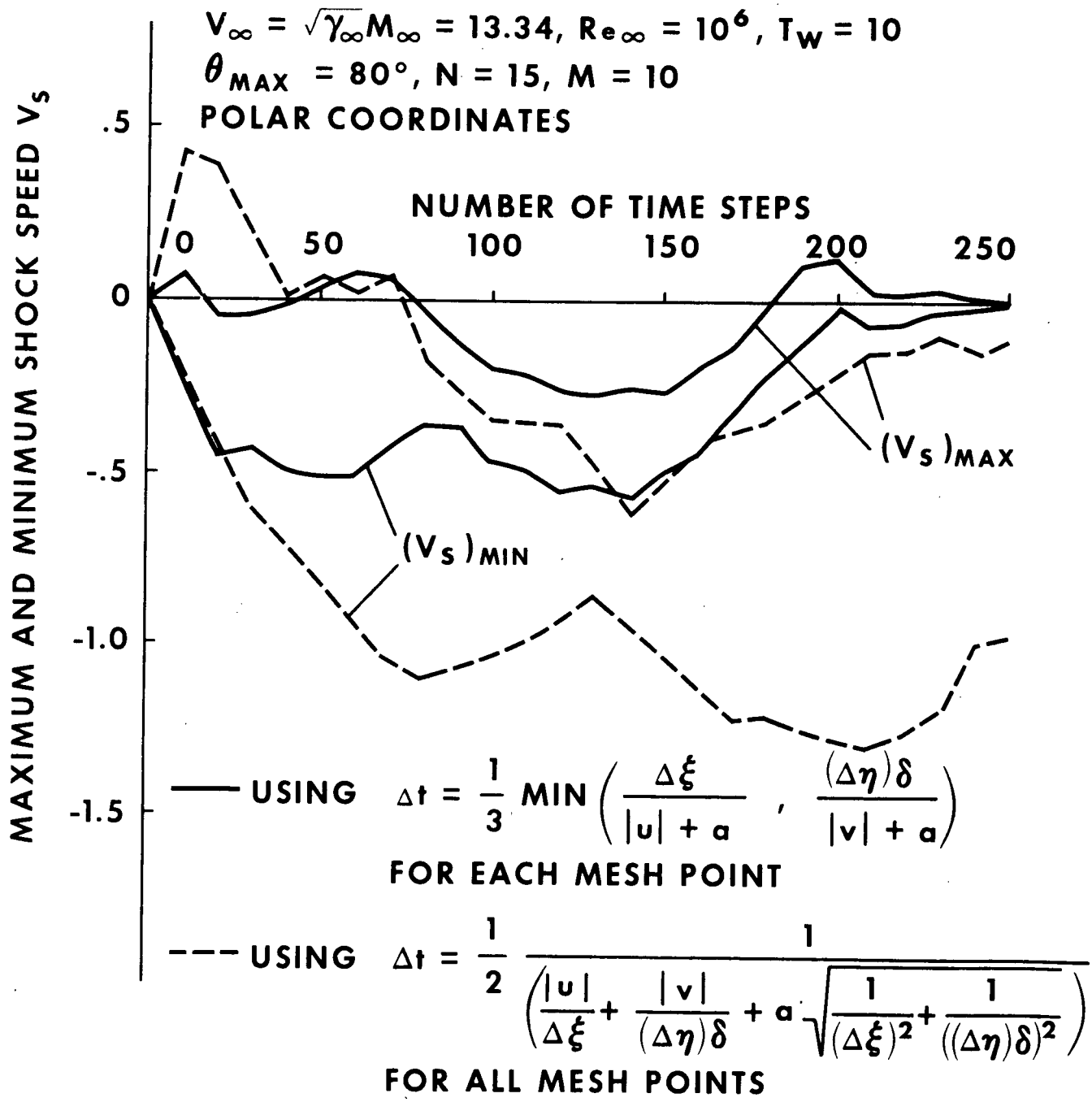
$V_\infty = \sqrt{\gamma_\infty} M_\infty = 13.34$, $Re_\infty = 10^6$, $T_W = 10$
$\theta_{MAX} = 80°$, N = 15, M = 10
POLAR COORDINATES
MAXIMUM AND MINIMUM SHOCK SPEED V_S
.5
0
-.5
-1.0
-1.5
NUMBER OF TIME STEPS
0
50
100
150
200
250
$(V_S)_{MAX}$
$(V_S)_{MIN}$
USING $\Delta t = \frac{1}{3} \text{MIN}\left(\frac{\Delta\xi}{|u| + a}, \frac{(\Delta\eta)\delta}{|v| + a}\right)$
FOR EACH MESH POINT
USING $\Delta t = \frac{1}{2} \frac{1}{\left(\frac{|u|}{\Delta\xi} + \frac{|v|}{(\Delta\eta)\delta} + a\sqrt{\frac{1}{(\Delta\xi)^2} + \frac{1}{((\Delta\eta)\delta)^2}}\right)}$
FOR ALL MESH POINTS

FIGURE 4

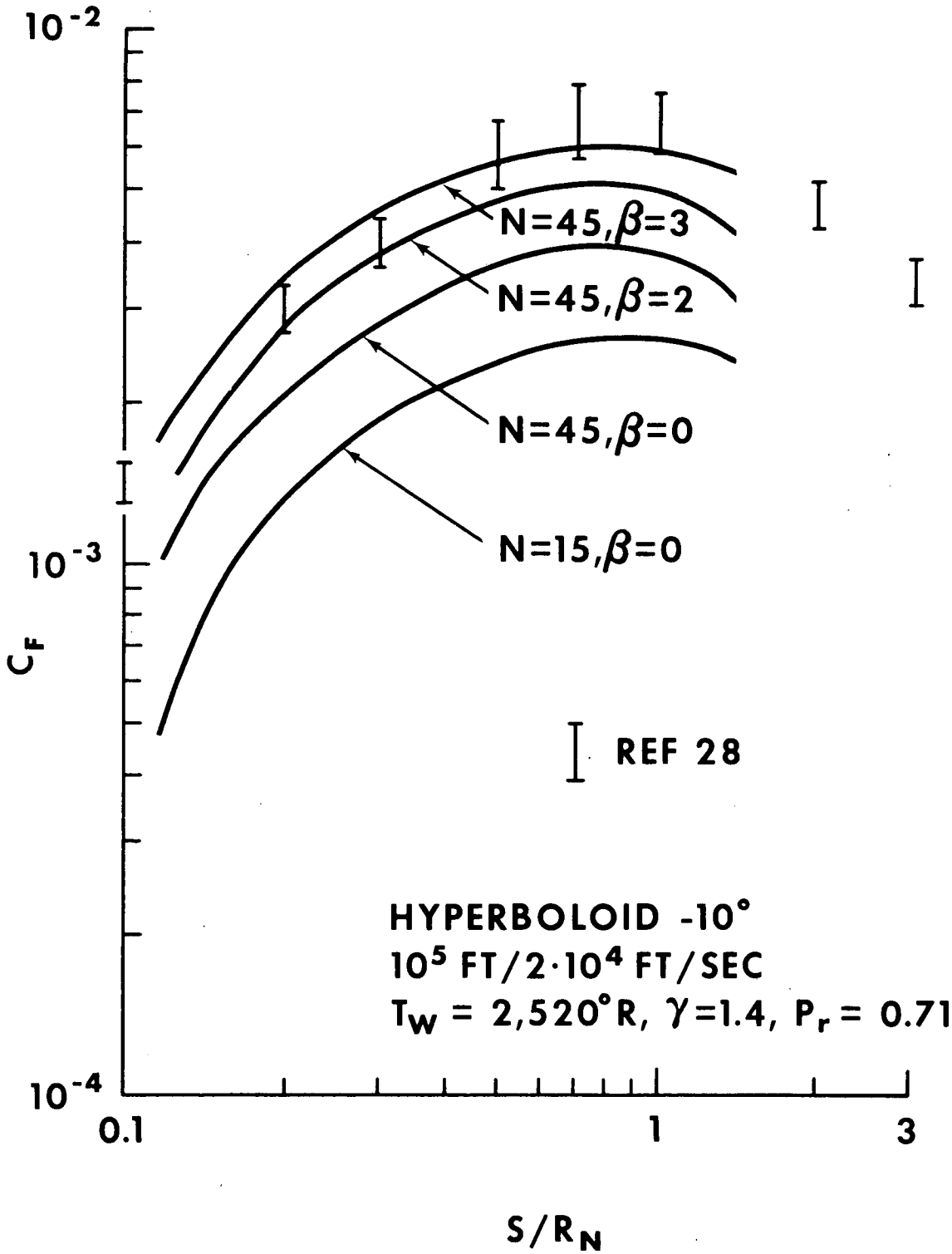
10^{-2}
10^{-3}
10^{-4}
C_F
N=45,β=3
N=45,β=2
N=45,β=0
N=15,β=0
REF 28
HYPERBOLOID -10°
10^5 FT/$2\cdot10^4$ FT/SEC
T_W = 2,520°R, γ=1.4, P_r = 0.71
0.1
1
3
S/R_N

FIGURE 5

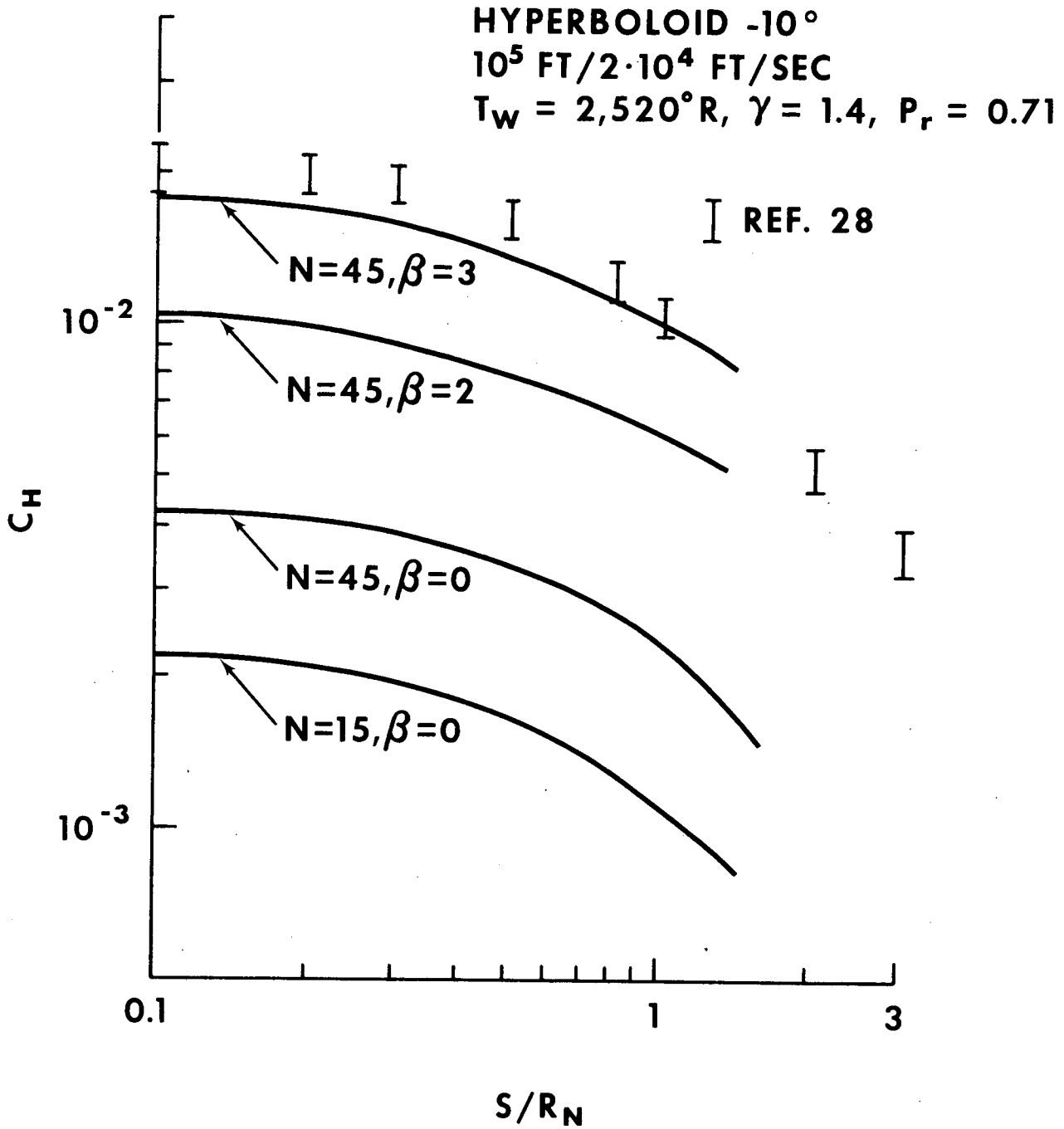
HYPERBOLOID -10°
10^5 FT/2·10^4 FT/SEC
T_W = 2,520°R, γ = 1.4, P_r = 0.71
REF. 28
N=45,β=3
N=45,β=2
N=45,β=0
N=15,β=0
10^-2
10^-3
C_H
0.1
1
3
S/R_N

FIGURE 5

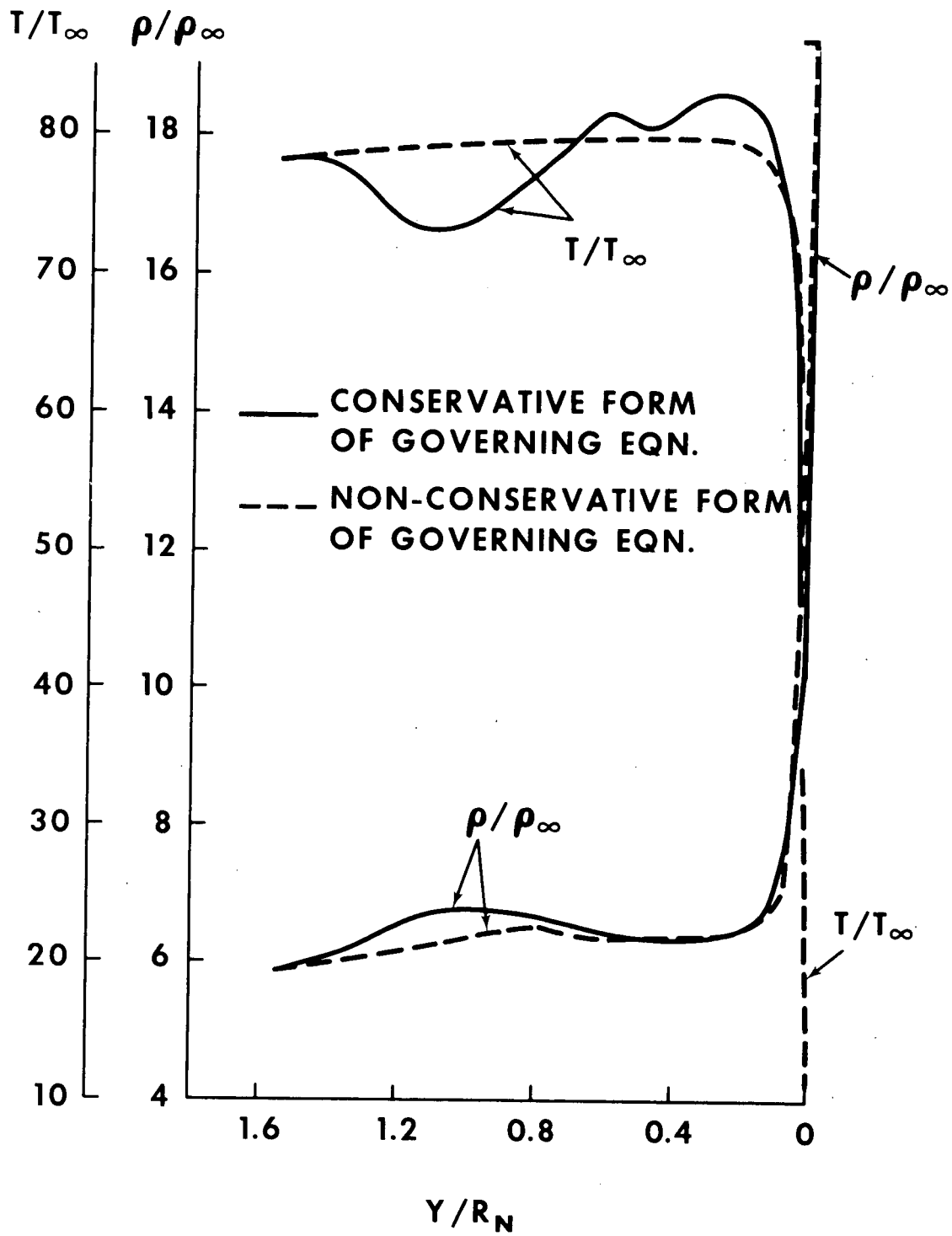
T/T∞
ρ/ρ∞
80
70
60
50
40
30
20
10
18
16
14
12
10
8
6
4
T/T∞
ρ/ρ∞
CONSERVATIVE FORM OF GOVERNING EQN.
NON-CONSERVATIVE FORM OF GOVERNING EQN.
ρ/ρ∞
T/T∞
1.6
1.2
0.8
0.4
0
Y/R_N

FIGURE 6

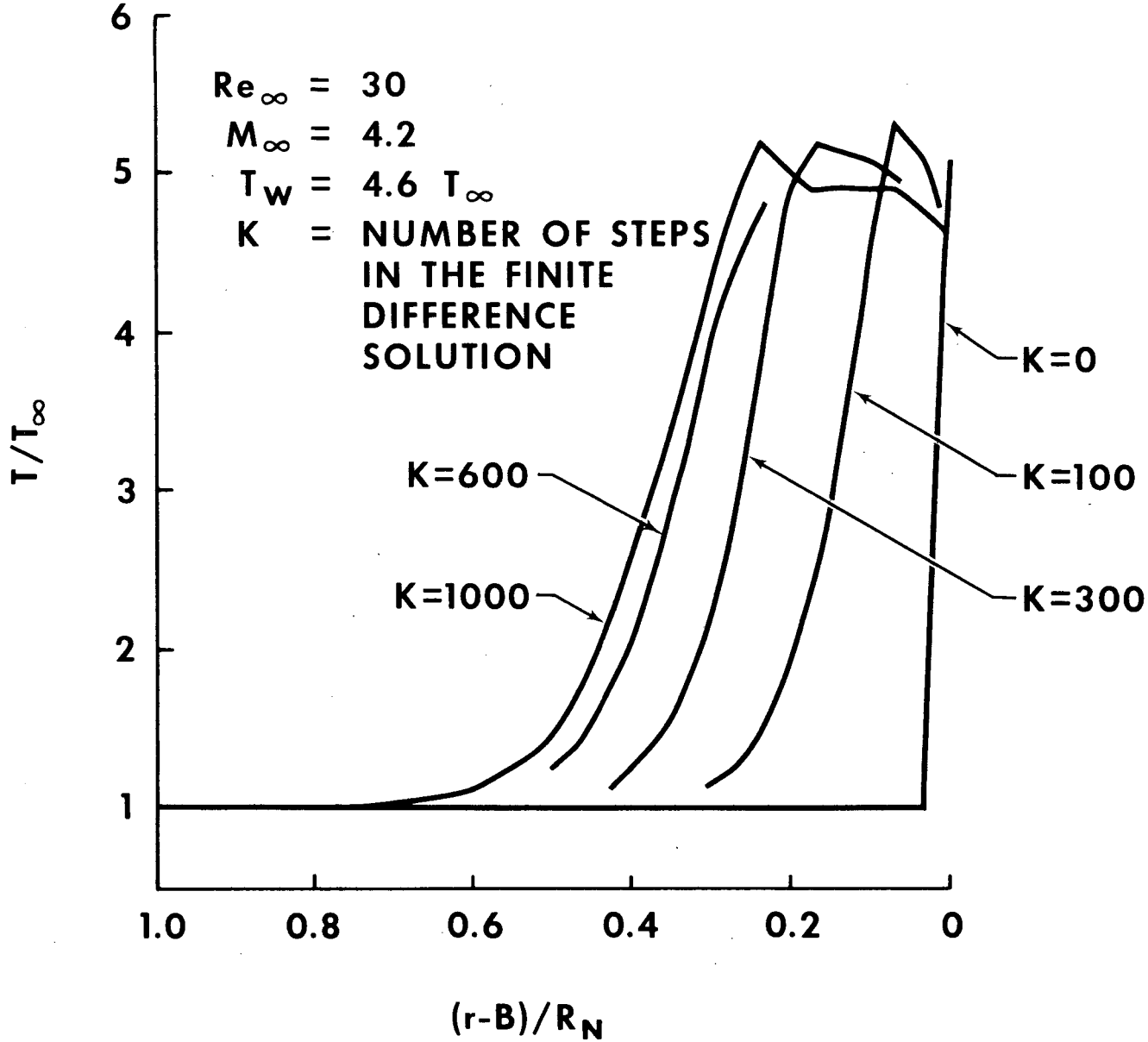
Re_∞ = 30
M_∞ = 4.2
T_W = 4.6 T_∞
K = NUMBER OF STEPS IN THE FINITE DIFFERENCE SOLUTION
K=0
K=100
K=300
K=600
K=1000
T/T_∞
$(r-B)/R_N$
6
5
4
3
2
1
1.0
0.8
0.6
0.4
0.2
0

FIGURE 7

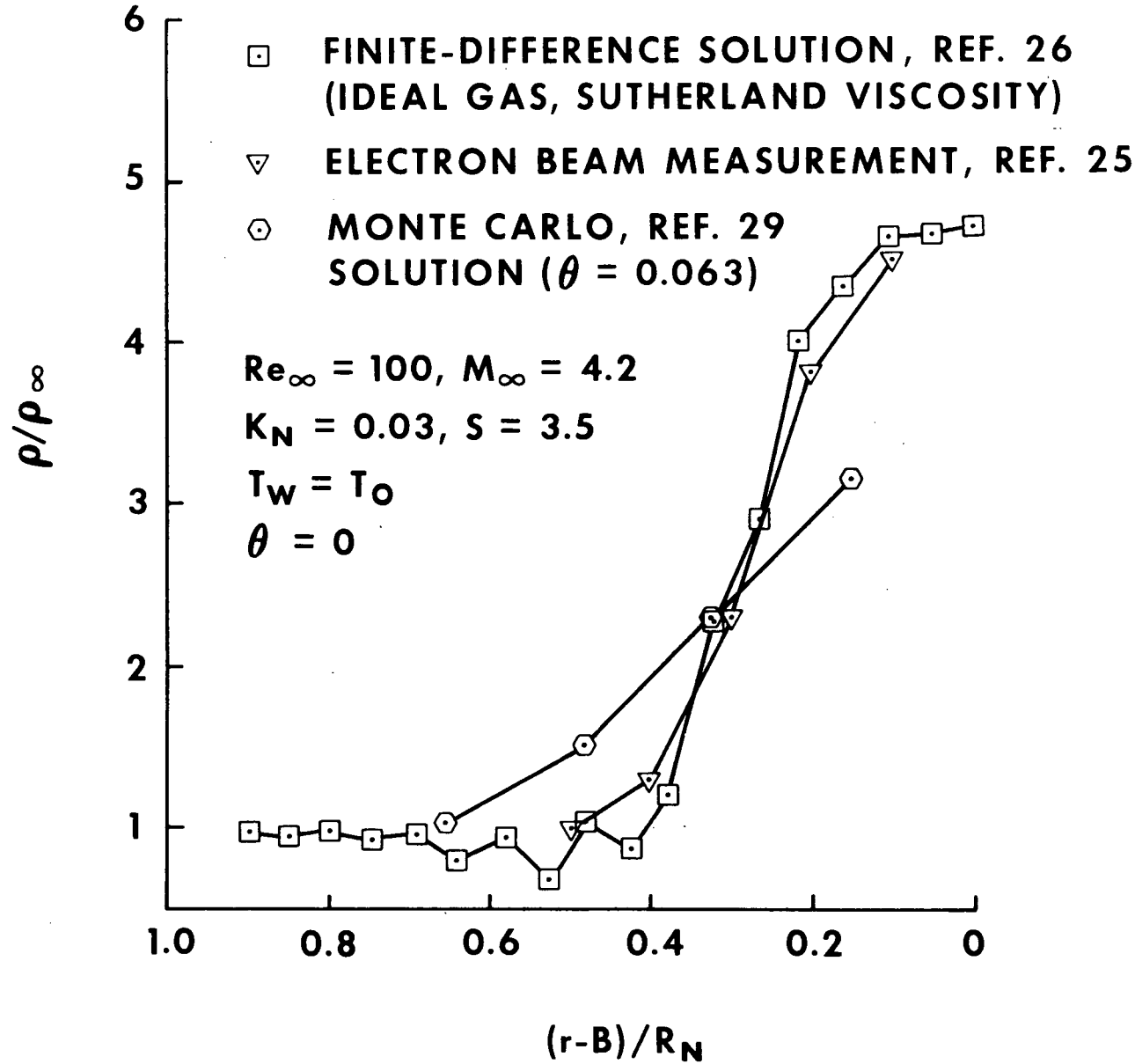
FINITE-DIFFERENCE SOLUTION, REF. 26
(IDEAL GAS, SUTHERLAND VISCOSITY)
ELECTRON BEAM MEASUREMENT, REF. 25
MONTE CARLO, REF. 29
SOLUTION (θ = 0.063)
Re∞ = 100, M∞ = 4.2
KN = 0.03, S = 3.5
TW = TO
θ = 0
ρ/ρ∞
6
5
4
3
2
1
1.0
0.8
0.6
0.4
0.2
0
(r-B)/RN

FIGURE 7

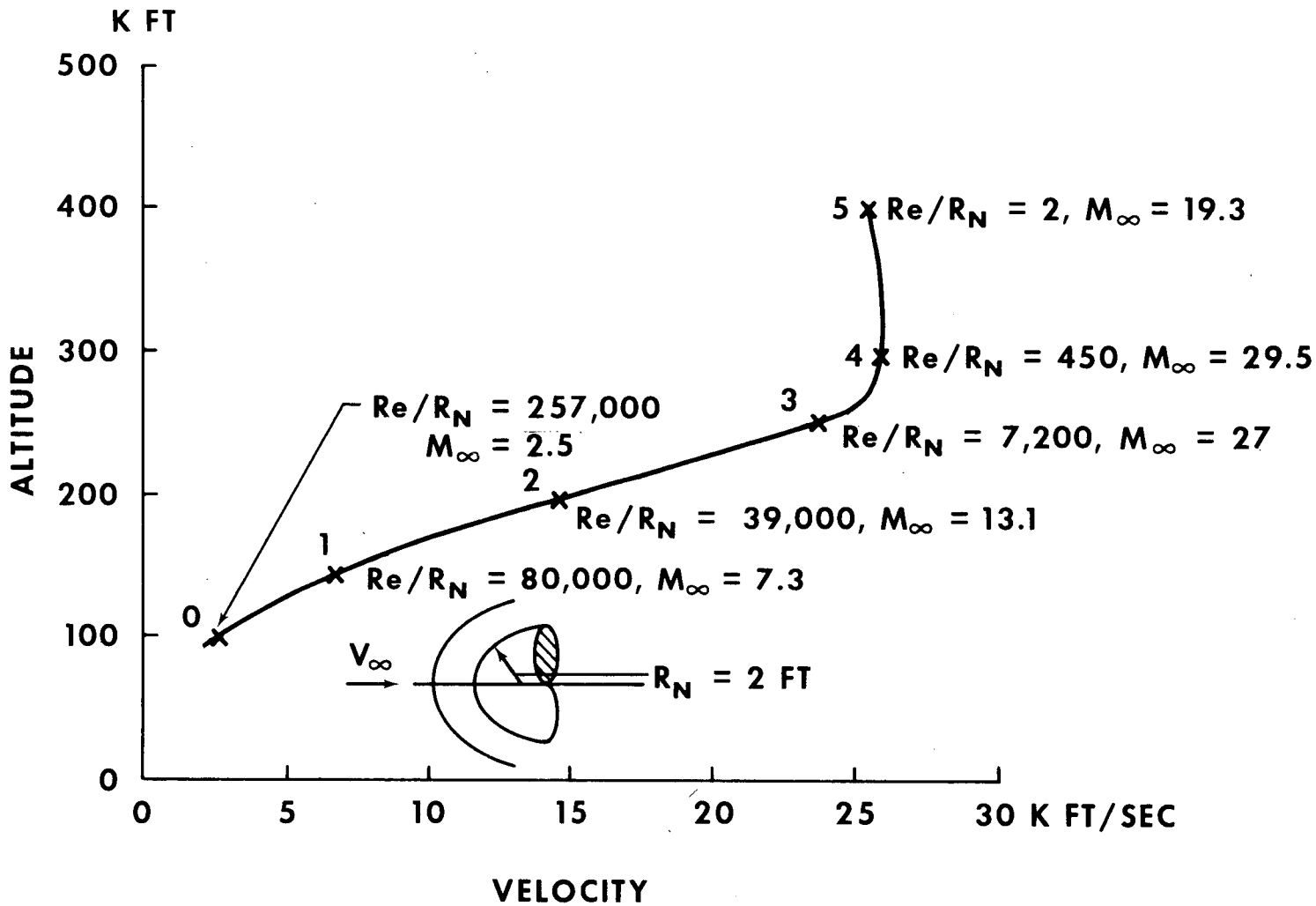
K FT
500
400
300
200
100
0
ALTITUDE
0
5
10
15
20
25
30 K FT/SEC
VELOCITY
5 Re/R_N = 2, M∞ = 19.3
4 Re/R_N = 450, M∞ = 29.5
3
Re/R_N = 7,200, M∞ = 27
2
Re/R_N = 39,000, M∞ = 13.1
1
Re/R_N = 80,000, M∞ = 7.3
0
Re/R_N = 257,000
M∞ = 2.5
V∞
R_N = 2 FT

FIGURE 8

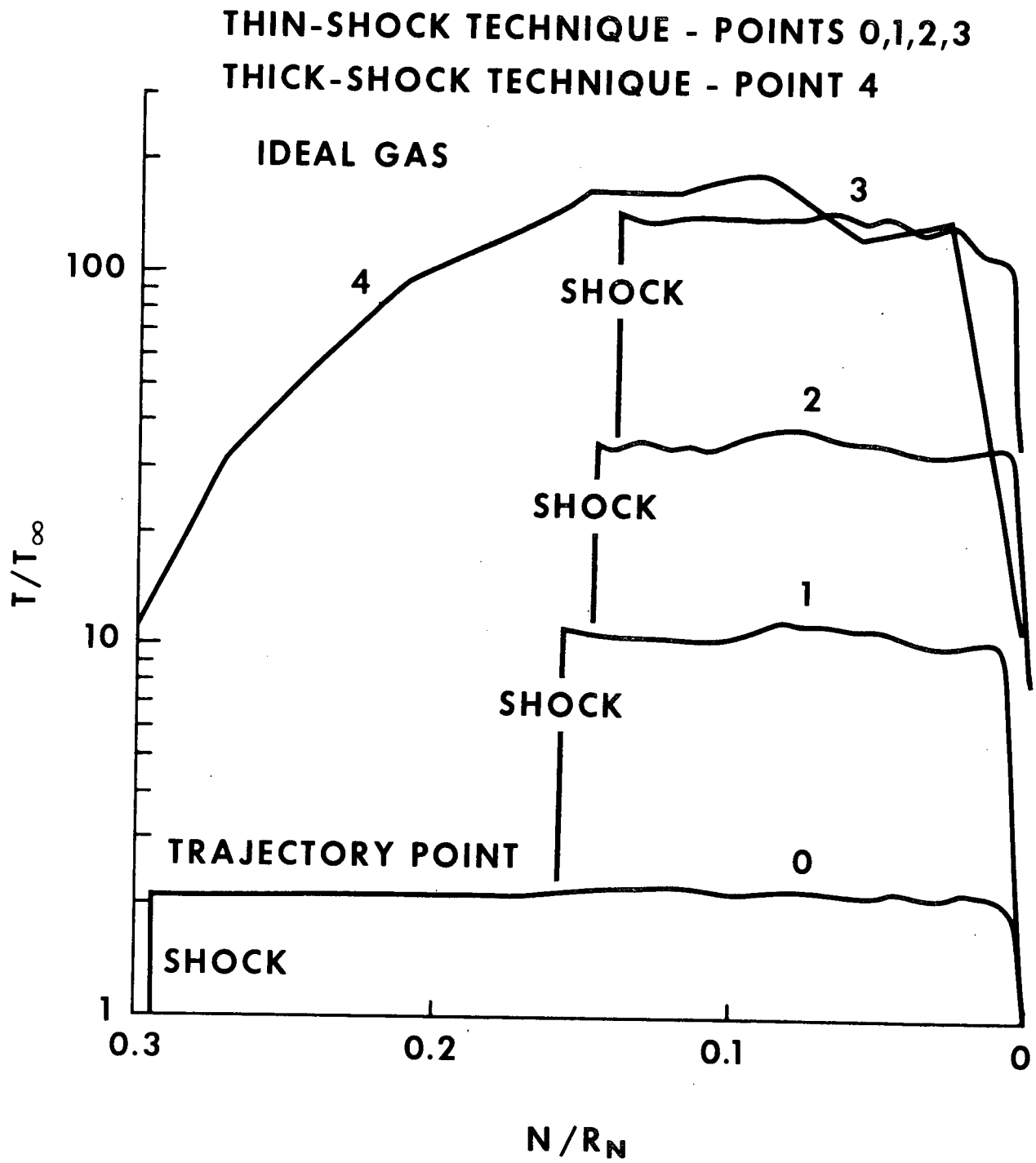
THIN-SHOCK TECHNIQUE - POINTS 0,1,2,3
THICK-SHOCK TECHNIQUE - POINT 4
IDEAL GAS
100
10
1
T/T∞
4
3
SHOCK
2
SHOCK
1
SHOCK
TRAJECTORY POINT
0
SHOCK
0.3
0.2
0.1
0
N/RN

FIGURE 9

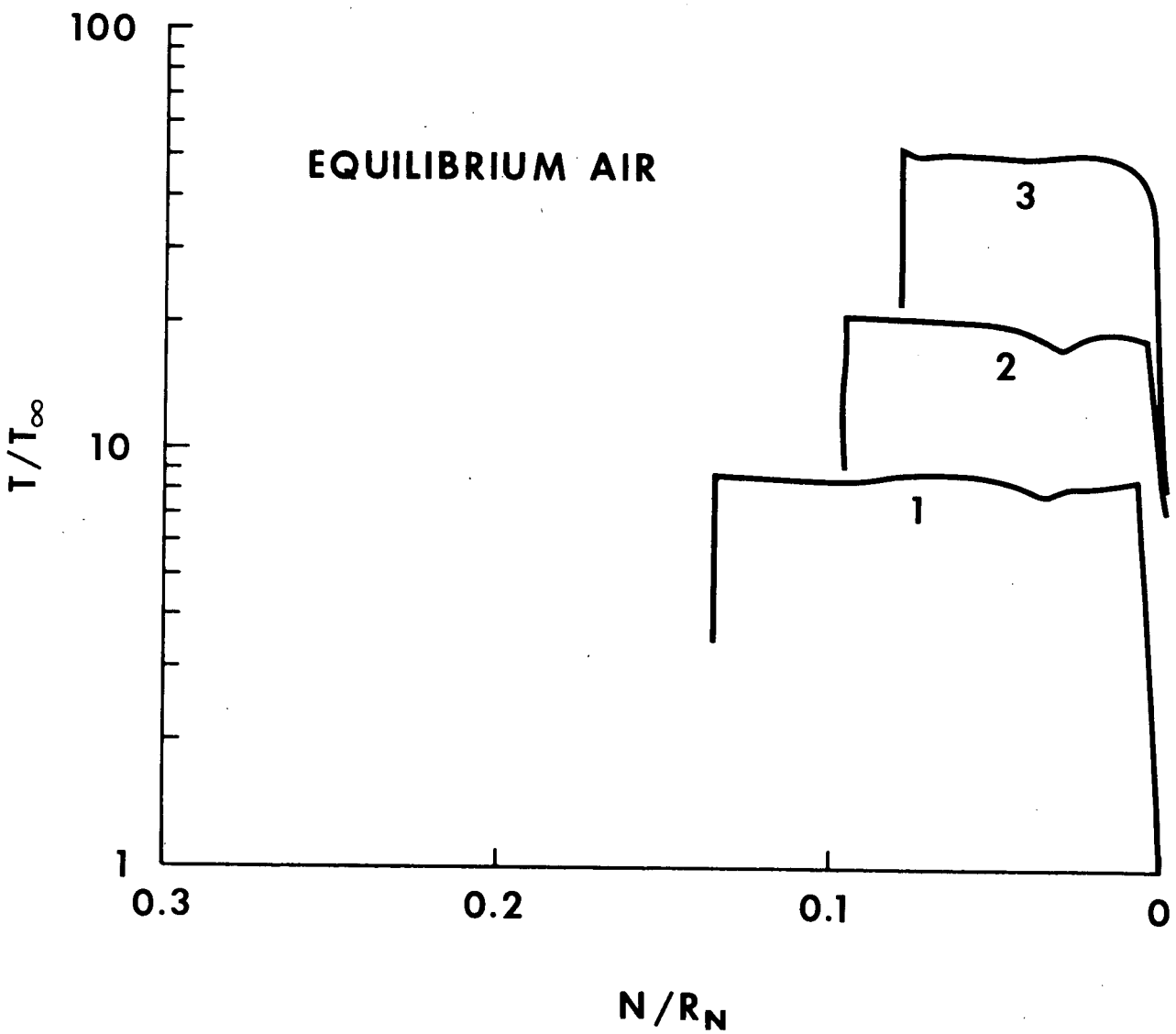

FIGURE 9

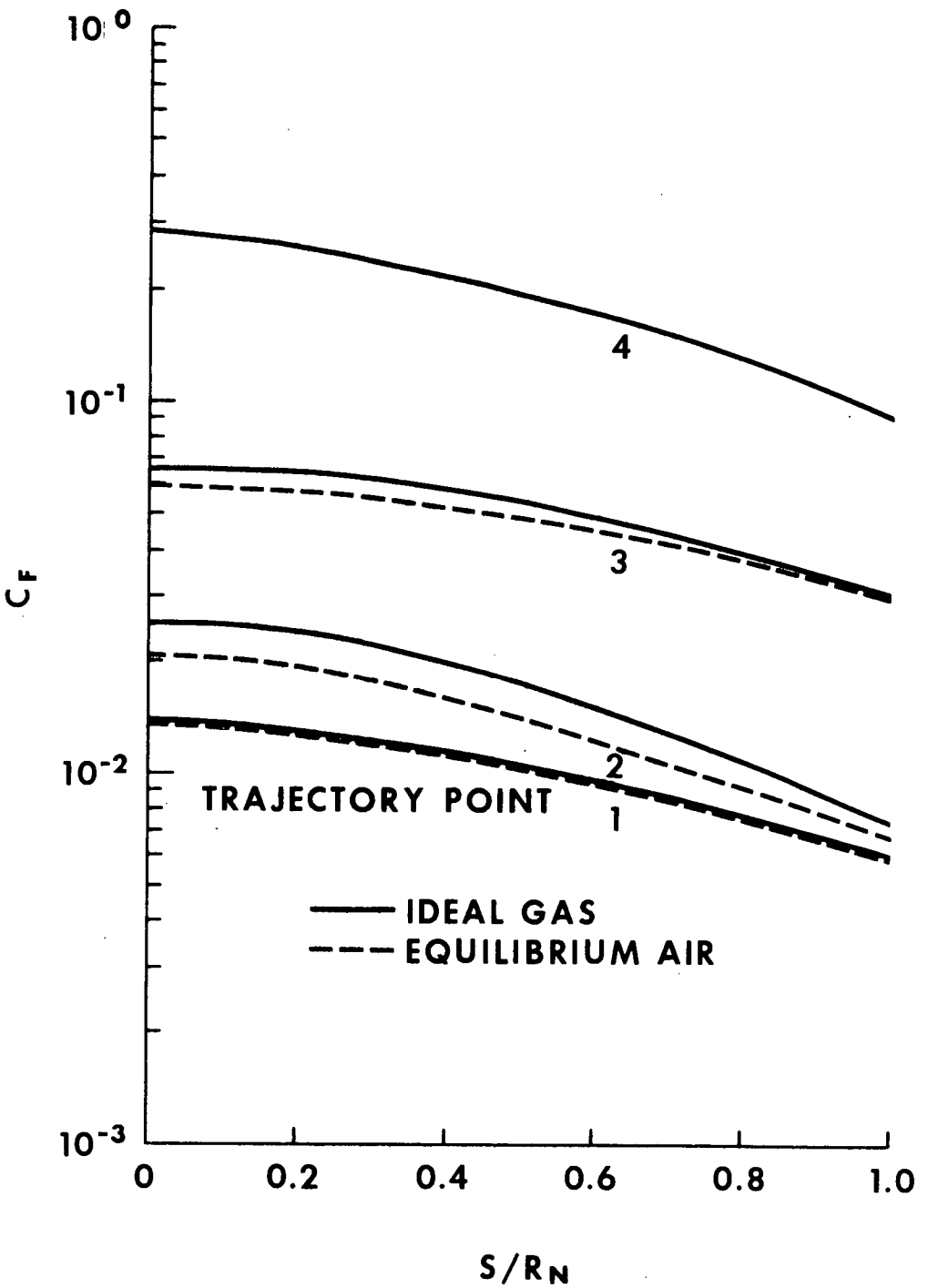
10^0
10^{-1}
10^{-2}
10^{-3}
C_F
4
3
2
1
TRAJECTORY POINT
IDEAL GAS
EQUILIBRIUM AIR
0
0.2
0.4
0.6
0.8
1.0
S/R_N

FIGURE 10

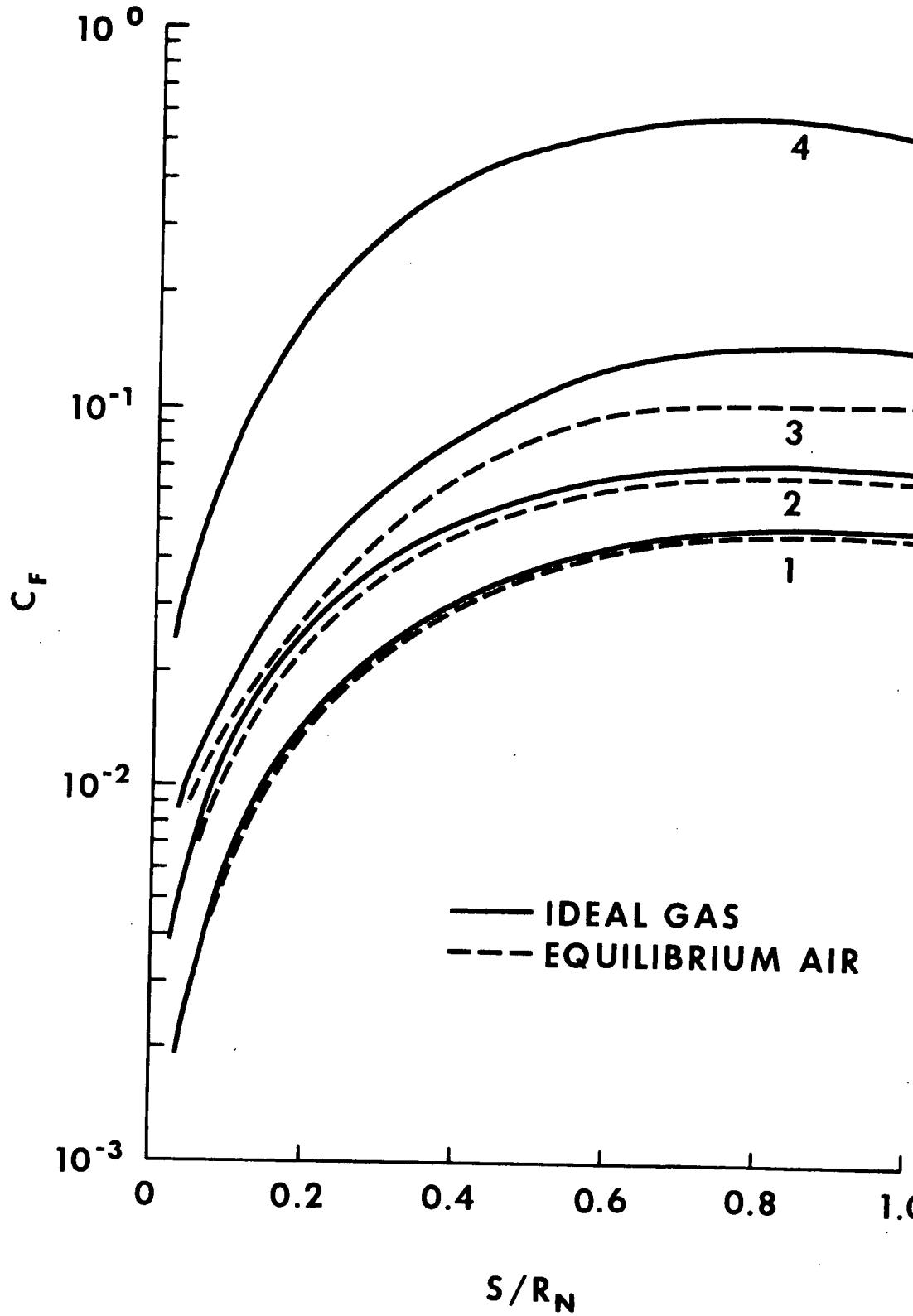
10^0
10^{-1}
10^{-2}
10^{-3}
C_F
4
3
2
1
IDEAL GAS
EQUILIBRIUM AIR
0
0.2
0.4
0.6
0.8
1.0
S/R_N

FIGURE 11

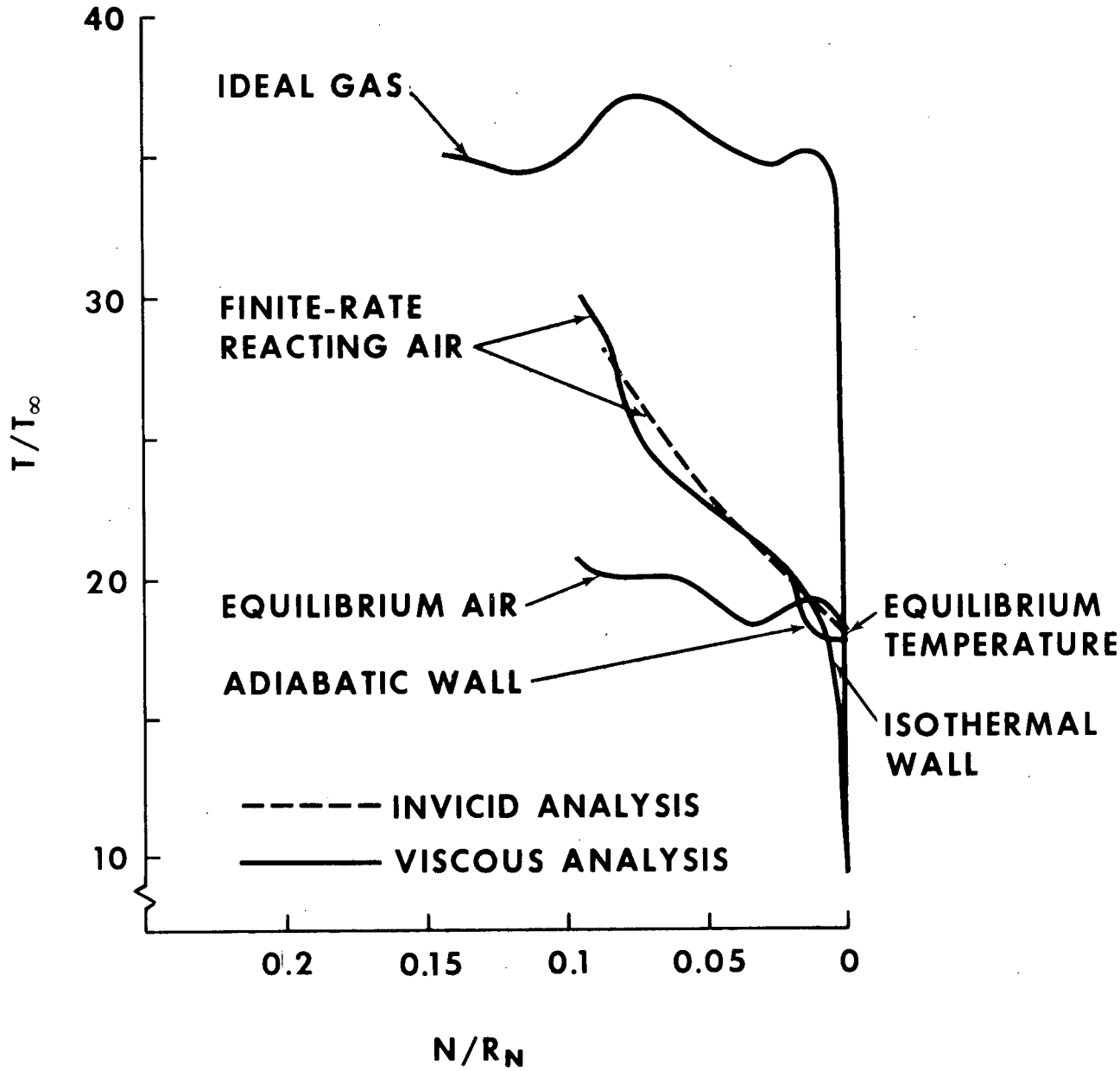

(a) $S/R_N = 0$

FIGURE 12

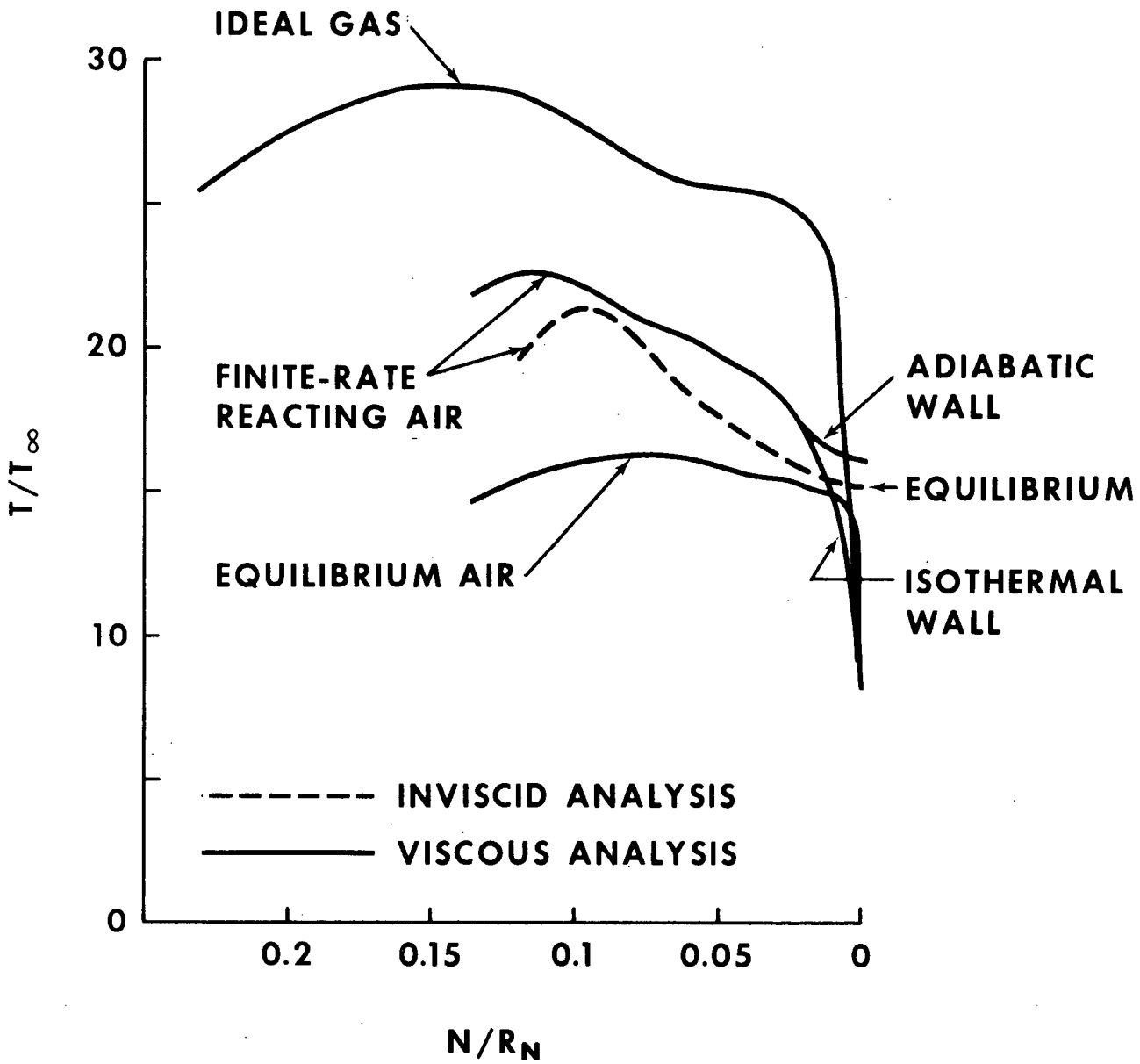

(b) $S/R_N = 0.7$

FIGURE 12

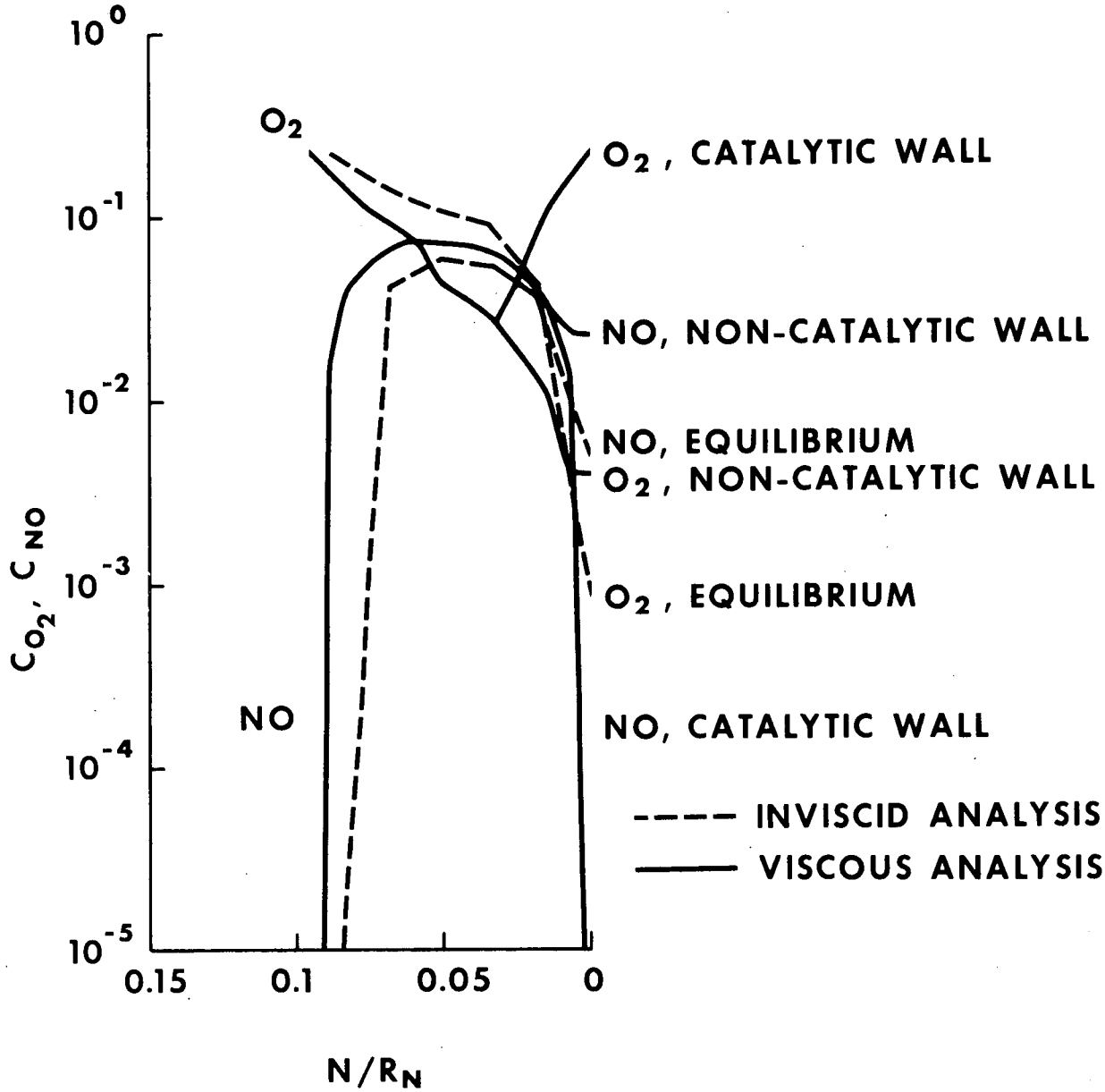

(a) $\left(\frac{\partial e}{\partial n}\right)_w = 0$

FIGURE 13

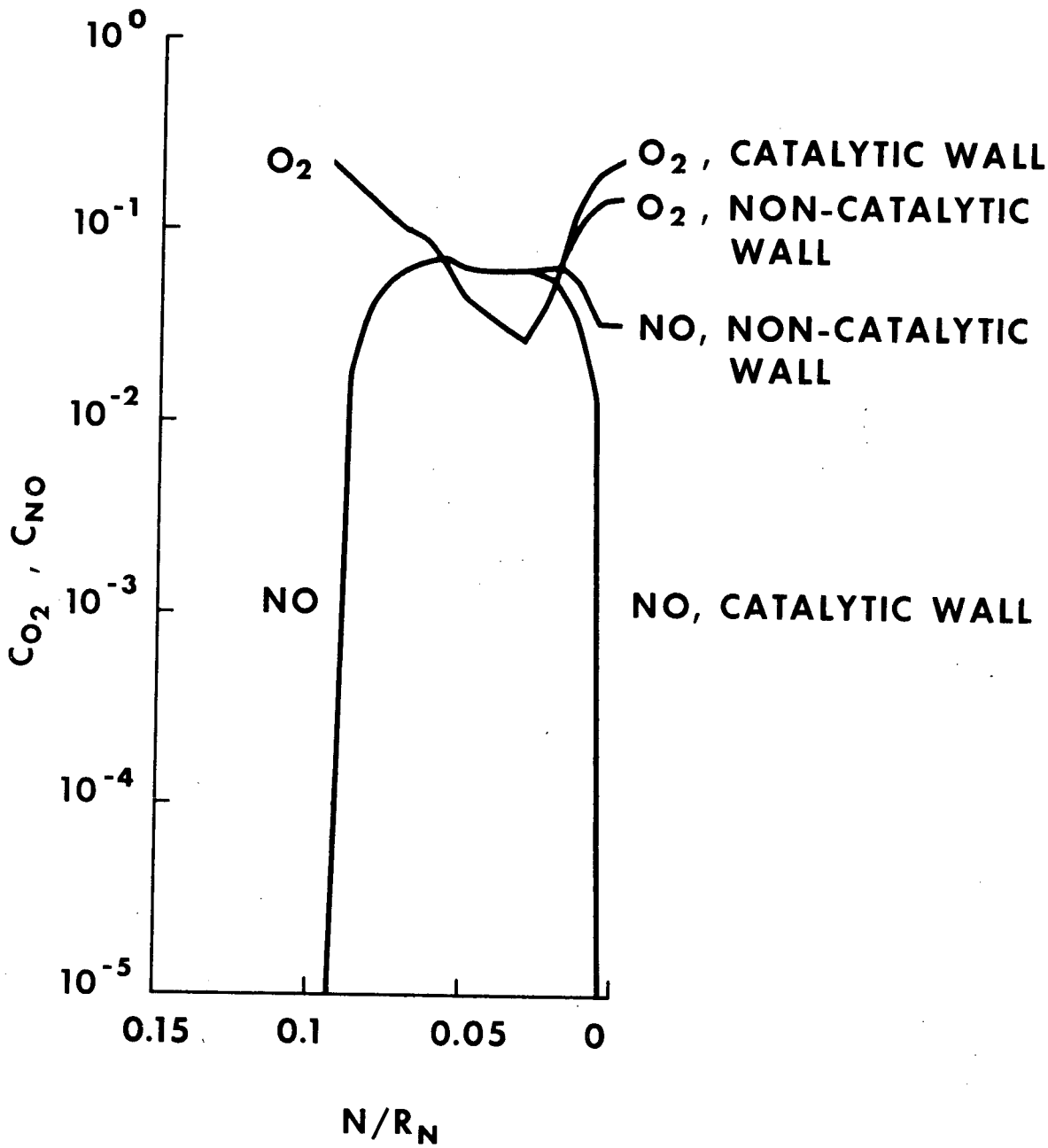

(b) $e_w = 8e_\infty$

FIGURE 13

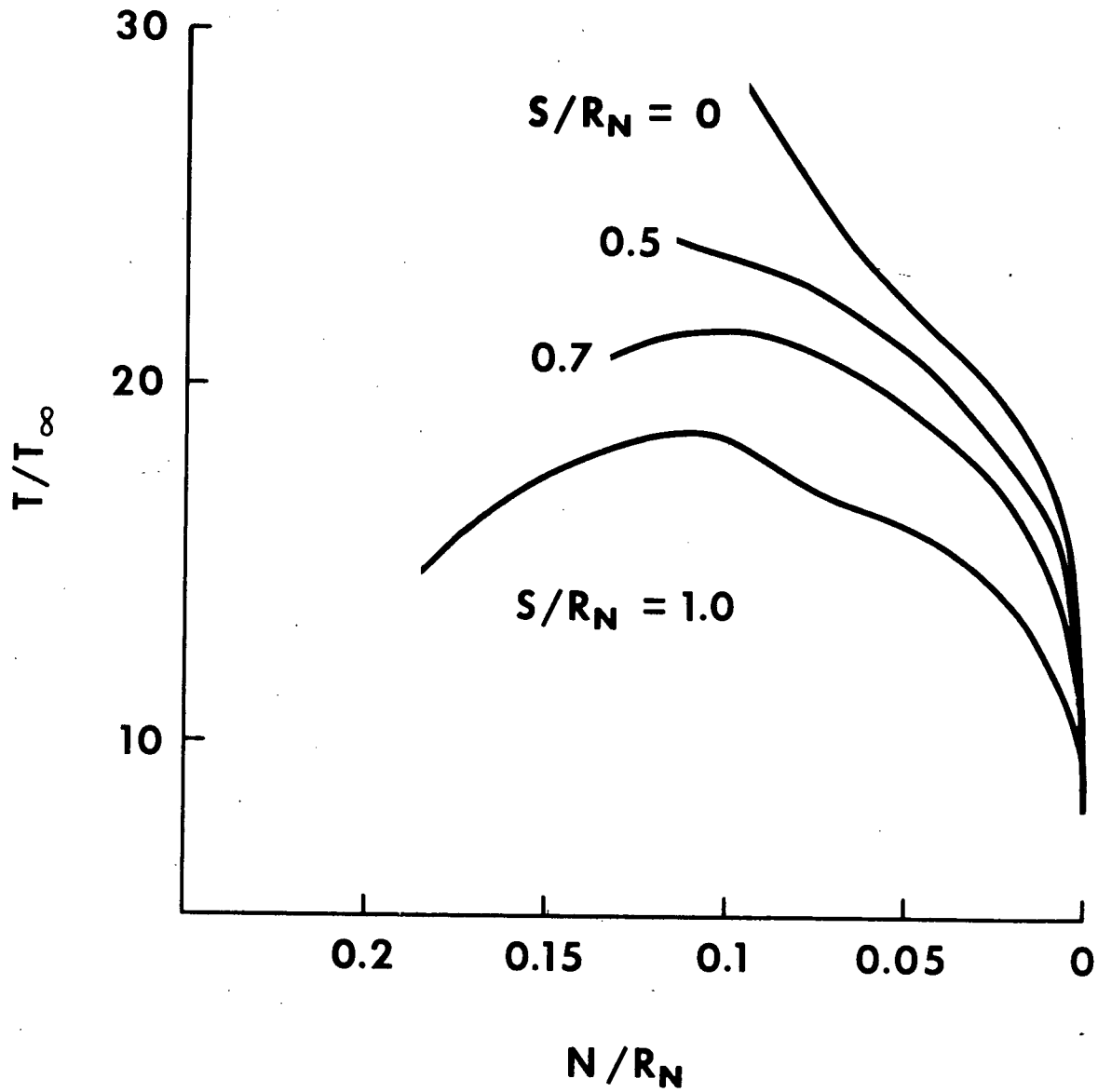

FIGURE 14

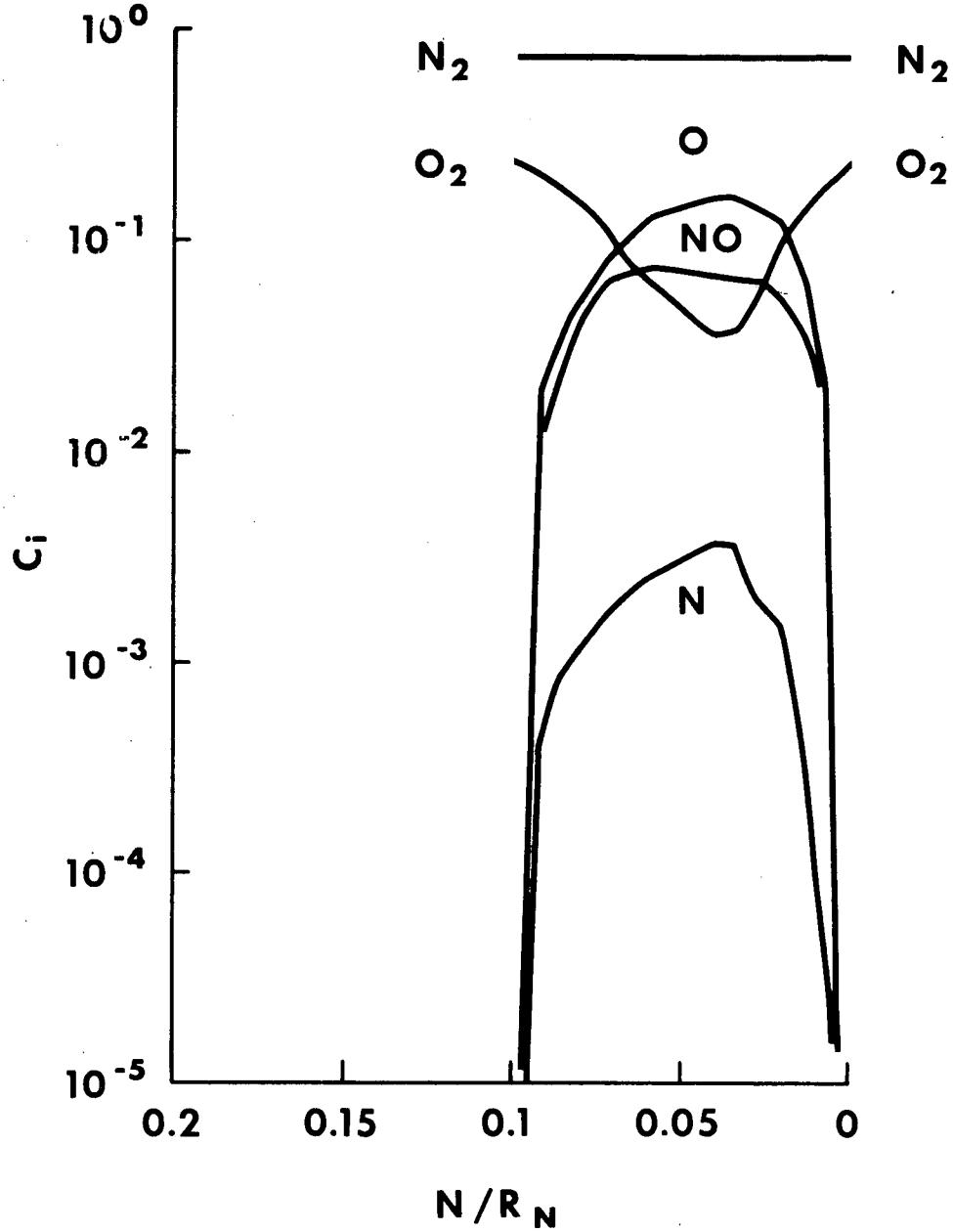

(a) $S/R_N = 0$

FIGURE 15

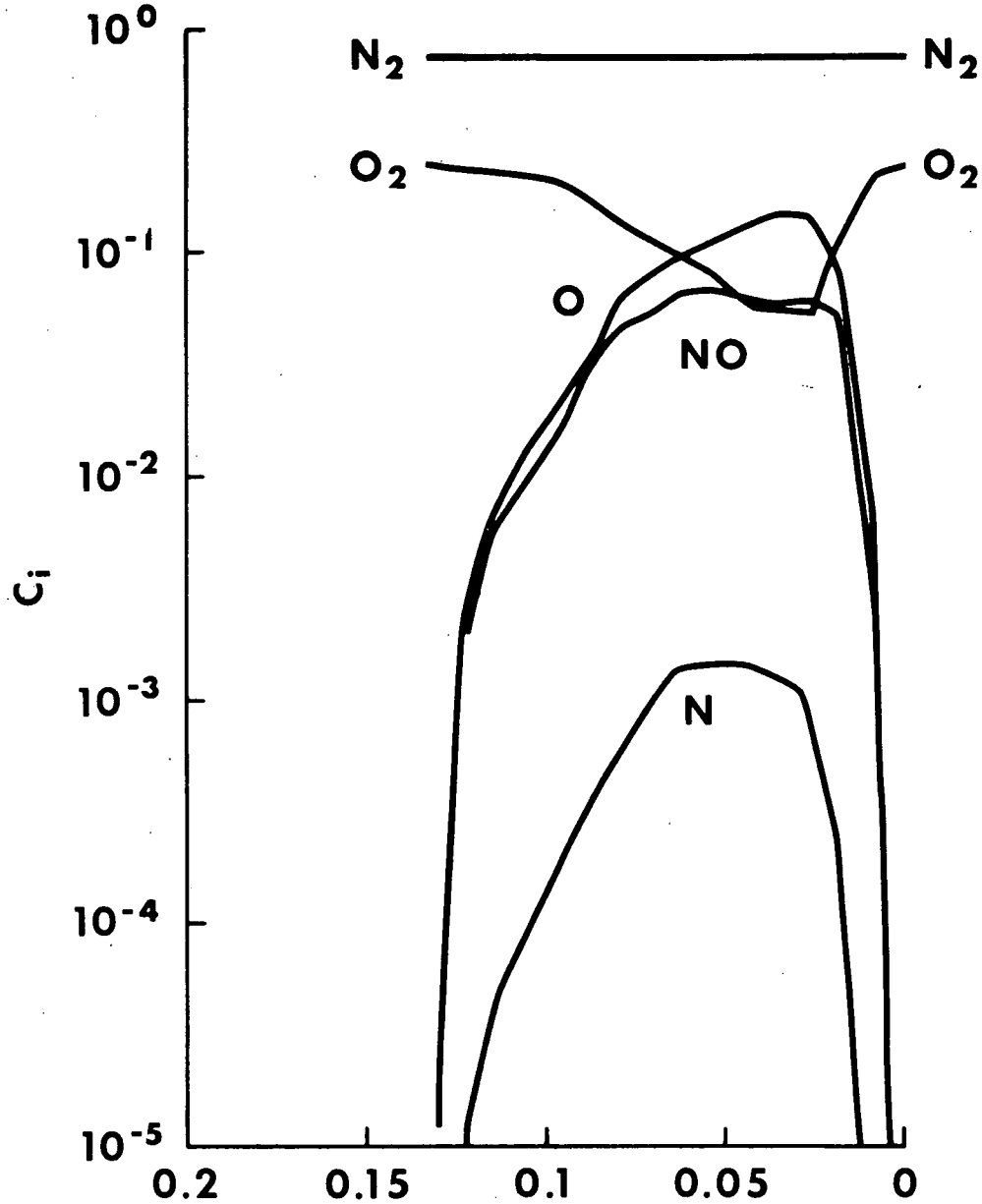

(b) $S/R_N = 0.7$

FIGURE 15

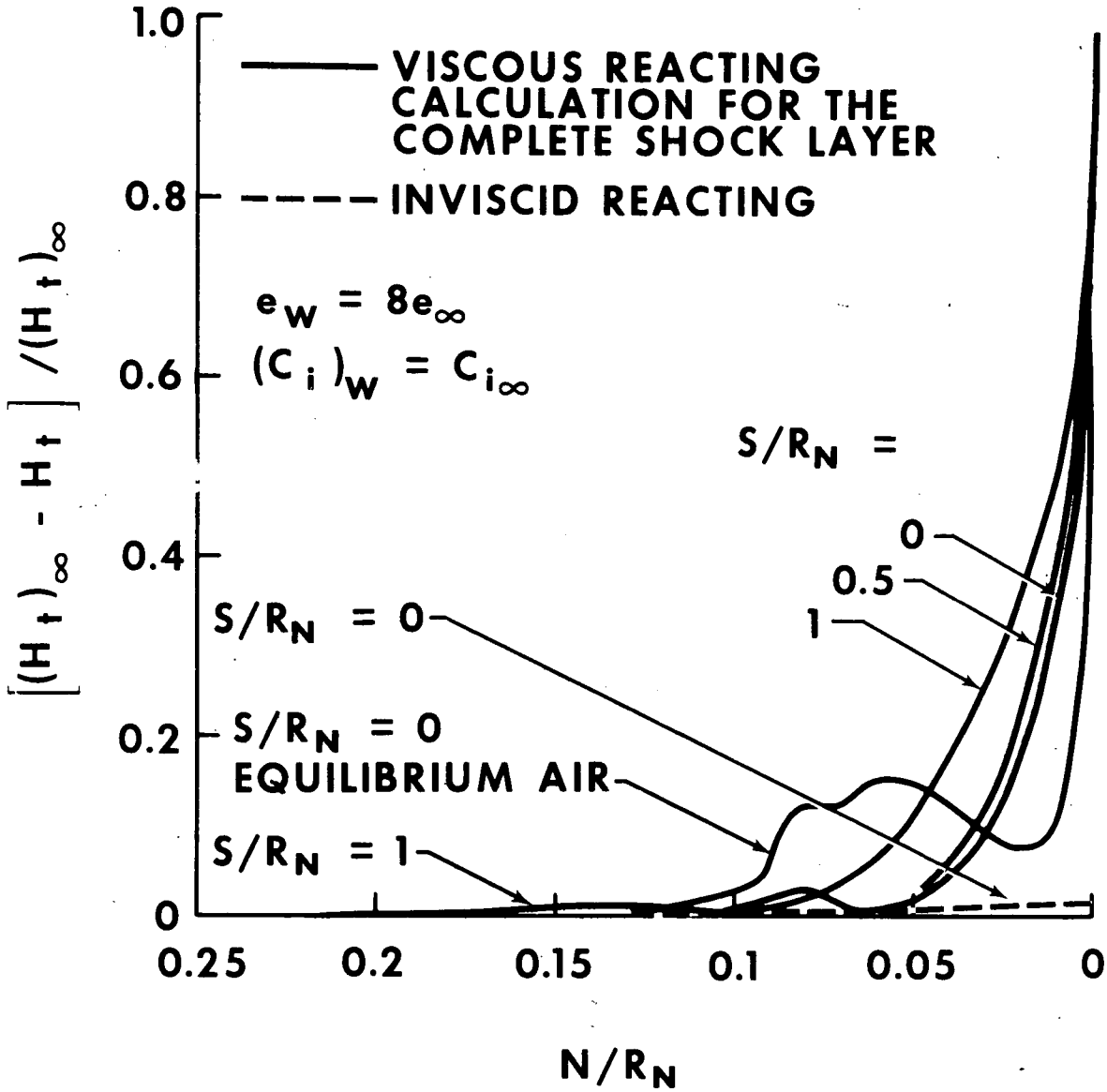
1.0
0.8
0.6
0.4
0.2
0
VISCOUS REACTING CALCULATION FOR THE COMPLETE SHOCK LAYER
INVISCID REACTING
$e_w = 8e_\infty$
$(C_i)_w = C_{i\infty}$
S/R_N =
0
0.5
1
S/R_N = 0
S/R_N = 0 EQUILIBRIUM AIR
S/R_N = 1
0.25
0.2
0.15
0.1
0.05
0
N/R_N
$\left[(H_t)_\infty - H_t\right]/(H_t)_\infty$

FIGURE 16

B

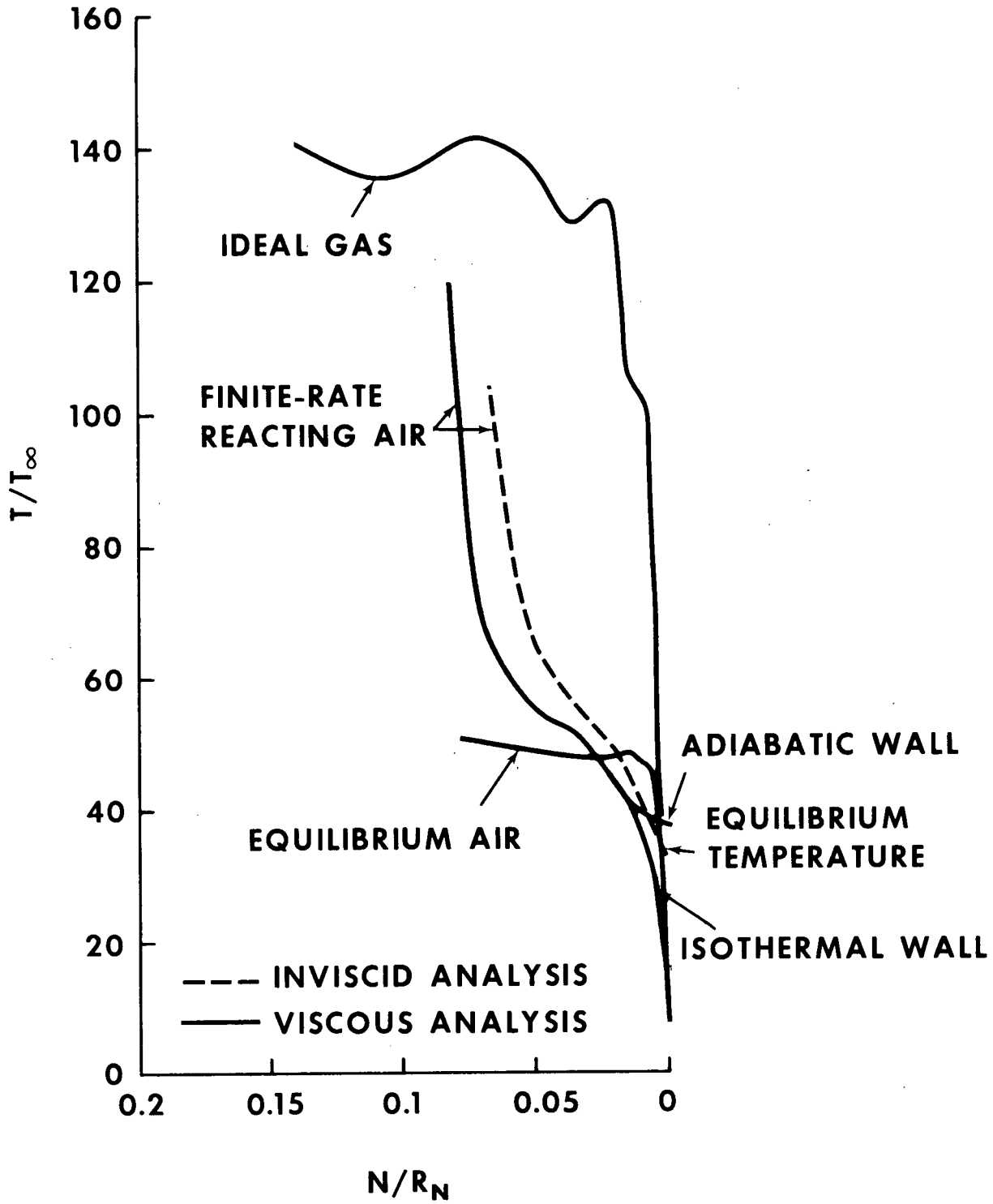

(a) $S/R_N = 0$

FIGURE 17

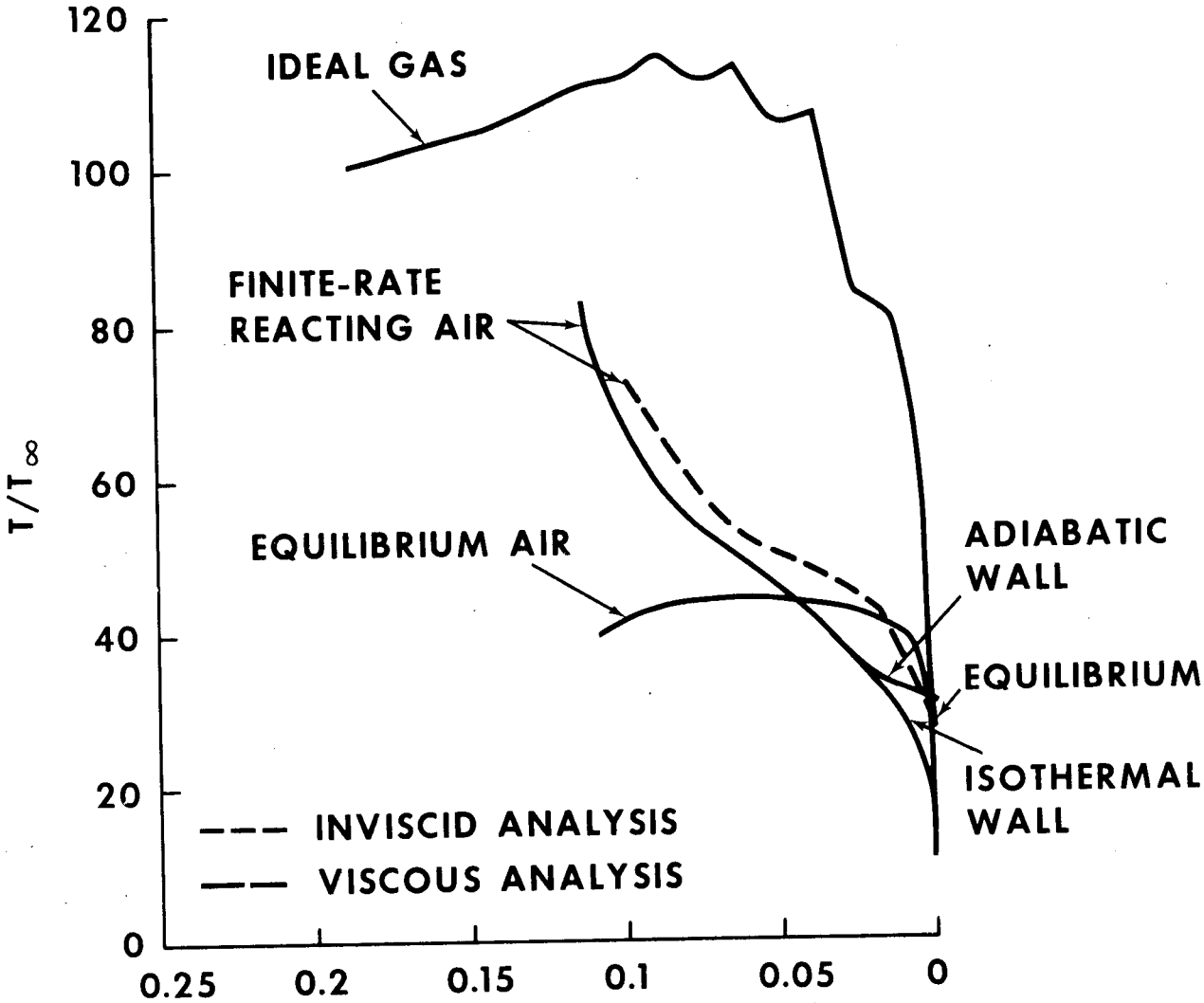

(b) $S/R_N = 0.7$

FIGURE 17

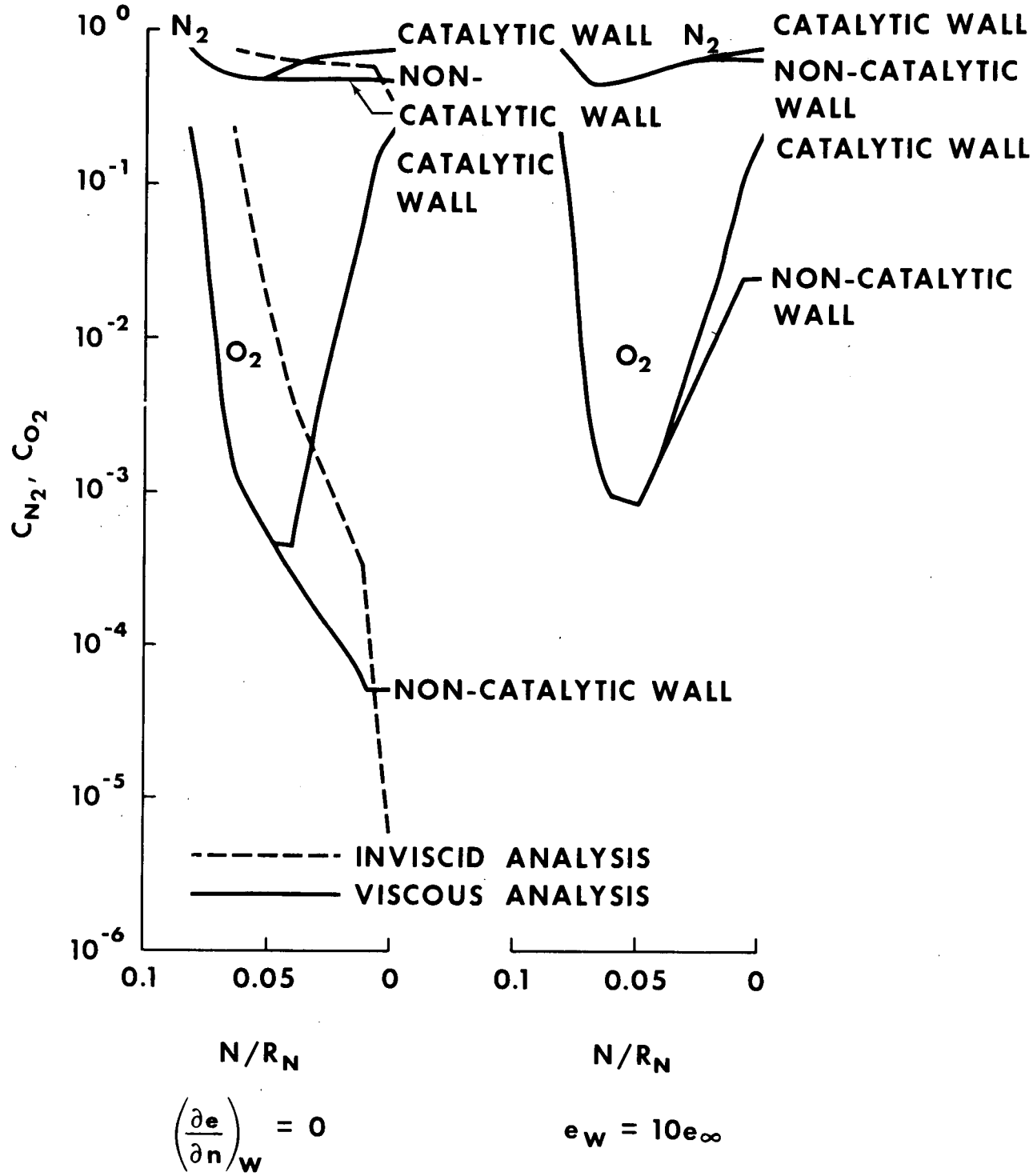
10^0
10^{-1}
10^{-2}
10^{-3}
10^{-4}
10^{-5}
10^{-6}
C_{N_2}, C_{O_2}
N_2
CATALYTIC WALL
NON-CATALYTIC WALL
O_2
INVISCID ANALYSIS
VISCOUS ANALYSIS
0.1
0.05
0
N/R_N
$\left(\frac{\partial e}{\partial n}\right)_w = 0$
$e_w = 10e_\infty$

FIGURE 18

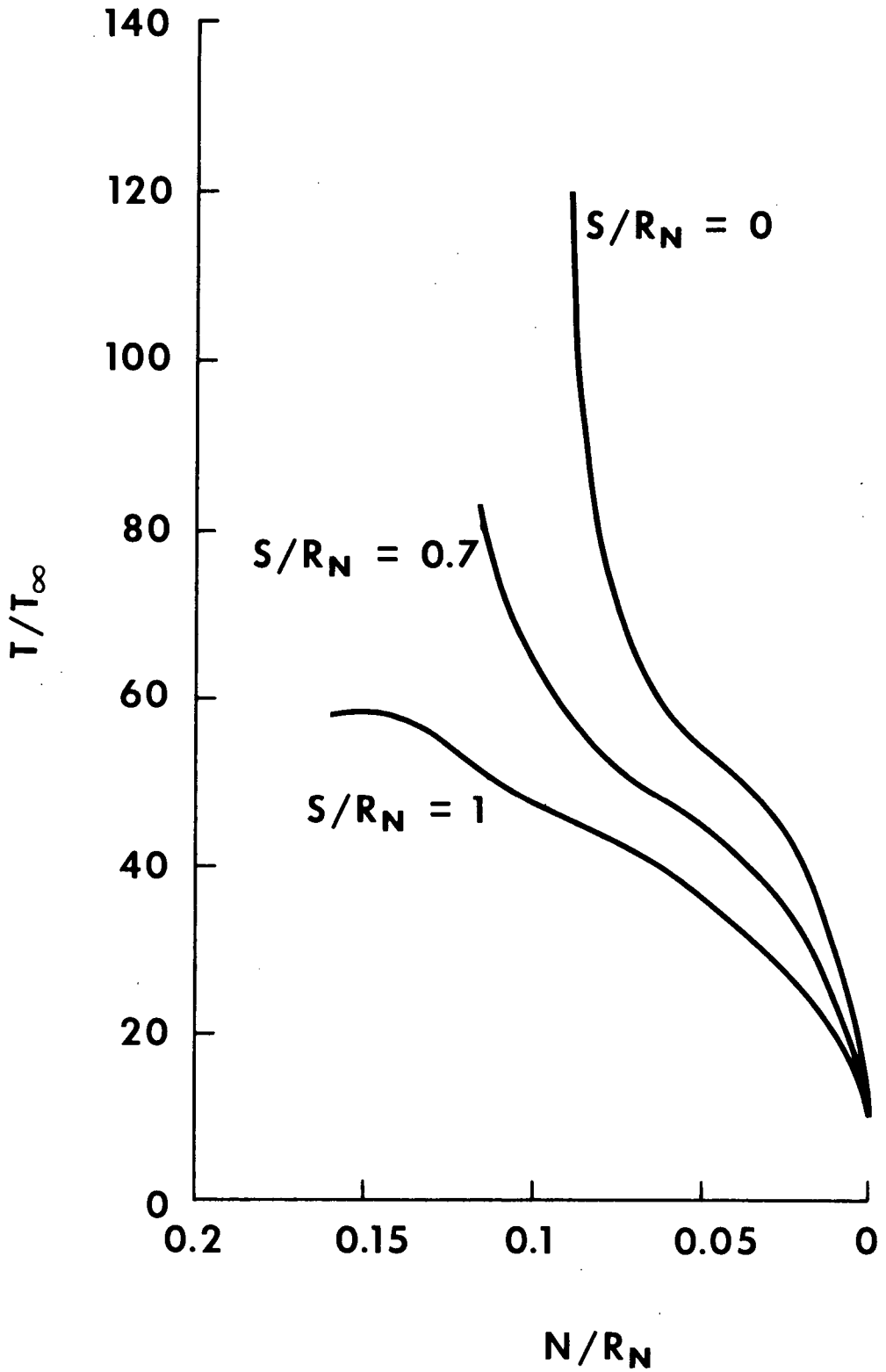

FIGURE 19

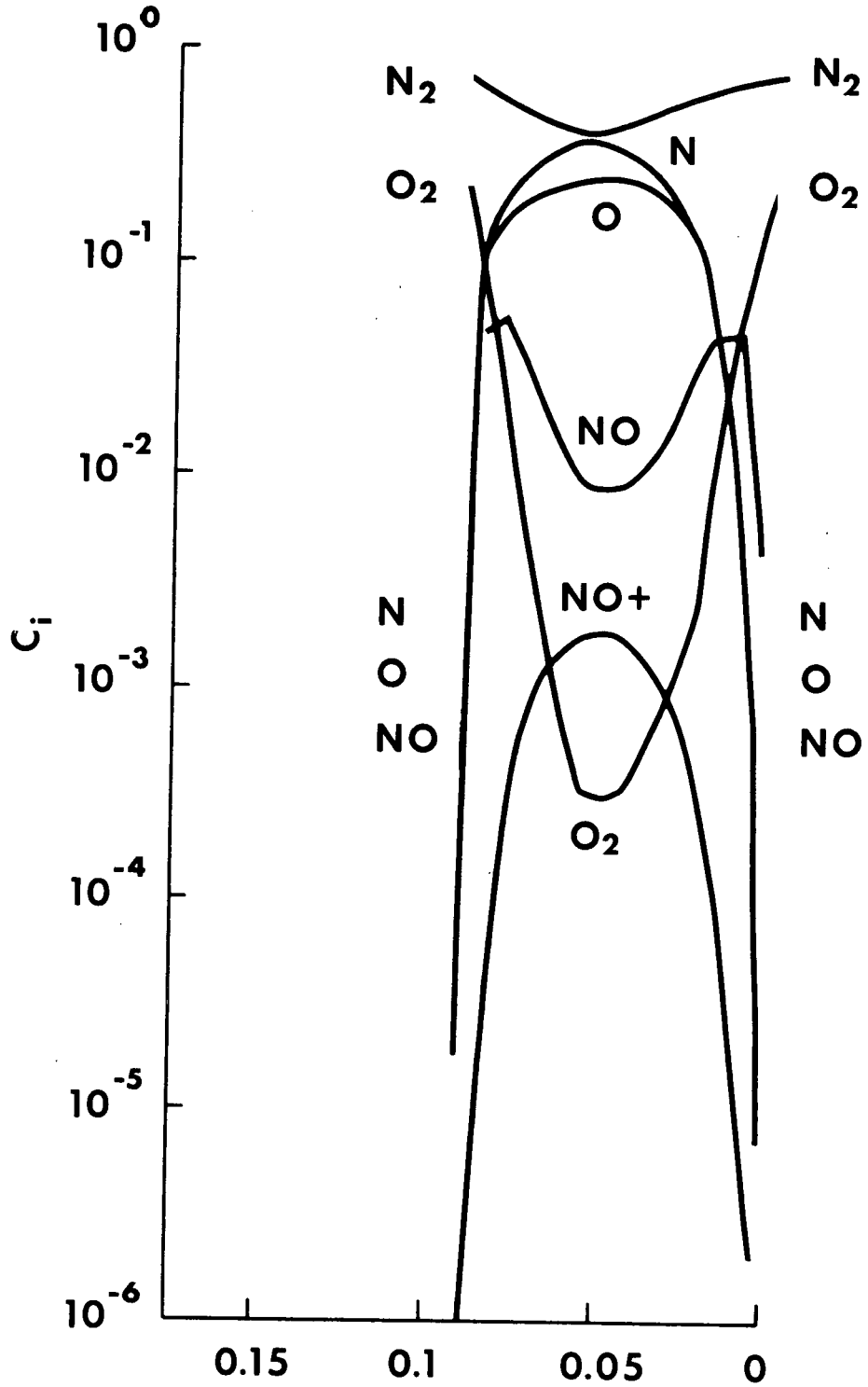

(a) $S/R_N = 0$

FIGURE 20

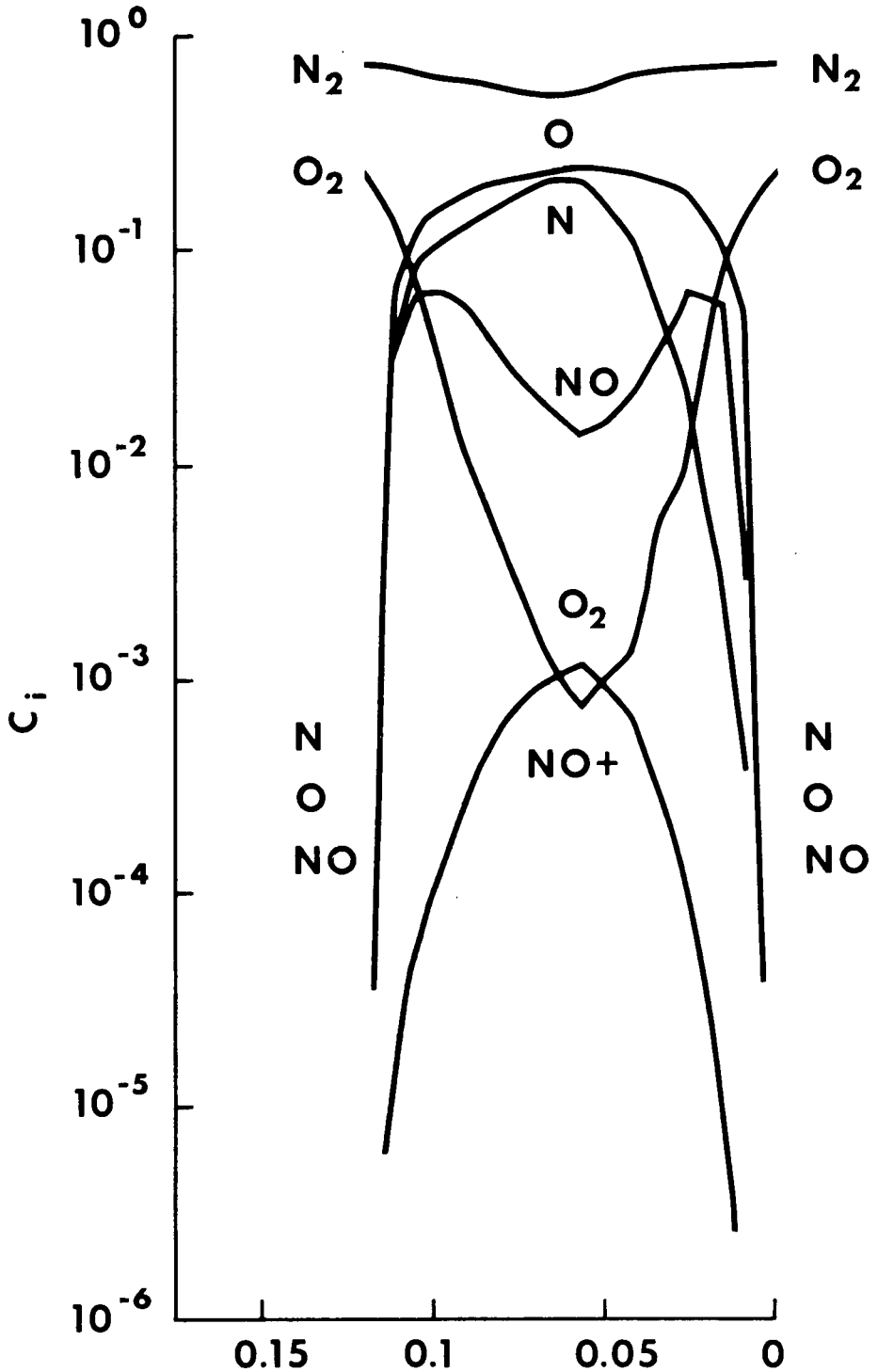

(b) $S/R_N = 0.7$

FIGURE 20

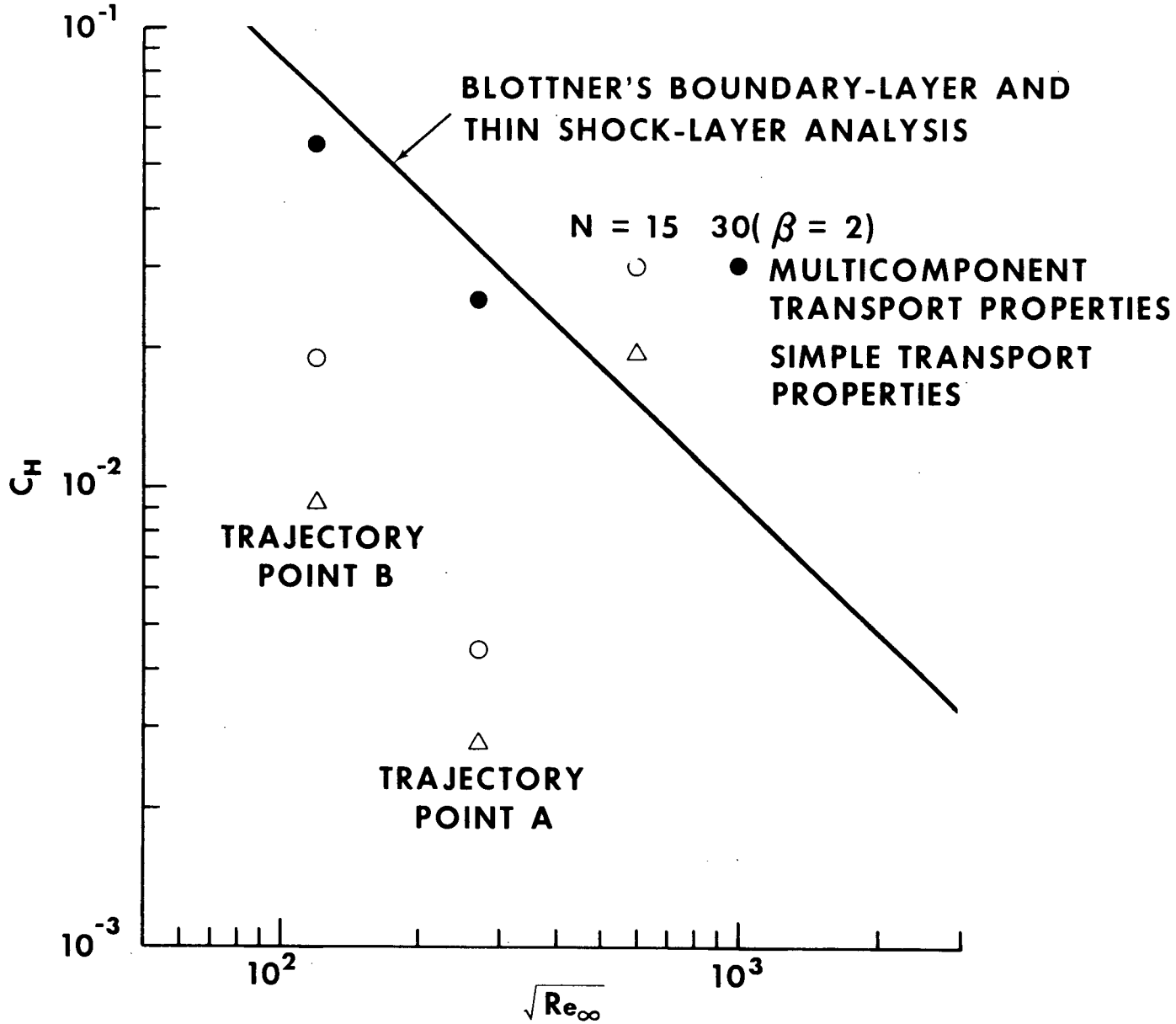
10^{-1}
10^{-2}
10^{-3}
C_H
BLOTTNER'S BOUNDARY-LAYER AND THIN SHOCK-LAYER ANALYSIS
N = 15 30(β = 2)
MULTICOMPONENT TRANSPORT PROPERTIES
SIMPLE TRANSPORT PROPERTIES
TRAJECTORY POINT B
TRAJECTORY POINT A
10^2
10^3
$\sqrt{Re_\infty}$

FIGURE 21

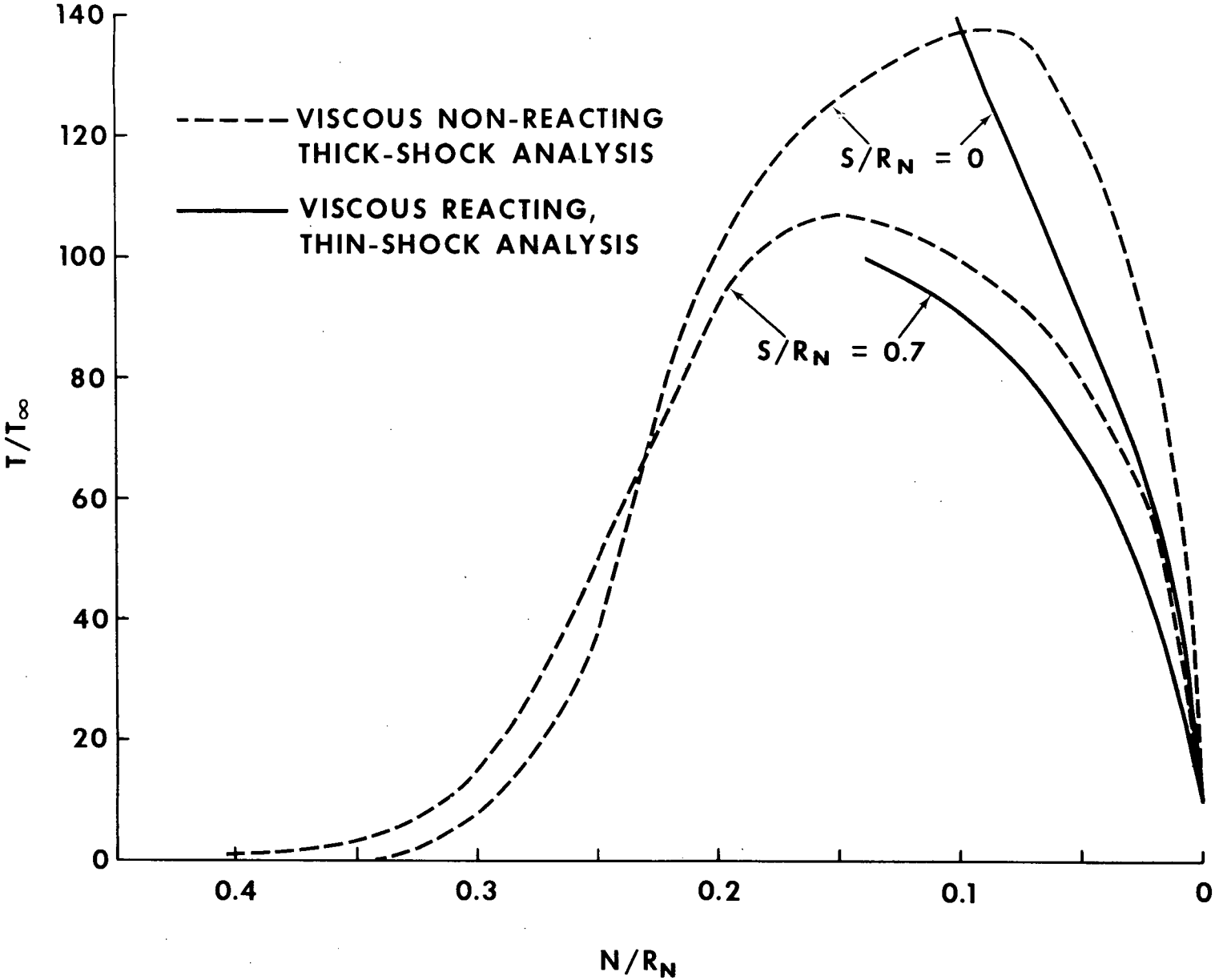
140
120
100
80
60
40
20
0
T/T∞
VISCOUS NON-REACTING
THICK-SHOCK ANALYSIS
VISCOUS REACTING,
THIN-SHOCK ANALYSIS
S/RN = 0
S/RN = 0.7
0.4
0.3
0.2
0.1
0
N/RN

FIGURE 22

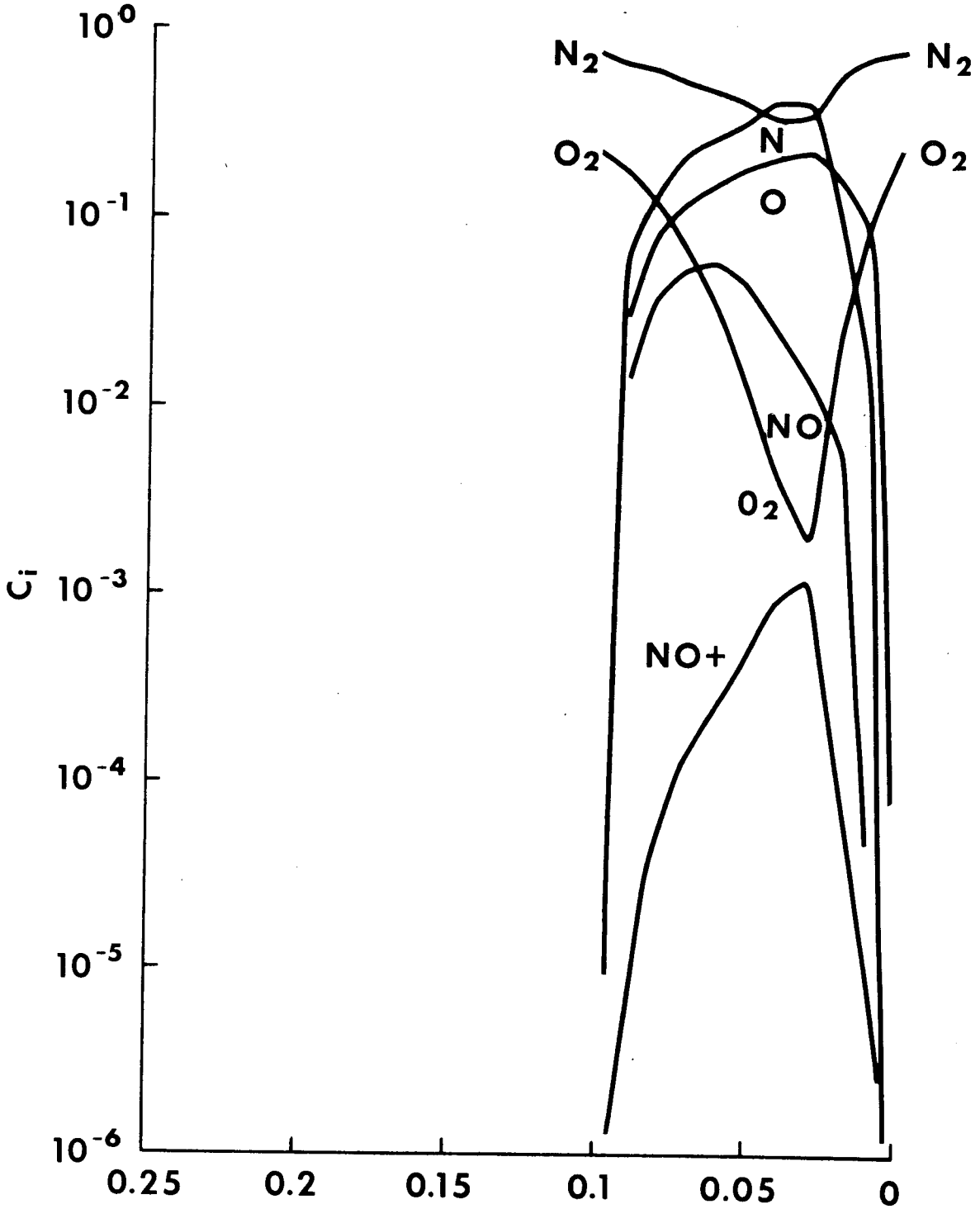
10^0
10^{-1}
10^{-2}
10^{-3}
10^{-4}
10^{-5}
10^{-6}
C_i
N_2
N_2
O_2
O_2
N
O
NO
O_2
NO+
0.25
0.2
0.15
0.1
0.05
0
N/R_N
(a) $S/R_N = 0$

FIGURE 23

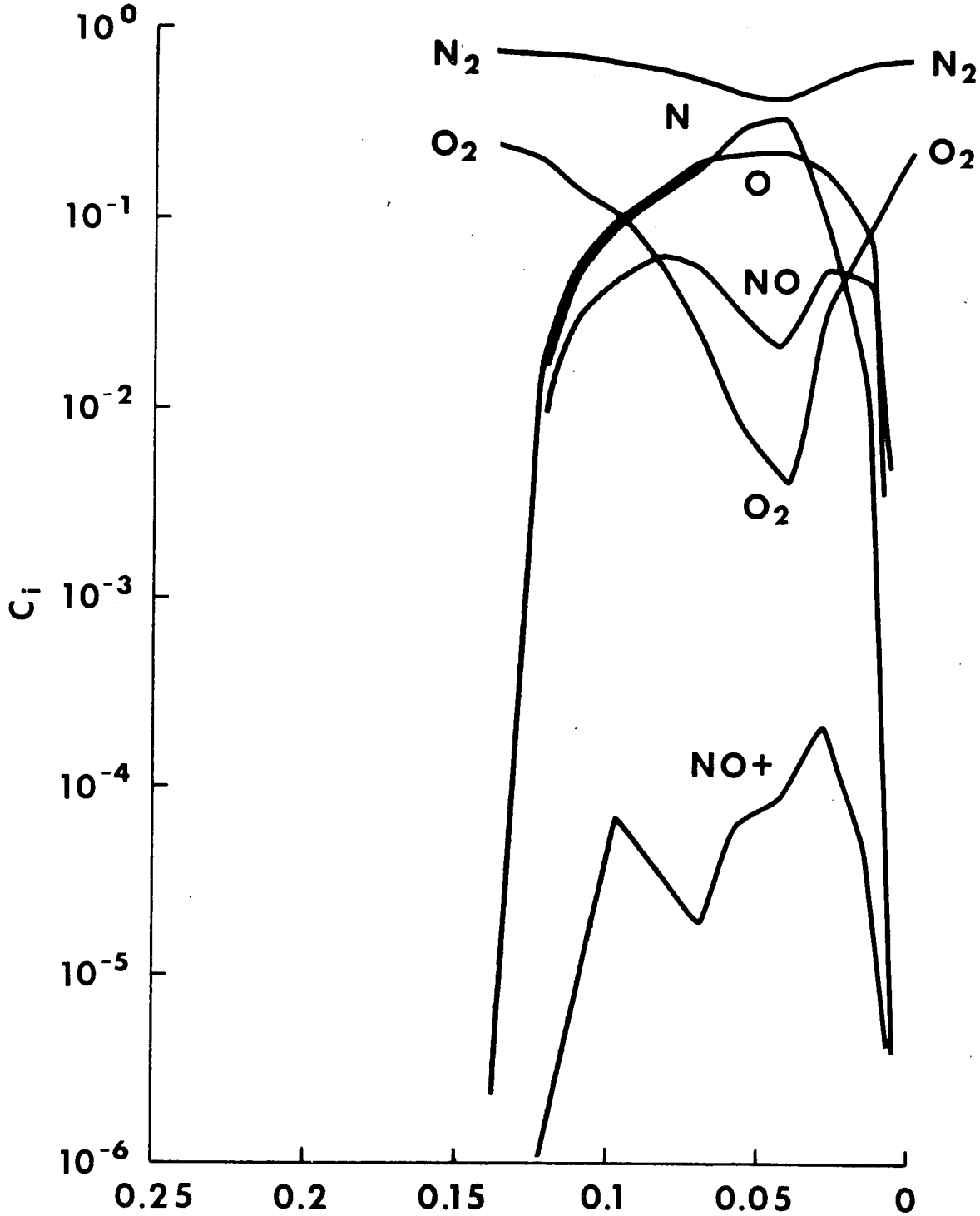

(b) $S/R_N = 0.7$

FIGURE 23

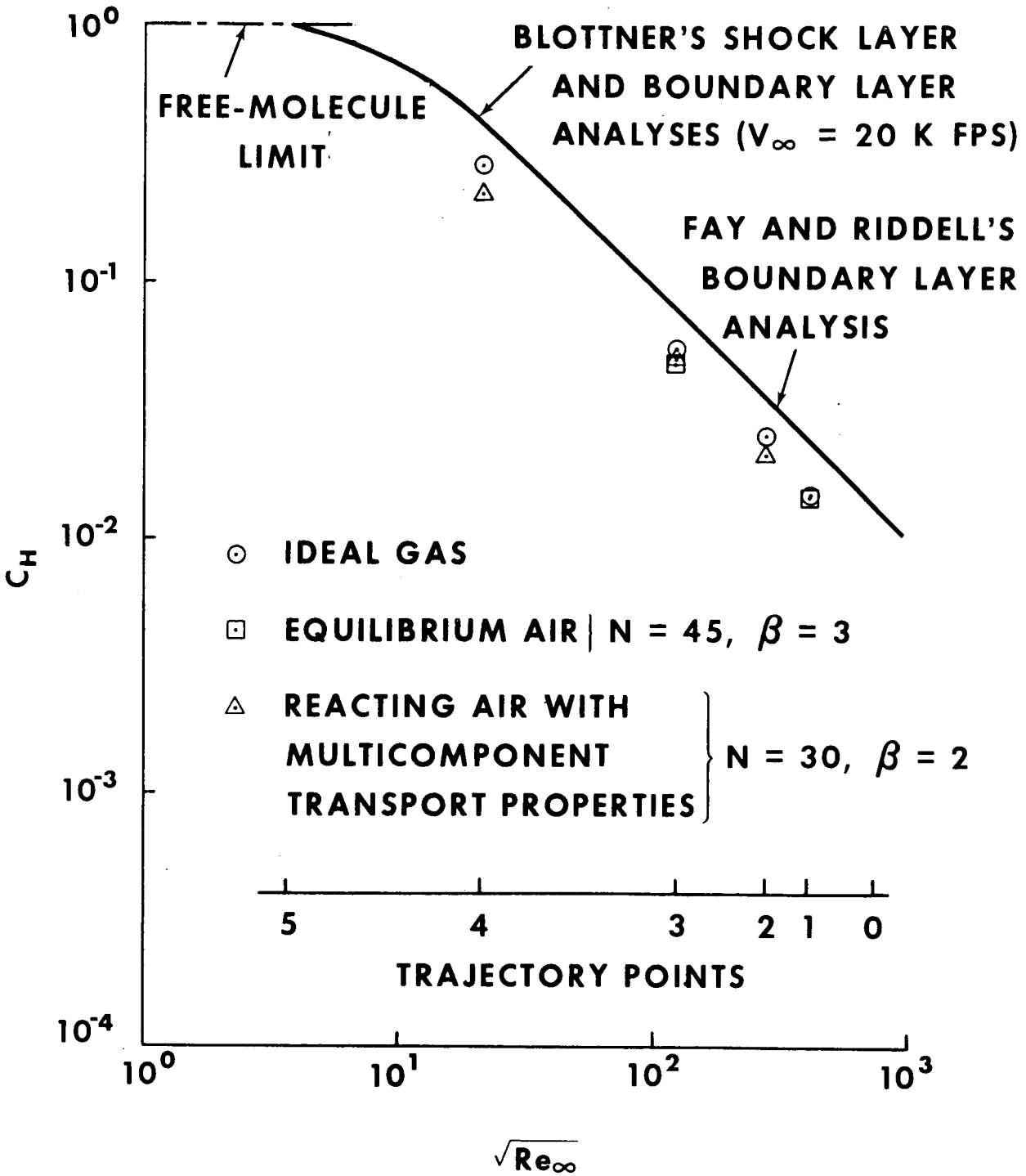

FIGURE 24

☆ U.S. GOVERNMENT PRINTING OFFICE: 1973—779-474/1899